Fisheries and Oceans Canada | Pêches et Océans Canada
Ecosystems and Oceans Science | Sciences des écosystèmes et des océans

Canadian Science Advisory Secretariat (CSAS)

Research Document 2022/018

Maritimes Region

Optical, Chemical, and Biological Oceanographic Conditions on the Scotian Shelf and in the eastern Gulf of Maine during 2020

B. Casault, C. Johnson, E. Devred, E. Head, L. Beazley, and J. Spry

Fisheries and Oceans Canada
Bedford Institute of Oceanography
1 Challenger Drive, PO Box 1006
Dartmouth, Nova Scotia B2Y 4A2

April 2022

Canada

Foreword

This series documents the scientific basis for the evaluation of aquatic resources and ecosystems in Canada. As such, it addresses the issues of the day in the time frames required and the documents it contains are not intended as definitive statements on the subjects addressed but rather as progress reports on ongoing investigations.

Published by:

Fisheries and Oceans Canada
Canadian Science Advisory Secretariat
200 Kent Street
Ottawa ON K1A 0E6

http://www.dfo-mpo.gc.ca/csas-sccs/
csas-sccs@dfo-mpo.gc.ca

© Her Majesty the Queen in Right of Canada, 2022
ISSN 1919-5044
ISBN 978-0-660-42530-6 Cat. No. Fs70-5/2022-018E-PDF

Correct citation for this publication:

Casault, B., Johnson, C., Devred, E., Head, E., Beazley, L., and Spry, J. 2022. Optical, Chemical, and Biological Oceanographic Conditions on the Scotian Shelf and in the eastern Gulf of Maine during 2020. DFO Can. Sci. Advis. Sec. Res. Doc. 2022/018. v + 82 p.

Aussi disponible en français :

Casault, B., Johnson, C., Devred, E., Head, E., Beazley, L., et Spry, J. 2022. Conditions océanographiques optiques, chimiques et biologiques sur le plateau néo-écossais et dans l'est du golfe du Maine en 2020. Secr. can. des avis sci. du MPO. Doc. de rech. 2022/018. v + 86 p.

TABLE OF CONTENTS

ABSTRACT

Ocean physical conditions in the Maritimes Region in 2020 were characterized by generally warm surface and bottom temperatures. The year 2020 was the third warmest of the 51-year time series with 2012 having been the warmest on record. Surface and deep nutrients inventories remained mainly near or below normal on the Scotian Shelf (SS) following the trend of the last 6–7 years. Higher-than-normal deep nitrate concentrations associated with warm salty water were observed in the fall on the eastern side of the Cabot Strait section and at the offshore stations of the Halifax section. The spring phytoplankton bloom on the central and the western SS was later than normal and shorter in duration with either near- or lower-than-normal magnitude. On the eastern SS, bloom conditions developed near the shelf break with normal onset timing and duration. Observations at the Halifax-2 (HL2) station indicated a continued pattern of mainly lower abundance of diatoms and higher abundance of ciliates and flagellates. Zooplankton indices (i.e., *Calanus finmarchicus*, *Pseudocalanus* spp., total copepods and non-copepods abundance, and mesozooplankton biomass) were mainly near or lower than average across most of the region but slightly above normal on the Browns Bank section. The abundance of copepod indicator species (i.e., Arctic *Calanus*, warm-offshore species and warm-shelf species) was generally near or slightly lower than normal, although spatial variability was observed. Observations at HL2 also indicate a continued pattern of generally higher-than-normal abundance of small cyclopoid copepods (e.g., *Oithona atlantica*).

Surface temperatures in Bedford Basin were, on average, slightly above normal in 2020, consistent with general trends observed across the SS. From January to September, bottom temperatures continued the trend of primarily negative anomalies observed in 2019. In October, both bottom temperature and salinity reverted to above-normal conditions, suggesting the occurrence of an offshore shelf-water intrusion event. Bottom nitrate, silicate, particulate organic carbon and nitrogen all reverted to below-normal conditions in October, coinciding with the timing of the suspected shelf-water intrusion event. Bottom chlorophyll and phytoplankton conditions were all below normal in 2020, marking a continuation of the primarily negative anomalies observed in these parameters since 2010.

The 2019 Continuous Plankton Recorder data indicated lower-than-normal annual abundances of diatoms and dinoflagellates on the Eastern Scotian Shelf (ESS) and Western Scotian Shelf (WSS), while the values of the phytoplankton colour index, a proxy for the phytoplankton biomass, were near (WSS) or above (ESS) normal. The annual abundances of *Calanus* CI–IV and *C. finmarchicus* CV–VI were above or near normal on the ESS and below normal on the WSS. Abundances of the other taxa (two arctic *Calanus* species, three small copepod taxa, two macrozooplankton taxa, and three acid-sensitive taxa) were near or lower than normal on the ESS and WSS, except for hyperiid amphipods, which were more abundant than normal on the ESS.

INTRODUCTION

The Atlantic Zone Monitoring Program (AZMP) was implemented in 1998 to enhance Fisheries and Oceans Canada's (DFO's) capacity to describe, understand, and forecast the state of the marine ecosystem (Therriault et al. 1998). The AZMP derives its information on the marine environment and ecosystem from data collected at a network of sampling locations (high-frequency sampling stations, cross-shelf sections, and ecosystem trawl surveys) in four DFO regions (Québec, Gulf, Maritimes, and Newfoundland), sampled at a frequency of twice-monthly to once-annually. The sampling design provides basic information on the variability in physical, chemical, and biological properties of the Northwest Atlantic continental shelf and slope on seasonal and inter-annual scales. Ecosystem trawl surveys and cross-shelf sections provide information about broad-scale environmental variability (Harrison et al. 2005) but are limited in their seasonal coverage. High-frequency sampling stations complement the broad-scale sampling by providing detailed information on seasonal changes in ocean properties. In recent years, data collected from buoys and gliders also complement the core observations with high-resolution temporal and/or spatial observations. In addition, the North Atlantic Continuous Plankton Recorder (CPR) survey provides monthly sampling along commercial shipping routes between Reykjavik and the New England coast, via the Scotian Shelf (SS). The CPR sampling extends a dataset started in 1960, allowing present-day observations to be set within a longer time frame than the AZMP core sampling. *In situ* sampling is also complemented by remote-sensing ocean colour measurements providing additional information of the distribution of phytoplankton in the surface layer on a broad scale. This report provides an assessment of the distribution and variability of nutrients, oxygen, and plankton on the SS and in the eastern Gulf of Maine (GoM), focusing on conditions observed during 2020 in the context of warmer conditions in the marine environment observed in recent years. It complements assessments for the physical environment of the Maritimes Region (Hebert et al. 2021) and for the state of the Canadian Northwest Atlantic shelf system as a whole (DFO 2021). Although not considered a core AZMP station, the Compass Buoy station located in the Bedford Basin has been sampled weekly since 1992 and a summary of the observed environmental and phytoplankton conditions is also presented in this report.

The SS is located in a transition zone influenced by both sub-polar waters, mainly flowing into the region from the Gulf of St. Lawrence and the Newfoundland Shelf, and warmer offshore waters of Gulf Stream origin. The deep-water properties of the western SS exhibit significant shifts in temperature, reflecting changes in the source of deep slope water to the shelf between cold, low-nutrient Labrador Slope Water, and warm, nutrient-rich Atlantic slope water that can be driven by changes in large-scale atmospheric pressure patterns (Petrie 2007). Temperature and salinity on the SS are also influenced by heat transfer between the atmosphere and ocean, local mixing, precipitation, and, to some extent, runoff from land. Changes in the physical pelagic environment influence both plankton community composition and annual biological production cycles, with implications for energy transfer to higher trophic-level production.

METHODS

Sample collection and processing conform to established standard protocols to the best extent possible (Mitchell et al. 2002). Non-standard measurements or derived variables are described below.

MISSIONS

AZMP-DFO Maritimes Region sea-going staff participated in three missions (two ecosystem trawl surveys and one seasonal cross-shelf oceanographic survey) during the 2020 calendar year, in addition to day trips to the two high-frequency sampling stations. The spring seasonal cross-shelf survey was cancelled due to the COVID-19 pandemic preventing at-sea activities. A total of 302 hydrographic station occupations were completed with net samples collected at 116 of these stations (Table 1).

High-Frequency Sampling Stations

The Halifax-2 (HL2) and Prince-5 (P5) high-frequency sampling stations (Figure 1) were sampled 12 and 8 times, respectively, in 2020. This is lower than sampling frequencies achieved in recent years and due to limited at-sea activities resulting from the COVID-19 pandemic. As a result, there was no sampling between mid-March and early July at HL2 or during the months of April, May, and June at P5. In addition, December sampling at P5 was cancelled due to inclement weather conditions.

The standard sampling suite for the high-frequency stations includes the following:

- Conductivity, Temperature, Depth (CTD; measured using a Sea-Bird instrument) profiles with dissolved oxygen, fluorescence, and Photosynthetically Active Radiation (PAR).
- Niskin water bottles sampled at standard depths for nutrient analyses, salinity and oxygen (for calibration of the CTD), and chlorophyll *a* analyses. Accessory phytoplankton pigments are also measured near the surface only but are not reported in this document.
- Niskin water bottles sampled for phytoplankton enumeration.
- Vertical ring net tows (202 µm mesh net) for zooplankton biomass (wet and dry weights), abundance, and community composition.
- Secchi depth measurement for light attenuation when possible.

Shelf Sections

During the spring and fall seasonal surveys, samples are collected on the four primary sections (Cabot Strait [CSL]; Louisbourg [LL]; Halifax [HL]; Browns Bank [BBL]; Figure 1) and a number of ancillary sections/stations (gray markers in Figure 2). However, results from the ancillary sections/stations are not reported in this document. In 2020, sampling on the shelf sections occurred in fall only (Table 1). Moreover, for the HL section, vertical net tows could not be completed at the core stations HL3 to HL6 due to inclement weather conditions, including high wind speeds. Annual estimates of zooplankton indices for HL are reported here, despite limited sampling in 2020, but they should be interpreted with caution.

The standard sampling suite for the cross-shelf section stations is the same as for the high-frequency sampling stations as listed above, except for phytoplankton enumeration. In addition to the standard suite of analyses from water samples, particulate organic carbon is measured at standard depths.

Ecosystem Trawl Surveys

AZMP-DFO Maritimes Region participated in two primary ecosystem trawl surveys in 2020. The March winter survey on the WSS and Georges Bank (GB) took place in two legs that were

assigned different mission identifiers (Table 1). The summer survey on the SS and in the eastern GoM took place from early July to mid-August.

The sampling suite for the ecosystem trawl survey stations includes the measurements listed above for the high-frequency sampling stations, but the standard set of water bottle sampling depths is reduced, and vertical ring net tows (202 µm mesh net) are only collected at a subset of stations (Table 1 and Figure 3).

The sum of nitrate and nitrite is reported here as “nitrate”. For the summer ecosystem trawl survey, bottom nitrate concentrations were interpolated on a three-minute latitude-longitude grid using optimal estimation (Petrie et al. 1996) to generate fields of bottom properties within the ecosystem trawl survey strata. The interpolation method uses the three nearest neighbours, with data near the interpolation grid point weighted proportionately more than those farther away. The weighting scheme is described in Petrie and Dean-Moore (1996), with horizontal length scales of 30 km, a vertical length scale of 15 m (for depth <50 m) or 25 m (for depths between 50 and 500 m). Bottom oxygen concentrations were optimally interpolated using the same technique as for nitrate. Oxygen concentrations were measured using a CTD-mounted oxygen sensor which was calibrated against oxygen concentrations measured by Winkler titration. Bottom oxygen saturation values are presented for the 2020 summer mission; however, the corresponding anomalies are not presented here as climatological means are not available due to insufficient availability of quality of oxygen data prior to 2015.

GEAR DEPLOYMENT

Conductivity, Temperature, Depth

The CTD is lowered to a target depth within 2 m of the bottom.

Standard depths for water samples include:

- High-frequency sampling stations:
    1. HL2: 1 m, 5 m, 10 m, 20 m, 30 m, 40 m, 50 m, 75 m, 100 m, 140 m
    2. P5: 1 m, 10 m, 25 m, 50 m, 95 m
- Seasonal sections: near-surface, 10 m, 20 m, 30 m, 40 m, 50 m, 60 m, 80 m, 100 m, 250 m, 500 m, 1000 m, 1500 m, 2000 m, near-bottom (depths sampled are limited by bottom depth)
- Ecosystem trawl surveys: 5 m, 25 m, 50 m, and near bottom when possible

Net Tows

Ring nets of a standard 202 µm mesh are towed vertically from near bottom to surface at approximately 1 $m \cdot s^{-1}$. In deep offshore waters, the maximum tow depth is 1000 m. Samples are preserved in buffered formalin and analyzed according to the protocol outlined in Mitchell et al. (2002).

DERIVED METRICS

Mixed Layer and Stratification Indices

Two simple indices of the vertical physical structure of the water column are computed and reported here:

1. The Mixed Layer (ML) depth is determined from CTD observations as the minimum depth where the density gradient is equal to or exceeds 0.01 $kg \cdot m^{-4}$.

2. The Stratification Index (SI) is calculated as:

$$SI\ (kg \cdot m^{-4}) = (\sigma_{t\text{-}50} - \sigma_{t\text{-}zmin})/(50 - z_{min})$$

where $\sigma_{t\text{-}50}$ and $\sigma_{t\text{-}zmin}$ are interpolated values of density (σ_t) at 50 m and z_{min}, the minimum depth of reliable CTD data, which is typically around 1 m or 2 m and always less than approximately 5 m.

Optical Properties

The optical properties of seawater (attenuation coefficient [K_d], euphotic depth [Z_{eu}]) are derived from *in situ* light attenuation measurements using a rosette-mounted PAR meter and from Secchi disk, according to the following procedures:

1. The downward vertical attenuation coefficient for PAR ($K_{d\text{-}PAR}$) is estimated as the slope of the linear regression of $\ln(E_d(z))$ as a function of depth z (where $E_d(z)$ is the value of downward irradiance at depth z) in the depth interval from minimum depth to around 50 m. The minimum depth is typically around 2 m although the calculation is sometimes forced below that target when near-surface PAR measurements appear unreliable.

2. The value of the light attenuation coefficient $K_{d\text{-}Secchi}$ from Secchi disc observations is found using:

$$K_{d\_secchi}\ (m^{-1}) = 1.44 / Z_{sd}$$

where Z_{sd} is the depth (in m) at which the Secchi disc disappears from view (Holmes 1970).

Estimates of the euphotic depth (Z_{eu}), defined as the depth where PAR is 1% of the surface value, are obtained using the following expression (Churilova et al. 2017):

$$Z_{eu}\ (m) = 4.6 / K_d$$

Vertically Integrated Variables

Integrated chlorophyll *a* and nutrient inventories are calculated over various depth intervals (e.g., 0–100 m for chlorophyll *a*, and 0–50 m and 50–150 m for nutrients) using trapezoidal numerical integration. When the maximum depth at a given station is shallower than the lower depth limits noted above, the inventories are calculated by setting the lower integration limit to the maximum depth at that station (e.g., 95 m for P5). Data at the surface (0 m) is taken as the closest-near-surface sampled value. Data at the lower depth is taken as:

1. the interpolated value when sampling is below the lower integration limit; or

2. the closest-deep-water sampled value when sampling is shallower than the lower integration limit.

Phytoplankton Taxonomic Groups

Phytoplankton abundance and taxonomic composition at the high-frequency sampling stations are estimated from pooled aliquots of water collected in the upper 100 m of the water column using the Utermöhl technique (Utermöhl 1931).

SATELLITE REMOTE SENSING OF OCEAN COLOUR

Near-surface chlorophyll *a* estimates from ocean colour data collected by the Moderate Resolution Imaging Spectroradiometer (MODIS) "Aqua" sensor are used for the purpose of constructing weekly composite time series for different statistical sub-regions. The MODIS time series extends from July 2002 to present for the selected stations (HL2 and P5) and sub-regions of the Maritimes Region(Cabot Strait [CS], Eastern Scotian Shelf [ESS], Central Scotian Shelf [CSS], Western Scotian Shelf [WSS], Lurcher Shoal [LS], Georges Bank [GB]; Figure 4). The OC3M band-ratio algorithm is used to derive chlorophyll *a* concentration from remote sensing reflectance as described in O'Reilly et al. (1998) with coefficients of the algorithm accessible on NASA's OceanColor Web chlorophyll-a website (accessed on November 23, 2021). The OC3M algorithm was modified to account for bias at low chlorophyll *a* concentration according to Hu et al. (2012). Basic statistics (mean and standard deviation) are extracted from weekly composites for the purpose of visualizing the annual cycle and the inter-annual variability of surface chlorophyll *a* for the sub-regions. Characteristics of the spring bloom are estimated from the weekly MODIS data using the shifted-Gaussian function of time model (Zhai et al. 2011). Four metrics are computed to describe the spring bloom characteristics: start date (day of year), cycle duration (days), magnitude (the integral of chlorophyll *a* concentration under the Gaussian curve), and amplitude (maximum minus the background chlorophyll *a* concentration). The application PhytoFit was used to compute the bloom metrics (Clay and Layton 2021).

ANNUAL ANOMALIES SCORECARDS

Scorecards of key indices, based on normalized, seasonally-adjusted annual anomalies, represent physical, chemical, and biological observations in a compact format. Annual estimates of water column inventories of nutrients, chlorophyll *a,* and the mean abundance of key zooplankton species or groups, at both the high-frequency sampling stations and as an overall average along each of the four standard sections, are based on general linear models (R Core Team 2021) of the form:

$$Density = \alpha + \beta_{YEAR} + \delta_{MONTH} + \varepsilon$$ for the high-frequency sampling stations, and

$$Density = \alpha + \beta_{YEAR} + \delta_{STATION} + \gamma_{SEASON} + \varepsilon$$ for the sections.

Density is in units of m^{-2} (or L^{-1} for microplankton abundance), α is the intercept and ε is the error. For the high-frequency sampling stations, β and δ are categorical effects for year and month, respectively. For the sections, β, δ *and* γ take into account the effect of year, station and season, respectively.

This approach is also used to calculate the seasonal estimates of zooplankton indices (i.e., zooplankton biomass and *Calanus finmarchicus* abundance) for the individual sections. In this case, a reduced model including the year and station effects is fitted to the seasonal data subsets. Note that for 2020, seasonal estimates were only calculated for the fall due to the absence of a spring mission.

The general linear model approach is also applied to the remote sensing data to calculate annual estimates of near-surface chlorophyll *a*. In this case, the model is fitted for each selected sub-region (i.e., HL2, P5, CS, ESS, CSS, WSS, LS and GB) using year and day of year as categorical variables.

Density in terms of surface chlorophyll *a* and chlorophyll *a* inventory is log-transformed [$log_{10}(n)$] to normalize the skewed distribution of the observations. For zooplankton and phytoplankton abundance, one is added to the log-transformed *Density* term [$log_{10}(n+1)$] to include observations for which the value equals zero. For the chlorophyll *a* inventory, estimates based

on both untransformed and log-transformed values are presented in this report for the purpose of comparison with estimates reported in previously published reports. Integrated inventories of nutrients and zooplankton biomass are not log-transformed. An estimate of the least-squares means based on Type III Sums of Squares (Lenth et al. 2020) is used as the measure of the overall year effect.

The zooplankton indices derived from the data collected during the ecosystem trawl surveys are calculated differently in this report compared to previous reports. The seasonal mean is calculated as the arithmetic mean of the zooplankton biomass or the log-transformed *C. finmarchicus* abundance data collected within each season/year and each Northwest Atlantic Fisheries Organization (NAFO) area. The reporting of the zooplankton indices based on the NAFO areas for the ecosystem trawl surveys conforms with similar reporting for the physical indices (e.g., DFO 2021) and with most fisheries stock assessment reports.

Annual anomalies are calculated as the deviation of an individual year from the mean of the annual estimates over the period 1999–2020. Note that in previous reports, annual anomalies were calculated relative to the 1999–2015 climatological period. For the remote sensing surface chlorophyll *a* and bloom metrics, a reference period of 2003–2020 is used due to missing data prior to 2003. The annual anomalies are expressed either in absolute units or as normalized quantities (i.e., by dividing by the standard deviation [sd] of the annual estimates over the same period). For the purpose of data interpretation, normalized anomalies are considered near normal when within ±0.5 sd, slightly above/below normal when between ±0.5 sd and ±1 sd, and above/below normal otherwise (i.e., larger/smaller than ±1 sd).

A standard set of indices representing anomalies of nutrient availability, phytoplankton biomass, and the abundance of dominant zooplankton species and groups (*C. finmarchicus*, *Pseudocalanus* spp., total copepods, and total non-copepods) are produced in each of the AZMP regions, including the Maritimes. To visualize Northwest Atlantic shelf scale patterns of variability, a zonal scorecard including observations from all of the AZMP regions is presented in DFO's Science Advisory Report (DFO 2021).

ACCESS TO DATA PRODUCTS

Data products presented in Figures 6, 8, 10, 11, 15, 18–20, and 23–34 are published on the Government of Canada's Open government website; a link to the data is available upon request to the corresponding author. Remote sensing chlorophyll *a* weekly estimates presented in Figures 16 and 21 are available at the DFO Maritimes MODIS FTP website (accessed on November 23, 2021) and bloom metrics used to generate Figures 17 and 22 are available upon request to the corresponding author.

BEDFORD BASIN MONITORING PROGRAM

The Compass Buoy station (44.69°N, 63.64°W) has been occupied weekly as part of the Bedford Basin Monitoring Program since 1992 (Li 2014). Regular occupations consist of a CTD equipped with a standard suite of sensors (accessed on November 23, 2021) and a vertical net tow for zooplankton identification and enumeration using AZMP protocols. Water samples are collected with Niskin bottles for a variety of analyses (accessed on November 23, 2021) at 2 m, 5 m, 10 m, and 60 m depths. Only zooplankton samples from 1999–2002 and 2012–2017 have been analyzed and archived in a local database; thus, only the CTD sensor and bottle observations are reported in this summary of 2020 conditions.

For ease of interpretation, surface conditions are expressed as the mean conditions at 2 m, 5 m, and 10 m. There is strong seasonal agreement among these depths for the physical and chemical conditions being measured and generally a minor difference in magnitude.

CONTINUOUS PLANKTON RECORDER

The Continuous Plankton Recorder (CPR) is an instrument towed by commercial ships that collects plankton at a depth of approximately 7 m, on a long continuous ribbon of silk (approximately 260 µm mesh). The position on the silk corresponds to the location of the different sampling stations. CPR data are analyzed to detect differences in the surface indices of phytoplankton (colour and relative numerical abundance of large taxa) and zooplankton (relative abundance) for different months, years, or decades in the Northwest Atlantic. The indices are used to indicate relative changes in concentration over time (Richardson et al. 2006). The sampling methods from the first surveys in the Northwest Atlantic (1960 for the continental shelf) to the present ones have been exactly the same so that valid comparisons can be made between years and decades.

The tow routes between Reykjavik and the GoM are divided into eight regions: WSS, ESS, the south Newfoundland Shelf, the Newfoundland Shelf, and four regions in the Northwest Atlantic sub-polar gyre, divided into 5 degrees of longitude bins (Figure 5). Only CPR data collected on the SS since 1992 are reported here, since these are comparable, to some extent, to AZMP survey results which date back to 1999 (Head et al. 2021). CPR data collected in all regions and all decades (i.e., including the four regions in the sub-polar gyre east of 45° W) are presented in annual Atlantic Zone Offshore Monitoring Program reports (e.g., Yashayaev et al. 2019). In 2019, there was CPR sampling during 12 months on the WSS and 8 months on the ESS.

Monthly log-transformed abundances [$log_{10}(n+1)$] of 14 taxa and the Phytoplankton Colour Index (PCI), a semi-quantitative measure of total phytoplankton abundance, are calculated by averaging values for all individual samples collected within either the WSS or ESS region for each month and year sampled. The examined taxa include: the PCI, diatoms and dinoflagellates (phytoplankton), four groups of *Calanus* species/stages, three representative small copepod taxa, two macrozooplankton taxa, and three acid-sensitive taxa.

Climatological seasonal cycles are obtained by averaging monthly averages for 1992–2015 for three indices of phytoplankton abundance and for the *Calanus* I–IV and *C. finmarchicus* V–VI taxa, and these are compared with values in the months sampled in 2019. Annual abundances and their anomalies are calculated for all 14 examined taxa for years during which there are 8 or more months of sampling, with no gaps of 3 or more consecutive months, conditions that were met in both regions in 2019.

OBSERVATIONS

MIXING AND OPTICAL PROPERTIES

At HL2, the ML is deepest and the SI lowest during the winter months when surface heating is weak and wind-driven mixing is strong (Figure 6). The ML shoals in the spring to minimum depth values from June to August and deepens in the last four months of the year. Similarly, SI increases in the spring to maximum values in August and September and then declines during the fall months. Since SI is calculated using a reference depth of 50 m, low values of the SI typically coincide with ML depths deeper than 50 m. Conversely, shallow ML depths (< 50 m) correspond to higher SI values that are determined by the strength of the pycnocline below the ML.

In 2020, the ML depth at HL2 was variable during the winter months (Figure 6). Sampling on February 4th and March 20th indicated MLs considerably shallower than normal which were associated with saltier water reaching higher in the water column (February 4th), and with cooling of the 25–40 m layer (March 20th). These shallower MLs appeared to have occurred respectively prior to, and closely following, periods of higher-than-normal wind gusts as registered at Halifax airport (Figure 7). The ML on March 1st was deeper than 50 m and, as expected, corresponded to the low SI value observed for that sampling day. Both the ML and the SI remained close to normal values during the summer and fall months when sampling occurred (Figure 6).

At P5, the ML is typically deeper and more variable, and stratification weaker, than at HL2 due to strong tidal mixing. The SI normally remains low (below 0.01 $kg \cdot m^{-4}$) for most of the year and ML depths vary from nearly full depth (90 m) in winter to approximately 40 m in summer (Figure 6). In 2020, the ML depth at P5 was variable during the winter months but mainly close to the seasonal values (Figure 6). The ML was shallower than normal during the summer months and deeper than normal during the fall months (Figure 6) despite wind gusts at Grand Manan being relatively close to normal values during the fall (Figure 7). This reinforced the predominance of tidal mixing in regulating the ML at P5. The SI was near normal in 2020 for each month where sampling occurred (Figure 6).

Euphotic depths (Z_{eu}) are generally deepest during the winter months and after the decline of the spring phytoplankton bloom, and shallowest during the period of the bloom when light attenuation in the water column is maximal (Figure 8). In 2020, Z_{eu} estimates were only available for the early winter and fall occupations at HL2 since summer occupations occurred at sunset or night time. PAR-based euphotic depths remained near normal values for the five available sampling dates at HL2 although more variability was observed in the Secchi-based euphotic depths (Figure 8).

At P5, Z_{eu} depth is relatively constant year-round since the primary attenuator is non-living suspended matter due to tidal action and continental freshwater input (Figure 8). In 2020, the PAR-based euphotic depths were near normal throughout the year at P5, with the exception of shallower-than-normal values in March and October where departure from the climatology was somewhat higher (Figure 8). Secchi-based euphotic depths closely followed the same temporal pattern as the PAR-based euphotic depths, with the exception of the October sampling where the estimated Z_{eu} depth was similar to the climatological value.

NUTRIENTS

The primary dissolved inorganic nutrients (nitrate, silicate, and phosphate) measured by the AZMP strongly co-vary in space and time (Petrie et al. 1999). For this reason and because the availability of nitrogen is most often associated with phytoplankton growth limitation in coastal waters of the Maritimes Region (DFO 2000), this report focuses mainly on variability patterns for nitrate, with information on silicate and phosphate concentrations presented mainly to help interpret phytoplankton taxonomic group succession at HL2 and P5.

High-frequency Sampling Stations

At HL2, the highest surface nitrate concentrations are observed in the winter when the water column is well mixed and primary production is low (Figure 9). Surface nitrate declines with the onset of the spring phytoplankton bloom, and the lowest surface nitrate concentrations are observed in the late spring through early fall. Deep-water nitrate concentrations are lowest in the late fall and early winter, and they increase from February to August, perhaps reflecting sinking and decomposition of the spring phytoplankton bloom (Petrie and Yeats 2000).

Nitrate levels in the upper 50 m were near or slightly higher than normal at HL2 in winter 2020 (Figure 10). The deep mixing event of March 1st appears to have contributed to the upward flux of nitrate resulting in the higher-than-normal surface inventory measured on March 20th (Figure 10). Surface nitrate levels were below climatological values in mid-July (Figure 10) due to a deeper-than-normal penetration of the depleted layer extending to around 40 m (Figure 9). Similarly, surface nitrate levels were mainly below climatological values in the fall (Figure 10) due to a longer-than-normal period of surface depletion that lasted until mid-December (Figure 9). The deep nitrate inventory was near or below normal during the winter months (Figure 10) mostly due to low concentrations observed in the 60–80 m depth range in January and February (Figure 9). The deep nitrate inventory was below normal in mid-July (Figure 10) due to a transient drawdown of bottom nitrate at that time (Figure 9). The deep nitrate inventory was mainly normal in the fall with the exception of a higher-than-normal value in mid-December (Figure 10) coinciding with an input of nitrate at the bottom of the water column (Figure 9). Overall, the surface and deep nitrate annual inventories at HL2 were slightly below average in 2020, following a trend that has been observed for the last 5 to 7 years (Figure 11). In parallel with the nitrate conditions, the surface and deep annual inventories of silicate and phosphate were also near or below normal at HL2 in 2020, continuing trends of the last 4 to 7 years (Figure 11).

The nitrate dynamics at P5 differ considerably from those at HL2 because of nutrient input from the effluent of the nearby St. John River, combined with the strong tidal mixing which contributes to a lower nitrate accumulation in the deep water while maintaining a higher overall surface inventory. The highest nitrate concentrations are observed in the winter and late fall, when the water column is well mixed from surface to bottom and phytoplankton growth is minimal due to light limitation (Figure 9). Nitrate concentrations start to decline in the upper water column when the spring phytoplankton bloom starts in April or May, and the lowest surface nitrate concentrations are typically observed from June to September.

At P5, nutrient measurements were only available for 6 occupations, thus preventing a comprehensive evaluation of the nutrients status for 2020. The two winter occupations both indicated below- or slightly below-normal levels of the surface and deep nitrate inventories, respectively (Figure 10). This appears to be due an earlier-than-normal nitrate decline throughout the water column (Figure 9). The four summer/early-fall occupations all indicated near-normal levels of the surface and deep nitrate inventories (Figure 10). Overall, the surface and deep nitrate annual inventories at P5 were slightly below average in 2020 for a sixth consecutive year (Figure 11). In parallel with the nitrate conditions, the surface and deep annual inventories were near normal for silicate and below normal for phosphate at P5 in 2020 (Figure 11).

Broad-scale Surveys

There was no seasonal survey in the spring of 2020 and, therefore, the analysis of the broad-scale nutrients on the core sections is limited to the fall observations. Consequently, nitrate levels in the upper 50 m indicated depleted conditions at nearly all stations of all sections (Figure 12). Anomalies of surface nitrate were near-zero or negative on most sections with the exception of the easternmost stations of CSL (CSL5 and CSL6), and the shelf-break station of HL (HL7) where positive anomalies were observed (Figure 12). Overall, anomalies of the annual estimates of surface nitrate were near normal for CSL and HL, and negative for LL and BBL (Figure 11). For the 50–150 m layer, positive anomalies were also observed on the eastern side of Cabot Strait (CSL5 and CSL6) and at the offshore stations of HL (HL6 and HL7) while anomalies were mixed at the offshore stations of LL (LL7, LL8, and LL9) and mainly negative on the offshore part of BBL (BBL6 and BBL7) (Figure 12). As a result, the annual estimates of deep

(> 50 m) nitrate levels were near normal or above normal on CSL and HL, respectively, and slightly below or below normal on LL and BBL, respectively (Figure 11). Surface and deep annual inventories of silicate and phosphate were below or slightly below normal on all sections in 2020, with strong negative anomalies of surface and deep phosphate on BBL especially (Figure 11). For deep silicate and phosphate, this continues a trend of mainly negative anomalies since 2014 (Figure 11).

Anomalies of bottom nitrate concentration for the 2020 summer ecosystem trawl survey showed high spatial variability between positive and negative values over the region. Positive anomalies were mainly observed along the west side of the Laurentian Channel (although sampling in that area was sparse), on the west side of the Gully, in the shallower waters of Emerald and Browns Banks, in the deeper waters of Georges and Jordan Basins, in the eastern GoM, and in the BoF (Figure 13). Negative anomalies mainly spread from east to west on the inner part of the SS and also on parts of the outer SS (e.g., Banquereau, Sable Island and Western Banks, and LaHave and Baccaro Banks) (Figure 13).

The lowest oxygen saturation levels are typically observed in deep basins and deep slope waters where nutrient concentrations are highest. In July 2020, bottom oxygen-saturation values near or below 60% were observed mainly in the deeper water on the west side of the Laurentian Channel, in Emerald and LaHave basins, the slope water off central SS, the Northeast Channel, and in the eastern GoM (Figure 14).

PHYTOPLANKTON

Although phytoplankton temporal and spatial variability is high in coastal and shelf waters, a recurrent annual pattern, including a pronounced spring diatom-dominated phytoplankton bloom followed by small secondary summer-fall blooms, is observed across the SS. A bloom develops as phytoplankton growth outpaces losses such as grazing and sinking (Behrenfeld and Boss 2014). Spring bloom initiation is thought to be regulated by the light environment of phytoplankton as well as temperature, starting when the water column stabilizes in late winter/early spring (Sverdrup 1953). Bloom magnitude is thought to be regulated largely by nutrient supply, while bloom duration is regulated by both nutrient supply and, to a lesser extent, by loss processes such as aggregation-sinking, grazing by zooplankton (Johnson et al. 2012) and lysis (Mojica et al. 2016).

High-frequency Sampling Stations

In 2020, the absence of *in situ* sampling at HL2 during the spring prevented any description of the spring phytoplankton bloom in terms of its onset, duration, amplitude, or magnitude. Sampling performed in March indicated lower-than-normal values of the integrated chlorophyll *a* despite the apparent shallowing of the ML observed for the March 20th sampling. The low values of the integrated chlorophyll *a* up to March 20th suggested that the onset of the bloom was considerably delayed compared to climatological conditions (Figure 15). Remote-sensing observations, although based on a limited number of pixels (maximum 5), suggested that the onset of the spring bloom at HL2 occurred slightly later than normal in early April, with a slightly shorter duration and near-normal magnitude (Figures 16 and 17). There was sub-surface production in the 30–50 m layer in July and August although the integrated chlorophyll remained near the climatological values (Figure 15). This sub-surface chlorophyll maximum appeared dominated by flagellates (Figure 18). Fall bloom conditions were observed in late-November/early-December likely in response to an upward flux of nitrate. The timing of the fall bloom was later than normal and its intensity only resulted in near-normal values of the chlorophyll *a* inventory, likely due to light limitations at that time of the year (Figure 15). The

phytoplankton community in the fall was also dominated by flagellates which appeared more dominant than normal (Figure 18). Overall at HL2, the annual estimate of the 0–100 m chlorophyll *a* inventory was slightly below normal in 2020 with near or slightly below normal values since 2016 (Figure 19). The estimated annual abundance of diatoms remained lower than average while those of flagellates and ciliates were higher than average in 2020, continuing the trend of the last 5 to 6 years (Figure 19). However, the annual estimates of the chlorophyll *a* inventory and the abundance of diatoms could be biased due to the absence of sampling during the critical spring timeframe during which these indices reach their maximum values.

Similar to HL2, the spring phytoplankton bloom at P5, which typically starts in March–April and peaks in June, could not be described from *in situ* measurements due to the absence of sampling during April, May, and June. Bloom metrics derived from remote-sensing observations for P5 must also be interpreted with caution due to limited number of pixels (maximum 2) used for their evaluation (Figures 16 and 17). Chlorophyll *a* concentrations typically decrease in July following the decline of the spring bloom. In July 2020, lower-than-normal chlorophyll *a* concentrations were observed below 15 m which resulted in the low value of the integrated chlorophyll *a*. However, bloom conditions were observed in August which indicated a shorter-than-normal bloom duration with a higher-than-normal intensity near the surface (Figures 15 and 16). The phytoplankton community during the August bloom was completely dominated by diatoms (Figure 18). Overall at P5, the chlorophyll *a* inventory was slightly below normal in 2020 for a third consecutive year (Figure 19). The abundance of diatoms remained lower than average while the abundance of dinoflagellates and ciliates was higher than average in 2020, continuing the trend of the last 10 to 12 years (Figure 19). Flagellates were also slightly lower than normal in 2020 for a third consecutive year although the pattern of the last 10 years indicates important inter-annual variability (Figure 19). Similar to HL2, the annual estimates of the chlorophyll *a* inventory and the abundance of diatoms could be biased due to the absence of sampling during the critical spring period.

Broad-scale Surveys and Satellite Remote Sensing

Anomalies in the 2020 annual integrated *in situ* chlorophyll *a* inventories indicated near-normal levels on CSL, HL, and BBL, and slightly above-normal level on LL (Figure 20). Near-surface chlorophyll *a* estimates from satellite remote sensing provide a complementary indicator of the 2020 status of phytoplankton abundance on a broad scale. Remote-sensing-based chlorophyll *a* anomalies were higher-than-normal across the region, and particularly on CSS and WSS where record-high anomalies were observed (Figure 20). Note that for CSS, the record-high positive anomaly can be partly attributed to the high chlorophyll *a* value observed in December (Figure 21a).

There is evidence of contradictory patterns between the *in situ* integrated chlorophyll *a* inventory and the remotely sensed surface chlorophyll *a*. Since 2016, the *in situ* integrated chlorophyll *a* inventory has shown predominantly negative anomalies across the region while the remotely sensed surface chlorophyll *a* has shown predominantly positive anomalies across the region (Figure 20). A similar contradictory pattern is also noticeable in previous years (e.g., 2003–2006, 2010). These apparent inconsistencies could be attributed in part to the inherent differences between the two indices, such as the vertical extent of the signal they capture (i.e., surface vs. water column integrated), the temporal resolution of the observations (weekly vs. semi-annual), and the spatial extent they represent (averaging over boxes vs. sections).

Based on the weekly surface chlorophyll *a* time series, the most intense spring bloom was observed in the CS sub-region where the peak surface concentration was more than twice the climatological value (Figure 21a). Weekly concentrations also suggested the spring bloom at CS

was earlier and slightly longer than normal (Figures 21a and 22). For the SS sub-regions, anomalies derived from the shifted-Gaussian model fit indicated near-normal or delayed onset and near-normal or shorter duration across the region, while the amplitude and magnitude were slightly below or below normal for ESS and CSS, and slightly above normal and near normal for WSS, respectively (Figure 22). For CSS, the estimates from the shifted-Gaussian model fit appear inconsistent with the time series of surface chlorophyll *a* concentrations (Figure 21a). Relatively low and variable surface chlorophyll *a* concentrations suggested weak spring bloom conditions for GB in 2020 (Figure 21b) although bloom metrics derived from the shifted-Gaussian model fit suggested an earlier and longer-than-normal spring bloom with record-low and record-high values, respectively (Figure 22). On the other hand, relatively high surface chlorophyll *a* concentrations revealed a long and intense fall bloom for GB in 2020 (Figure 21b). The low annual variability in the surface chlorophyll *a* in the tidally mixed LS sub-region is such that bloom conditions are hardly discernible (Figure 21b) and, therefore, the resulting bloom metrics should be interpreted with caution for that sub-region. Except for the amplitude, the spring bloom metrics shown in Figure 22 are highly subject to the ability of the shifted-Gaussian model to accurately detect the start and end of the spring bloom. Inaccurate predictions of the timing of the bloom in one or multiple years can introduce important bias in the resulting anomalies for a given sub-region.

ZOOPLANKTON

High-frequency Sampling Stations

Zooplankton biomass is presented in terms of the total wet biomass for zooplankton larger than 0.202 mm and the dry biomass for zooplankton in the size range of 0.202 mm to 10 mm. Consequently, the dry biomass estimates are a close representation of the mesozooplankton size class while the wet biomass estimates can represent both mesozooplankton and macrozooplankton, including gelatinous plankton. However, as Figure 23 suggests, there is strong similarity in the annual variability pattern of dry and wet biomass at both the HL2 and P5 stations.

At HL2, zooplankton biomass and total abundance are typically lowest in January and February, and increase to maximum values in April, similar to the spring phytoplankton bloom peak timing, before declining to low levels again in the fall (Figure 23 and 24). In 2020, biomass was near or below normal in winter and remained lower than normal until late March when it typically starts to increase (Figure 23). However, the increase in biomass was not observed due to the absence of sampling during spring. Biomass was near normal levels during the summer with the exception of the mid-July sampling where it was more than twice the climatological value. During the fall, biomass was again near normal levels, except for the late October sampling, which indicated a lower-than-normal value (Figure 23). A similar pattern was observed for the total zooplankton abundance with lower-than-normal abundance in late-March and late-October, and higher-than-normal abundance in mid-July (Figure 24). Overall, the zooplankton biomass was normal at HL2 in 2020 (Figure 25) although the annual mean is likely biased by the large value observed in mid-July.

At P5, zooplankton biomass and total abundance are typically lowest in January–May and increase to maximum values in July–October, lagging the increase in phytoplankton by about a month, before declining to low levels again in the late fall (Figure 23 and 24). In 2020, zooplankton biomass was near normal during most months where sampling occurred, with the exception of the lower-than-normal biomass in August (Figure 21), which was perhaps a consequence of the lower-than-normal standing stock of phytoplankton observed in July (Figure 15). Winter biomass levels, despite being typically low during that period, were even

slightly lower than the climatological values (Figure 23). Overall, the annual mean mesozooplankton biomass was slightly below normal in 2020 (Figure 25). Total zooplankton abundance in 2020 was near normal during winter but variable in summer and early fall with larger-than-normal levels observed in July and September (Figure 24).

The zooplankton community at HL2 in 2020 was dominated by copepods, representing roughly 90% or more of the total zooplankton abundance during the months where sampling occurred (Figure 24). The total zooplankton abundance reached a minimum value in early October, which also coincided with a higher-than-normal relative abundance of non-copepods zooplankton (Ampiphoda, Gastropoda, Limacina, Bryozoa and *Themisto* spp.) grouped as “Others” (Figure 24). Overall at HL2 in 2020, the abundance of copepods and non-copepods were both below normal (Figure 25). At P5 in 2020, the annual mean abundance of copepods was near normal and that of non-copepods was higher than normal (Figure 25). Higher relative abundance of ascidians and cirripedes (Others) in January and March, respectively, *Fritillaria* spp. (Appendicularia) in January-March, *Podon leuckartii* (Cladocera) in July, and euphausiids in August appear to have contributed to higher overall abundance of non-copepods.

At HL2 in 2020, the abundance of *C. finmarchicus* was lower than normal in late-winter (March 1st and 20th) with a higher-than-normal proportion of stage CVI (Figure 26) suggesting an earlier arousal from diapause. During the summer, the abundance of *C. finmarchicus* reached a peak level more than twice the climatological value (Figure 26), which coincided with the extreme zooplankton biomass and total zooplankton abundance levels reported earlier (Figure 23 and 24). The absence of a second generation, which typically develops during the summer months, likely resulted in the lower than normal abundance of *C. finmarchicus* and the predominance of stage CV during the fall (Figure 26). Overall at HL2, the abundance of *C. finmarchicus* was lower than normal in 2020 (Figure 25). At P5, the abundance of *C. finmarchicus* was slightly lower or lower than normal during each of the months where sampling occurred in 2020 (Figure 26). In July, the *C. finmarchicus* population was completely dominated by stage CI (Figure 26), which coincided with near-zero *C. finmarchicus* abundance and the lower-than-normal standing stock of phytoplankton observed at that time (Figure 15). A second generation of *C. finmarchicus*, albeit at low abundance, appeared to be developing in the fall (Figure 26), perhaps in response to the phytoplankton bloom conditions observed in August (Figure 15). Overall at P5, the abundance of *C. finmarchicus* was below normal in 2020 (Figure 25).

At HL2, the pattern of total copepods abundance (Figure 27a) followed that of zooplankton biomass (Figure 23), total zooplankton abundance (Figure 24) and *C. finmarchicus* abundance (Figure 26) as described earlier, with lower-than-normal levels in late winter and fall, and a higher-than-normal peak value in mid-July. *Metridia* spp. and the smaller copepod *Oithona atlantica* were slightly or more abundant than normal in 2020 (Figure 28) while most of the other dominant and sub-dominant copepod species were less abundant than normal (Figure 28), including *Pseudocalanus* spp. (Figure 25 and 28). At P5 in 2020, the total copepod abundance (Figure 27b) followed a pattern similar to that of total zooplankton abundance (Figure 24) with higher-than-normal values recorded in July and September. The abundance of the dominant *Pseudocalanus* spp. was near normal in 2020 (Figure 25 and 28). *Microcalanus* spp. was absent from all samples collected at P5 in 2020, hence the strong negative annual anomaly (Figure 28). The sub-dominant *Acartia* spp., *Temora longicornis*, and *Eurytemora* spp. had the strongest positive annual anomalies in 2020 (Figure 28).

Broad-scale Surveys

In 2020, net tow sampling on the HL section occurred at only 3 stations during the fall survey. Consequently, there is possibly important bias introduced in the seasonal and annual estimates

of the zooplankton indices for the HL section due to the lack of observations. For this reason, patterns in the broad-scale zooplankton indices are discussed only for the CSL, LL, and BBL sections, and the ecosystem surveys. Mesozooplankton biomass during the fall 2020 survey was slightly lower than normal on CSL and LL, and near normal on BBL (Figure 29). This pattern was also observed to some extent in the annual biomass anomalies estimated with the statistical model (Figure 25). The slightly positive biomass anomaly observed in the fall on BBL appeared to be driven by the relatively high biomass value recorded at station BBL4 (Figure 29). Mesozooplankton dry biomass during the 2020 winter ecosystem survey indicated a slightly negative anomaly on area 5Ze, a sharp contrast from 2019 when a record-high positive anomaly was observed for that area (Figure 30). Mesozooplankton dry biomass during the SS summer ecosystem survey was near normal for areas 4V and 4X, and higher than normal for area 4W (Figure 30). For area 4W, the positive summer anomaly appeared to be driven by relatively high biomass values observed in the western part of area 4W (Figure 30).

The abundance of *C. finmarchicus* during the fall 2020 survey was normal on CSL and LL, and slightly above normal on BBL (Figure 31). The same pattern was also observed in the annual anomalies of the *C. finmarchicus* abundance estimated from the statistical model (Figure 25). The abundance of *C. finmarchicus* was below average for area 5Ze during the 2020 winter ecosystem survey (Figure 32). The abundance of *C. finmarchicus* during the SS summer ecosystem survey was near normal for areas 4V and 4X, and higher than normal for area 4W (Figure 30). For area 4W, the positive summer anomaly also appeared to be driven by relatively high abundance values observed in the western part of area 4W (Figure 32).

The annual abundance of *Pseudocalanus* spp. in 2020, a dominant small copepod species on the SS, was below normal on CSL and LL, and slightly above normal on BBL (Figure 25). Total copepods abundance was near normal for CSL and LL, and slightly above normal for BBL in 2020 (Figure 25). The abundance of non-copepods was mainly slightly lower than normal for CSL and LL, and slightly above normal for BBL in 2020 (Figure 25). Abundance anomalies of appendicularians, euphausiids, and ostracods were particularly low in 2020 (Figure 33). For the ostracods, this continued a robust 5-year trend of negative anomalies (Figure 33). On the other hand, chaetognathes, polychaetes, echinoderms, and amphipods were near or above-normal levels in 2020 (Figure 33). For the chaetognathes, polychaetes, and echinoderms, this represented a shift from negative to positive abundance anomalies from 2019 to 2020 (Figure 33).

Indicator Species

Indicator species provide insights into the response of the copepod community to changes in water mass properties. Arctic *Calanus* species (*Calanus hyperboreus* and *Calanus glacialis*) have been mainly less abundant than normal on the SS since 2012. However, mixed signals were observed in 2020, with mainly lower-than-normal abundance recorded for CSL, LL, and P5, while BBL and HL2 showed near and slightly above-normal abundances, respectively (Figure 34). Warm offshore species (*Clausocalanus* spp., *Mecynocera clausi*, and *Pleuromamma borealis*) have been generally more abundant than normal on the SS since 2012. In 2020, abundance anomalies were mainly near normal or slightly negative, with the exception of HL2 where a positive anomaly was recorded (Figure 34). Abundance anomalies for the warm-shelf copepod species (the summer-fall copepods *Paracalanus* spp. and *Centropages typicus*) were mixed in 2020 (Figure 34). In most cases, this represented a shift from near-normal or negative to positive abundance anomalies, or vice-versa, from 2019 to 2020 (Figure 34).

IMPACTS OF MISSED SEASONAL SURVEYS

As described in the Methods section, annual means of key indices, such as chlorophyll *a* and nutrients inventories, and zooplankton abundance or biomass, are estimated using a General Linear Model (GLM). The GLM reduces bias in the estimates of annual means under sampling shortages (e.g., stations on a section not sampled during a given survey). Since the spring survey was cancelled in 2020, a sensitivity analysis was developed to assess the bias introduced in the annual estimated means and anomalies resulting from the missing mission.

The analysis was performed for each of the key indices that are reported as part of the spring and fall seasonal surveys on the core sections as shown in Figures 11, 20, 25, and 34. For each index, the annual means were calculated for the years where data are available at all stations of a section in both spring and fall seasons. This condition of full occupation ensures that bias in the annual estimates from the GLM is eliminated as annual means calculated from the model under full occupation coincide with the arithmetic annual means calculated directly from the data. Years for which there was full occupation varied slightly among the different indices and sections (Figures 35a and 35b). For each index and section, annual anomalies were calculated with respect to pseudo-climatological means. The term pseudo-climatological mean refers to the subset of years with full annual occupation for a given index and section. In order to assess the bias associated with missing surveys, model estimates and their resulting anomalies were calculated by successively setting the spring data as missing within each targeted year for each index and section. For each index, the two year-specific estimated means (i.e., full occupation and spring excluded) were compared visually in a scatterplot to assess overall differences between the two (Figures 36a and 36b). The difference between the two estimates, expressed as normalized anomalies, provides a measure of the bias in the anomalies resulting from excluding the spring data, which were then plotted over time to examine patterns in their magnitudes (Figures 37a and 37b). The annual and the seasonal fall anomalies for the full occupation years were also compared to assess whether the estimated annual anomaly resulting from missed spring sampling can be inferred from its seasonal fall counterpart as calculated from available seasonal fall data (Figure 38a and 38b). The relationship between annual and fall anomalies was assessed using Pearson correlation coefficients. The estimated annual and calculated seasonal fall anomalies for 2020 were then compared alongside each other in light of their respective correlation to qualitatively assess the degree of confidence and coherence between the two quantities (Figure 39).

No systematic shifts toward higher or lower estimated annual means resulting from excluding spring data were observed when compared to the unbiased annual means, for any of the indices (Figures 36a and 36b). Scatter around the identity line indicates relatively high variability for the surface nitrate, surface silicate, and the chlorophyll *a* inventory, which are indices characterized by a strong annual cycle. On the other hand, deep nutrients, which are characterized by a weaker seasonality, show lower variability. For the zooplankton indices, the variability is moderate, except for the dry biomass which shows the lowest overall variability (Figures 36a and 36b).

As observed for the annual means, there is no evidence for any of the indices of any robust trends toward overestimation or underestimation of the annual normalized anomalies resulting from excluding spring data when compared to the unbiased annual anomalies (Figure 37a and 37b). However, the large scatter indicates greater uncertainty when spring sampling is missing. Anomalies resulting from missing spring data are typically within ±2 sd of the unbiased anomalies, although extreme values reaching close to ±4 sd are also observed (Figures 37a and 37b).

For several indices, there is a strong correlation between the annual and the fall anomaly values (Figures 38a and 38b). Positive correlations are particularly strong for the deep nutrient indices and most of the zooplankton indices, as data points closely align along the identity line. On the other hand, weaker correlations are observed for the surface nitrate, surface silicate, and the chlorophyll *a* inventory. The strength of the correlation relates to the level of confidence in inferring the estimated annual anomaly on the basis of its seasonal fall counterpart, while the sign of the correlation coefficient indicates the degree of coherence between the two quantities.

A summary of the correlation coefficients, along with the estimated annual and the calculated seasonal fall anomalies for 2020, is presented in Figure 39 for each index and section. A negative correlation, albeit weak, is only observed for chlorophyll *a* 0–100 m for BBL. Since most correlations are positive, the estimated annual anomalies are expected to take the same sign as the fall anomaly, which is generally observed for the majority of indices and sections for 2020, with the exception of warm offshore zooplankton species abundance for LL and zooplankton dry biomass for HL, although the correlation in the latter case is weak. On the other hand, weak correlations are associated with higher uncertainty in the estimated annual anomalies, which is the case for surface nitrate and silicate on CSL and BBL, chlorophyll *a* inventory on LL and BBL, and zooplankton biomass on HL. Note that for HL, there is additional uncertainty in the fall zooplankton anomalies as samples were collected at only 3 of 7 stations in 2020. There is, therefore, a high level of uncertainty associated with the estimated annual anomalies of the zooplankton indices for that section, despite some moderate to large correlation coefficients calculated for those indices.

In summary, the analysis described in this section has provided insight into the indices and sections for which the estimated annual anomalies for 2020 must be interpreted with caution. Based on data collected in previous years, surface nitrate and silicate, and chlorophyll *a* inventory have the highest level of uncertainty owing to: i) the high variability in the estimated annual means and anomalies resulting from excluding spring data, and ii) low inference of the annual estimated anomaly from the measured fall anomaly due to the weak correlation between the two quantities. In addition, anomalies for the zooplankton indices on the HL section for 2020 must be interpreted with caution due to the low overall sampling effort for that section.

DISCUSSION

In the Maritimes Region, the SS is characterized by a strong annual cycle of temperature and stratification, and spatial variability in the form of longitudinal and cross-shelf gradients. While the temperature annual cycle and its perturbations are mostly driven by meteorological forcing, spatial variability is mostly the result of interacting water inputs with the advection of cold fresh waters onto the inshore ESS from the Gulf of St. Lawrence in the northeast and the intrusion of warm and salty slope waters onto the WSS and CSS in the southwest. These temporal and spatial patterns result in different water masses having direct and indirect influences on the distribution and dynamics of plankton and nutrients in the region.

Ocean temperatures on the SS and in the GoM have exhibited strong inter-decadal variability since the 1950s, with recent years (2010 and onward) being generally warmer than the long-term average. A composite index, consisting of 23 ocean temperature time series from surface to bottom across the region, indicated that 2020 was the 3rd warmest of 51 years of observations, with 2012 being the warmest on record (Hebert et al. 2021). For several indices, this represented a shift from 2019, when cooler conditions were observed. Surface water temperatures showed spatial variability with near- to above-normal temperatures across the region. Deep or bottom water temperatures were above normal across the region. Stratification on the SS was significantly lower in 2020 than in 2019 due to the presence of saltier and

warmer surface water and it remained below the trend of the 73-year time series which shows increasing stratification. The volume of the Cold Intermediate Layer (CIL) was slightly below normal in 2020 and the CIL minimum temperature was above normal. Warmer ocean temperatures observed in recent years may be directly or indirectly responsible for changes observed in the nutrient conditions and the two trophic levels (phytoplankton and zooplankton) surveyed in this report.

The nutrient environment on the SS is influenced directly or indirectly by water inputs from upstream, for example the Labrador Current and the outflow from the Gulf of St. Lawrence, as well as by intrusions of slope water and Gulf Stream meanders (Pepin et al. 2013). Surface nutrients display a strong seasonality associated with phytoplankton production, with higher production typically associated with surface nutrient depletion. Deep nutrients, on the other hand, provide a better representation of the nutrient pool available for new primary production. Deep nutrient concentrations have been mainly lower than normal since 2013 for silicate and phosphate, and since 2016 for nitrate. With the exception of CSL and HL, the pattern of lower-than-normal deep nitrate concentrations has persisted across the region in 2020. For CSL and HL, nutrient-rich water was associated with warm, salty water observed in the fall on the eastern side of the strait in the 100–150 m layer and at the offshore stations of the HL section in the 50–150 m layer (Hebert et al. 2021). The recent shift in deep-nutrients inventory is likely linked to changes in shelf circulation, changes in the Gulf Stream transport, and, to some extent, changes in the export of surface particulate nitrogen and its remineralisation at depth. A decrease in the deep nutrient concentrations coupled with the observed increase in stratification on the SS (Hebert et al. 2021) could imply lower primary productivity, with potential impacts on the structure and functioning of the food web.

In ocean regions where annual-scale environmental variability is a dominant frequency, plankton life history, behavior, and physiology provide adaptations that focus reproductive effort on favorable times of year and minimize exposure to risk at unfavorable times of year. However, unpredictable perturbations in the range of environmental seasonality and in seasonal timing can disrupt these adaptations (Greenan et al. 2008, Mackas et al. 2012). Large-scale shifts in water mass boundaries also influence local plankton community composition (e.g., Keister et al. 2011). The main recurring feature of the phytoplankton dynamics on the SS and in the GoM is the spring bloom, which develops under favourable conditions of increased insolation, warming water temperatures, and water column stratification. However, Ross et al. (2017) observed spring blooms on the SS when stratification was at its lowest, water temperature at its coldest, and when the surface mixed layer was still much deeper than the euphotic depth, in apparent contradiction with the critical-depth hypothesis. Phytoplankton biomass declines after the bloom peak as grazing increases or growth becomes nutrient limited. In summer, sporadic occurrences of sub-surface chlorophyll peaks reflect primary production fuelled by regenerated nutrients within the stratified upper water column. Sub-surface summer production is a significant contribution to the annual primary production on the SS (Ross et al. 2017).

The characteristics of the spring phytoplankton bloom, as inferred from remote-sensing ocean color observations, collected within the pre-defined statistical sub-regions, mainly indicated a delayed initiation, shorter-than-normal duration, and lower-than-normal magnitude on the SS in 2020. This pattern concurs with observations by Friedland et al. (2018), suggesting negative correlations between start day and duration, and between start day and magnitude. However, bloom metrics for the pre-defined sub-regions can be misleading due to spatial patchiness in the surface chlorophyll. Weekly satellite composite images showed bloom conditions developing around Sable Island during the second week of March 2020 and progressing westward along the shelf break over the following two weeks, suggesting near-normal onset and duration. However, metrics for ESS and CSS did not capture those bloom conditions as they occurred

just outside the limits of those sub-regions. Weekly images also showed relatively high surface chlorophyll *a* concentrations appearing near the coast during the 3rd week of March but only propagated southward across the CSS and WSS during the 2nd week of April and declined during the 3rd week of April, confirming a delayed onset and shorter duration for those sub-regions. Bloom conditions on the SS in 2020 thus followed, to some extent, the general pattern of westward progression (Song et al. 2010).

Observations at HL2 have indicated the recent period (2015 to present) to be characterised by mainly lower-than-normal abundance of diatoms and dinoflagellates, and higher-than-normal abundance of ciliates and flagellates. The CPR observations in recent years also provide evidence of changes toward lower abundance of diatoms and dinoflagellates on the WSS and higher abundance of flagellates on the ESS. A decrease in the abundance of diatoms affects the ecosystem at different levels. On the SS, diatoms typically dominate the phytoplankton biomass during the spring bloom and a decrease in their abundance is likely resulting in lower overall annual primary production. Diatom abundance can also be linked to secondary production as large copepods preferentially feed on larger cells. Diatoms also contribute to the deep nitrate pool as a result of fast sedimentation of senescent cells and copepod faecal pellets, and subsequent remineralisation of particulate nitrate in the deep water. A shift toward smaller phytoplankton taxa could be driven by the warmer ocean conditions on the SS, as has been observed in other areas of the ocean (Doney et al. 2012).

Zooplankton biomass on the SS and in the eastern GoM is normally dominated by large, energy-rich copepods, mainly *C. finmarchicus*, which are important prey for planktivorous fish such as herring and mackerel, North Atlantic right whales, and other pelagic species. The population responses of *C. finmarchicus* to environmental changes are complex due to interactions among several processes, such as transport by ocean circulation, annual primary production cycles, and *Calanus* life history. The latter focuses reproductive effort on spring bloom production of diatoms and includes a period of late-juvenile-stage dormancy in deep water during less productive seasons. The winter abundance level of *C. finmarchicus* is an indicator of initial conditions for production, while the late-fall abundance level is an indicator of the overwintering stock for production in the following year. *Pseudocalanus* spp. are smaller than *Calanus* spp. and less energy-rich, but they are also important prey for small fish due to their high abundance and wide spatial distribution.

A persistent change in the zooplankton assemblage on the SS has been evident since 2011, marked most notably by the decline in the abundance of *C. finmarchicus*, and a similar decline in the mesozooplankton biomass over that same period as *C. finmarchicus* is a biomass-dominant member of zooplankton assemblage. The year 2011 marked a regime shift to lower biomass of *Calanus* spp. on the SS which also coincided with a shift to warmer temperatures (Sorochan et al. 2019). Apart from the HL section, where the annual estimated abundance and biomass are uncertain due to the overall lack of sampling on that section, the trend of lower abundance of *C. finmarchicus* and lower zooplankton biomass has persisted over most of the region in 2020, with the exception of the southwest area where both metrics were above or slightly above normal levels. At the seasonal scale, *C. finmarchicus* abundance was below normal during winter on GB and near or above normal during summer on the SS in 2020. This is in contrast to observations in the GoM where warming has been linked to a decline in the summer and fall abundance of *C. finmarchicus*, and an increase in their winter abundance since 2010 (Pershing and Stamieszkin 2020, Record et al. 2019). High proportions of *C. finmarchicus* adult stages in winter may indicate an impact of higher deep water temperatures on the diapausing population, resulting in increased developmental rates and early exit from diapause well before the spring phytoplankton bloom. Along with the overall decline in the abundance of *C. finmarchicus* and zooplankton biomass, observations at HL2 have indicated consistent

changes in the copepods community with generally higher-than-normal abundance of small copepods since around 2014, especially *Centropages* spp., *Oithona atlantica,* and *Temora longicornis*. On the other hand, *Pseudocalanus* spp. have been generally less abundant than normal during nearly the same period. Small copepods are preferred prey for larval stages of many fish stocks due to their high abundance, appropriate size, and good nutritional value, which promotes larval fish survival and subsequent recruitment (Shi et al. 2020). The decline in the abundance of Arctic *Calanus* species since 2011 is perhaps the most direct response to warmer temperatures observed over that period on the SS.

In recent years, the sampling at the high-frequency sampling stations, cross-shelf sections, and ecosystem trawl surveys has been compromised as a result of ship unavailability and/or pandemic conditions limiting at-sea activities. Due to the increased frequency of cancelled seasonal missions (e.g., fall 2019, spring 2020), it has become necessary to address the impact of missing sampling on the annual estimates of the different metrics reported in this document in order to provide sound scientific advice. The sensitivity analysis presented in this report focused on missing spring sampling in the context the 2020 seasonal surveys. The analysis indicated that the uncertainty in the annual anomalies resulting from missing spring sampling is highly variable and typically in the range of ±2 standard deviations. The analysis also suggested that for several indices, it was possible to infer qualitatively the annual anomaly with respect to the fall anomaly due to strong correlation between the two values. For future reference, such analysis should be extended to missing fall seasonal missions and the methodology further developed to address sampling gaps in other measurement protocols (e.g., high-frequency sampling stations).

The relationships among environmental and plankton conditions are complex and their interpretation from a deterministic perspective requires a comprehensive analysis that is beyond the scope of this report. However, observations in recent years provide increasing evidence of warmer ocean conditions and decreased deep-nutrient availability, coupled with a shift in both phytoplankton and zooplankton communities away from the dominance of large phytoplankton cells and large, energy-rich copepods like *C. finmarchicus* toward smaller phytoplankton and copepod species. Since “classical” food webs, dominated by diatoms and *C. finmarchicus,* are associated with more efficient transfer of energy to higher trophic level pelagic animals than are food webs dominated by small phytoplankton cells and small zooplankton taxa, this shift may indicate a change to less-productive conditions for planktivorous fish, North Atlantic right whales, and pelagic-feeding seabirds in the Maritimes Region.

BEDFORD BASIN MONITORING PROGRAM

PHYSICAL CONDITIONS

Due to the impacts of COVID-19 on the ability to conduct field programs at the Bedford Institute of Oceanography, only 22 sampling events occurred at the Compass Buoy station in Bedford Basin in 2020, with sampling performed from January 9 to March 16, and from September 29 to December 22. Since the annual anomalies for bottom and surface (2 m, 5 m, and 10 m values combined) conditions were based on only 7 months from the winter and late summer/fall seasons, rather than the net average of all 12 normalized monthly anomalies (Li 2014), interpretation of annually-averaged conditions should be done with caution.

The annual sea surface temperature was slightly above normal (+0.27 sd; Figure 40) in 2020 compared to the 1999–2020 reference period. This is in contrast to 2019, when the annual surface temperature anomaly was negative (-0.40 sd). Monthly anomalies in surface temperature in 2020 showed a similar pattern (Figure 41) and were either at or slightly above

normal for all months sampled, with the exception of October, which was below normal (-1.69 sd) and the third coolest on record for this month since the start of the time series in 1992.

While annual average bottom (60 m) temperature was near normal (+0.09 sd) in 2020 (Figure 42), monthly anomalies in bottom temperature showed at or slightly below normal conditions for the first 3 months of the year (January to March), and at or above normal conditions during the latter part of the year (October to December; Figure 43). This is in contrast to the monthly temperature anomalies observed in 2019 when they were below normal for nearly the entire year (February to December; Figure 43). Monthly anomalies in bottom salinity showed a similar pattern, and were below normal from January to March and above normal from September to December (Figure 44), with October experiencing the most saline conditions (+2.35 sd) on record.

The Bedford Basin is stratified seasonally by temperature and year round by salinity, with the latter occurring as a result of local freshwater input into the basin (Kerrigan et al. 2017). The water column in Bedford Basin is also influenced by wind-induced vertical mixing during periods of weaker stratification in winter, and lateral mixing with saltier waters from the SS resulting from strong alongshore winds, large tides, and/or storm events that occur during the spring and fall seasons (Kerrigan et al. 2017). The higher salinities observed in the deeper waters of Bedford Basin from October to December in 2020 suggest an offshore origin. Section plots of the temperature, salinity, and density time series and their anomalies in relation to the 1999–2020 reference period (Figure 45) revealed cooler-than-normal temperatures down to 30 m depth in late October/early November, following a period of warming that occurred in late September/early October. Note that the latter is based only on one sampling event on September 29, 2020. At the same time, higher-than-normal temperatures and salinities occurred in the bottom 20 m of the water column during the same month, the latter of which persisted for the remainder of the year. This suggests that a more saline and warmer-than-average water mass infiltrated the basin during the month of October. Such intrusions are common in the fall and are thought to occur during periods of sustained southwesterly winds and strong tides that result in coastal upwelling of shelf waters into Halifax Harbour and over the sill of Bedford Basin (Platt et al. 1972, Petrie et al. 1987, Burt et al. 2013). While these events are typically short-lived and do not alter the vertical stratification of the basin, they do have a profound effect on the biogeochemistry of its bottom waters (Punshon and Moore 2004, Burt et al. 2013, Haas et al. 2021).

NUTRIENTS AND PLANKTON CONDITIONS

Annual anomalies in surface and bottom nitrate were at or slightly above normal in 2020, while nitrite, ammonia, phosphate, and silicate were all near or slightly below normal (Figures 40 and 42). Surface phosphate was the lowest on record (-1.24 sd), marking a continuation of the monotonic, downward trend observed in this inorganic nutrient since 2011. Evaluation of monthly anomalies in nutrients revealed bottom nitrate was anomalously high in September (+1.94 sd) and subsequently declined to slightly below-normal conditions in October and November (Figure 46). A similar pattern was also observed in bottom silicate, particulate organic carbon (POC), and nitrogen (PON) (results not shown). These shifts coincided with the suspected intrusion event from the shelf that occurred in October (Figure 45).

Annual anomalies in surface chlorophyll, POC, and PON, and other metrics describing the phytoplankton community (e.g., HPLC pigments) were at or slightly above normal in 2020 (Figure 40). This is in contrast to 2019 and 2018 where, with the exception of POC and PON in 2019, these conditions were all slightly below normal. Chlorophyll and other plankton metrics measured at 60 m showed the opposite pattern to conditions at the surface (Figure 42). Bottom anomalies in chlorophyll and PON were near or above normal in 2020, while all other metrics

related to phytoplankton were below normal. Apart from 2016, the annual anomalies of bottom chlorophyll and other phytoplankton metrics have been primarily near normal or negative since 2010.

CONTINUOUS PLANKTON RECORDER

PHYTOPLANKTON

Average monthly PCI values and diatom abundances (1992–2015) on the ESS and WSS show the spring bloom occurring in March–April, with low values in summer (Figure 47). In fall and winter, the PCI is low, but diatom abundance increases over the fall, remaining relatively high in winter. Dinoflagellate abundance shows no clear seasonal cycle. In 2019, PCI values were generally close to normal on the SS, except in April when they were higher than normal on the ESS. Monthly diatom abundances were below normal in late winter (Feb–Mar) and fall (Oct–Nov) on the WSS and in late spring (May–Jun) on the ESS. Otherwise, diatom levels were close to normal in both regions. On the WSS, dinoflagellate abundances were generally below normal in fall and winter, normal in spring, and above normal in summer, while on the ESS values were below normal, except in August. Annual anomalies were positive (ESS) or neutral (WSS) for the PCI in 2019, and abundance anomalies were negative for diatoms and dinoflagellates (Figure 48). Since 1999, diatom abundance has shown a downward trend on both the WSS and ESS, while on the ESS the PCI has trended upward and dinoflagellate abundance has trended downward. These observations are consistent with the observations of Casault et al. (2020) and support their suggestion that the phytoplankton community is changing to one composed of smaller taxa.

ZOOPLANKTON

CPR-derived climatological (1992–2015) seasonal cycles for *Calanus* I–IV (mostly *C. finmarchicus*) and *C. finmarchicus* CV–VI have broad spring–summer (April–July) peaks in abundance on the WSS (Figure 49). On the ESS, *Calanus* CI–IV abundance has a similar, lower-magnitude peak, but *C. finmarchicus* CV–VI does not. In 2019, monthly abundances for *Calanus* I–IV on the WSS were lower than normal during the spring–summer peak and close to normal for the rest of the year (Figure 49). *C. finmarchicus* V–VI levels on the WSS were below normal between March and July, and otherwise close to normal. On the ESS in 2019, monthly abundances for *Calanus* I–IV were close to normal in January and April, dropping to near zero in June, and increasing to levels slightly above normal in late summer-fall; *C. finmarchicus* V–VI monthly abundances on the ESS showed a similar pattern (Figure 49). Vertical net tow sampling at HL2 has indicated relatively low annual abundances for *C. finmarchicus* since 2011, which had not previously been evident in CPR data for either the WSS or ESS (Casault et al. 2020). The inclusion of data from 2019, however, now yields significant downward trends in annual *Calanus* I–IV and *C. finmarchicus* V–VI CPR abundances on the WSS starting in 2014 (Figure 48).

Annual abundances of the Arctic *Calanus* taxa (*C. glacialis*, *C. hyperboreus*) were at near-normal levels in both SS regions in 2019, while the small copepod taxa (copepod nauplii, *Para-Pseudocalanus*, *Oithona*) were at or below normal levels. Annual abundances of hyperiid amphipods were at (WSS) or above (ESS) normal levels, while euphausiid levels were near (WSS) or below (ESS) normal (Figure 48).

ACID SENSITIVE ORGANISMS

In 2019, abundances of all three acid-sensitive taxa (coccolithophores, foraminifera, *Limacina* spp.) were near (WSS) or mainly below (ESS) normal levels (Figure 48).

SUMMARY

- In 2020, the sampling protocol for the high-frequency sampling stations, seasonal surveys, and Bedford Basin monitoring program was compromised due to the COVID-19 pandemic preventing at-sea activities. Consequently, there is increased uncertainty in the annual means of key indices reported in this document due to substantial gaps in the input data used for their estimation.
- Observations provided evidence that warmer conditions, lower overall nutrient inventories, and changes in the plankton community observed in recent years have generally persisted in 2020. These changes are likely to alter the fate of production in the ecosystem with negative impacts having already been observed (e.g., feeding habitat for specialized planktivores such as North Atlantic right whales).
- In 2020, surface and deep inventories of nitrate, silicate, and phosphate were mainly near or lower than average on the SS following the trend of the last 6–7 years. However, higher-than-normal deep nitrate concentrations associated with warm salty water were observed in the fall on the eastern side of the CSL section and at the offshore stations of the HL section.
- Phytoplankton spring bloom on the CSS and WSS, as observed from satellite remote sensing, was later than normal, shorter in duration with either near- or lower-than-normal magnitude. For the eastern part of the SS, the spring bloom developed near the shelf break with normal onset timing and duration. At HL2, the spring bloom could not be observed *in situ* due to the absence of sampling during spring.
- Observations at HL2 indicate a continued pattern of mainly lower abundance of diatoms and higher abundance of ciliates and flagellates over the last 5–6 years. The abundance of dinoflagellates was mainly lower than normal over that same period although slightly above normal in 2020.
- With the exception of the HL section where the annual zooplankton indices are unreliable due to limited sampling in 2020, the abundance of *C. finmarchicus*, *Pseudocalanus* spp., total copepods, and non-copepods was mainly near or lower than average across most of the region but slightly above normal for BBL. A similar spatial pattern was also observed for the mesozooplankton biomass.
- Anomalies of copepod indicator species abundance were mixed in 2020. With the exclusion of the HL section, the abundance of Arctic *Calanus*, warm-offshore species, and warm-shelf species was generally near or slightly lower than normal although spatial variability was observed. Observations at HL2 indicate a continued pattern of generally higher-than-normal abundance of small copepods, particularly *O. atlantica*.
- Average annual surface and bottom temperatures in Bedford Basin were at or slightly above normal in 2020, which is in contrast to the below-normal conditions that were observed in the basin in 2019. During the month of October, surface temperatures fell drastically to

below-normal conditions. At the same time, bottom temperatures and salinities, which were below normal at the beginning of the year, increased to above-normal conditions, likely as a result an offshore shelf-water intrusion event.

- Surface chlorophyll, particulate organic carbon and nitrogen, and other metrics describing the phytoplankton community were at or above normal in 2020. Conversely, these conditions at the bottom were either neutral or below normal relative to the 1999–2020 reference period, continuing the trend of primarily negative anomalies observed in these conditions since 2010.
- In 2019, CPR observations indicated that annual average PCI values were close to (WSS) or above (ESS) normal, while diatom and dinoflagellate abundances were below normal in both regions.
- In 2019, CPR observations indicated that annual abundances for the *Calanus* copepodite I–IV (mostly *C. finmarchicus* CI–IV) and *C. finmarchicus* CV–VI taxa were below normal for the WSS and near or higher than normal for ESS. Average annual abundances for all other taxa (two arctic *Calanus*, three small copepod taxa, two macrozooplankton, three acid-sensitive taxa) were lower than or close to normal in both regions, except for hyperiid amphipods on the ESS, which were more abundant than normal.

ACKNOWLEDGEMENTS

The authors thank the personnel at the Bedford Institute of Oceanography and St. Andrews Biological Station who contributed to sample collection, sample analysis, data analysis, data management, and data sharing. We also thank the officers and crews of the Canadian Coast Guard Ships *Alfred Needler, Hudson, Sigma-T*, *Teleost,* and *Viola M. Davidson* for their assistance in the collection of oceanographic data during 2020. Reviews by David Bélanger et Stéphane Plourde improved the manuscript.

REFERENCES CITED

Behrenfeld, M.J., and Boss, E.S. 2014. Resurrecting the Ecological Underpinnings of Ocean Plankton Blooms. Annu. Rev. Mar. Sci. 6: 167–194.

Burt, W.J., Thomas, H., Fennel, K., and Horne, E. 2013. Sediment-water column fluxes of carbon, oxygen and nutrients in Bedford Basin, Nova Scotia, inferred from ^{224}Ra measurements. Biogeosciences 10:53–66.

Casault, B., Johnson, C., Devred, E., Head, E., Cogswell, A., and Spry, J. 2020. Optical, Chemical, and Biological Oceanographic Conditions on the Scotian Shelf and in the eastern Gulf of Maine during 2019. DFO Can. Sci. Advis. Sec. Res. Doc. 2020/071. v + 64 p.

Churilova, T., Suslin, V., Krivenko, O., Efimova, T., Moiseeva, N., Mukhanov, V., and Smirnova L. 2017. Light Absorption by Phytoplankton in the Upper Mixed Layer of the Black Sea: Seasonality and Parametrization. Frontiers in Mar. Sci., 4, 90.

Clay, S., and Layton, C. 2021. BIO-RSG/PhytoFit: First release (Version v1.0.0). Zenodo.

DFO. 2000. Chemical and Biological Oceanographic Conditions in 1998 and 1999 – Maritimes Region. DFO Sci. Stock Status Rep. G3-03 (2000).

DFO. 2021. Oceanographic Conditions in the Atlantic Zone in 2020. DFO Can. Sci. Advis. Sec. Sci. Advis. Rep. 2021/026.

Doney, S.C., Ruckelshaus, M., Duffy, J.E., Barry, J.P., Chan, F., English, C.A., Galindo, H.M., Grebmeier, J.M., Hollowed, A.B., Knowlton, N., Polovina, J., Rabalais, N.N., Sydeman, W.J., and Talley, L.D. 2012. Climate change impacts on marine ecosystems. Annu. Rev. Mar. Sci. 4:11–37.

Friedland, K.D., Mouw, C.B., Asch, R.G., Ferreira, A.S.A, Henson, S., Hyde, K.J.W., Morse, R.E., Thomas, A.C., and Brady, D.C. 2018. Phenology and time series trends of the dominant seasonal phytoplankton bloom across global scales. Glob. Ecology Biogeography. 27(5):551–569.

Greenan B.J.W., Petrie B.D., Harrison W.G., Strain P.M. 2008. The onset and evolution of a spring bloom on the Scotian Shelf. Limnol. Oceanogr. 53.

Harrison, G., Colbourne, E., Gilbert, D., and Petrie, B. 2005. Oceanographic Observations and Data Products Derived from Large-scale Fisheries Resource Assessment and Environmental Surveys in the Atlantic Zone. AZMP/PMZA Bull. 4: 17–23.

Haas, S., Robicheau, B.M., Rakshit, S., Tolman J., Algar, C.K., LaRoche, J., and Wallace, D.W.R. 2021. Physical mixing in coastal waters controls and decouples nitrification via biomass dilution. Proc. Natl Acad. Sci. USA 118 (18), e2004877118.

Head, E.J.H., Johnson, C.L., and Pepin, P. 2021. Plankton monitoring in the Northwest Atlantic: a comparison of zooplankton abundance estimates from vertical net tows and Continuous Plankton Recorder sampling on the Scotian and Newfoundland shelves, 1999–2015. ICES J. Mar. Sci. fsab208.

Hebert, D., Layton, C., Brickman, D. and Galbraith, P.S. 2021. Physical Oceanographic Conditions on the Scotian Shelf and in the Gulf of Maine during 2020. DFO Can. Sci. Advis. Sec. Res. Doc. 2021/070. iv + 55 p.

Holmes, R.W. 1970. The Secchi Disk in Turbid Coastal Waters. Limnol. Oceanogr. 15(5): 688–694.

Hu, C., Lee, Z., and Franz, B. 2012. Chlorophyll *a* algorithms for oligotrophic oceans: A novel approach based on three-band reflectance difference. Journal of Geophysical Research, 117(C1).

Johnson, C., Harrison, G., Head, E., Casault, B., Spry, J., Porter, C., and Yashayaev, I. 2012. Optical, Chemical, and Biological Oceanographic Conditions in the Maritimes Region in 2011. DFO Can. Sci. Advis. Sec. Res. Doc. 2012/071.

Keister, J.E., Di Lorenzo, E., Morgan, C.A., Combes, V., and Peterson, W.T. 2011. Zooplankton species composition is linked to ocean transport in the Northern California Current. Global Change Biol. 17: 2498–2511.

Kerrigan, E.A., Kienast, M., Thomas, H., and Wallace, D.W.R. 2017. Using oxygen isotopes to establish freshwater sources in Bedford Basin, Nova Scotia, a Northwestern Atlantic fjord. Estuar. Coast. Shelf. Sci. 199, pp. 96–104.

Lenth, R., Singmann, H., Love, J., Buerkner, P., and Herve, M. 2021. emmeans: Estimated Marginal Means, aka Least-Squares Means. R package version 1.6.2-1.

Li, W.K.W. 2014. The state of phytoplankton and bacterioplankton at the Compass Buoy Station: Bedford Basin Monitoring Program 1992–2013. Can. Tech. Rep. Hydrogr. Ocean Sci. 304.

Mackas, D.L., Greve, W., Edwards, M., Chiba, S., Tadokoro, K., Eloire, D., Mazzocchi, M.G., Batten, S., Richardson, A.J., Johnson, C., Head, E., Conversi, A., and Pelosi, T. 2012. Changing zooplankton seasonality in a changing ocean: Comparing time series of zooplankton phenology. Progr. Oceanogr. 97-100: 31–62.

Mitchell, M., Harrison, G., Pauley, K., Gagné, A., Maillet, G., and Strain, P. 2002. Atlantic zonal monitoring program sampling protocol. Can. Tech. Rep. Hydrogr. Ocean Sci. 223.

Mojica, K.D.A., Huisman, J., Wilhelm, S.W., and C.P.D. Brussaard. 2016. Latitudinal variation in virus-induced mortality of phytoplankton across the North Atlantic Ocean. ISME J 10, 500–513.

O'Reilly, J.E., Maritorena, S., Mitchell, B. G., Siegel, D. A., Carder, K. L., Garver, S. A., Kahru, M., and McClain, C. R. 1998. Ocean color chlorophyll algorithms for SeaWiFS. J. Geophys. Res. 103, 24937–24953.

Pepin, P., Maillet, G.L., Lavoie, D., and Johnson, C. 2013. Temporal trends in nutrient concentrations in the Northwest Atlantic basin. Ch. 10 (p. 127–150) In: Aspects of climate change in the Northwest Atlantic off Canada [Loder, J.W., G. Han, P.S. Galbraith, J. Chassé and A. van der Baaren (Eds.)]. Can. Tech. Rep. Fish. Aquat. Sci. 3045: x + 190 p.

Pershing, A.J. and Stamieszkin, K. 2020. The North Atlantic Ecosystem, from Plankton to Whales. Annu. Rev. Mar. Sci. 12(1):339–359.

Petrie, B. 2007. Does the north Atlantic oscillation affect hydrographic properties on the Canadian Atlantic continental shelf? Atmos. Ocean 45(3): 141–151.

Petrie, B., and Dean-Moore, J. 1996. Temporal and Spatial Scales of Temperature and Salinity on the Scotian Shelf. Can. Tech. Rep. Hydrogr. Ocean Sci. 177.

Petrie, B., Drinkwater, K., Gregory, D., Pettipas, R., and Sandström, A. 1996. Temperature and Salinity Atlas for the Scotian Shelf and the Gulf of Maine. Can. Data. Rep. Hydrog. Ocean Sci. 171.

Petrie, B., Topliss, B.J., and Wright, D.G. 1987. Coastal upwelling and eddy development off Nova Scotia. J. Geophys. Res. 92 (C12):12979–12991.

Petrie, B., and Yeats, P. 2000. Annual and interannual variability of nutrients and their estimated fluxes in the Scotian Shelf - Gulf of Maine region. Can. J. Fish. Aquat. Sci. 57: 2536–2546.

Petrie, B., Yeats, P., and Strain, P. 1999. Nitrate, Silicate and Phosphate Atlas for the Scotian Shelf and the Gulf of Maine. Can. Tech. Rep. Hydrogr. Ocean Sci. 203.

Platt T., Prakash, A., and Irwin, B. 1972. Phytoplankton nutrients and flushing of inlets on the coast of Nova Scotia, Nat. Can. 99:253–261.

Punshon, S., and Moore, R. M. 2004. Nitrous oxide production and consumption in a eutrophic coastal embayment. Mar. Chem. 91(1-4):37–51.

R Core Team. 2021. R: A language and environment for statistical computing. R Foundation for Statistical Computing, Vienna, Austria.

Record, N.R., et al. 2019. Rapid Climate-Driven Circulation Changes Threaten Conservation of Endangered North Atlantic Right Whales. Oceanography. 32(2) : 162-169.

Richardson, A.J., Walne, A.W., John, A.W.G., Jonas, T.D., Lindley, J.A., Sims, D.W., Stevens, D., and Witt, M. 2006. Using continuous plankton recorder data. Progr. Oceanogr. 68: 27–74.

Ross, T., Craig, S.E., Comeau, A., Davis, R., Dever, M., and Beck, M. 2017. Blooms and subsurface phytoplankton layers on the Scotian Shelf: Insights from profiling gliders. J Marine Syst. 172, 118–127.

Shi, Y., Wang, J., Zuo, T., Shan, X., Jin, X., Sun, J., Yuan, W., and Pakhomov, E.A. 2020. Seasonal Changes in Zooplankton Community Structure and Distribution Pattern in the Yellow Sea, China. Frontiers in Mar. Sci., 7, 391.

Song, H., Ji, R., Stock, C., and Wang, Z. 2010. Phenology of phytoplankton blooms in the Nova Scotian Shelf–Gulf of Maine region: remote sensing and modeling analysis. J. Plankton Res., 32(11), 1485–1499.

Sverdrup, H.U. 1953. On Conditions for the Vernal Blooming of Phytoplankton. J. Cons. Perm. Int. Explor. Mer. 18: 287–295.

Therriault, J.-C., Petrie, B., Pepin, P., Gagnon, J., Gregory, D., Helbig, J., Herman, A., Lefaivre, D., Mitchell, M., Pelchat, B., Runge, J., and Sameoto, D. 1998. Proposal for a Northwest Atlantic Zonal Monitoring Program. Can. Tech. Rep. Hydrogr. Ocean Sci. 194.

Utermöhl, von H. 1931. Neue Wege in der quantitativen Erfassung des Plankton.(Mit besonderer Berücksichtigung des Ultraplanktons.). Verh. Int. Verein. Theor. Angew. Limnol., 5, 567–595.

Yashayaev, I., Ringuette, M., Peterson, I., Wang, Z., Head, E., Punshon, S., Devred, E., and Azetsu-Scott, K. 2019. Environmental Conditions in the Labrador Sea during 2018. NAFO SCR Doc. 19/039. Serial N6960. 50 p.

Zhai, L., Platt, T., Tang, C., Sathyendranath, S., and Hernández Walls, R. 2011. Phytoplankton Phenology on the Scotian Shelf. ICES J. Mar. Sci. 68:781–791.

TABLES

Table 1. Atlantic Zone Monitoring Program sampling missions in the Maritimes Region in 2020.

Group	Location	Mission ID	Dates	# Hydro Stations	# Net Stations
Ecosystem Trawl Survey	Western Scotian Shelf	TEL2020-102	Mar 07–09	37	11
Ecosystem Trawl Survey	Georges Bank	TEL2020-002	Mar 11–20	31	9
Ecosystem Trawl Survey	Scotian Shelf	NED2020-025	Jul 03–Aug 10	163	37
Seasonal Sections	Scotian Shelf	HUD2020-063	Oct 03–15	51	41
High-frequency Stations	Halifax-2	BCD2020-666	Jan 01–Dec 31	12(5)[1]	11(5)[1]
	Prince-5	BCD2020-669	Jan 01–Dec 31	8	7
			Total:	*302*	*116*

[1]Total station occupations, including occupations during trawl surveys and seasonal sections (dedicated occupations with mission ID as listed at left are in parentheses).

FIGURES

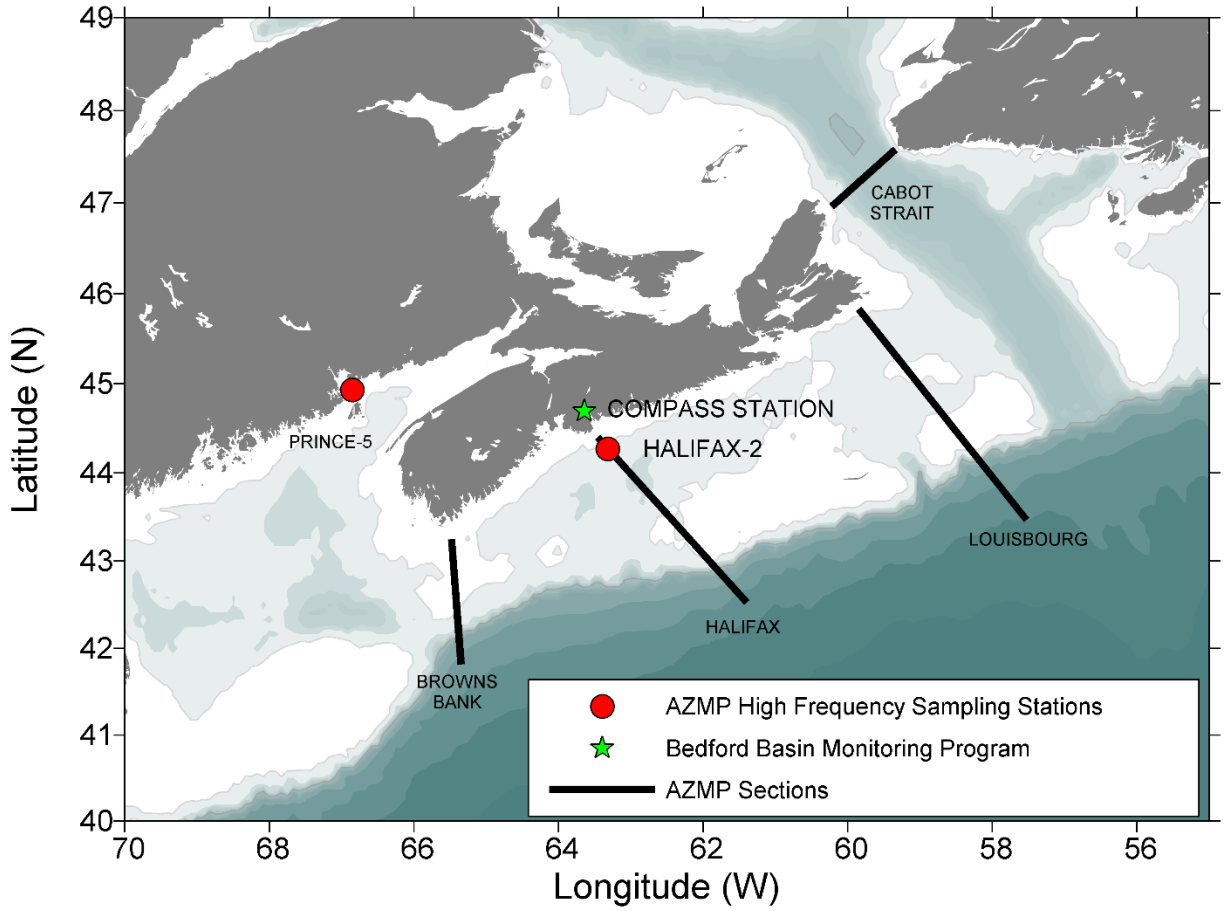

Figure 1. Map of primary sections (Cabot Strait [CSL]; Louisbourg [LL]; Halifax [HL]; Browns Bank [BBL]) and high-frequency sampling stations (Halifax-2 [HL2]; Prince-5 [P5]) sampled in the DFO Maritimes Region. The Compass Buoy station is sampled as part of the Bedford Basin Monitoring Program.

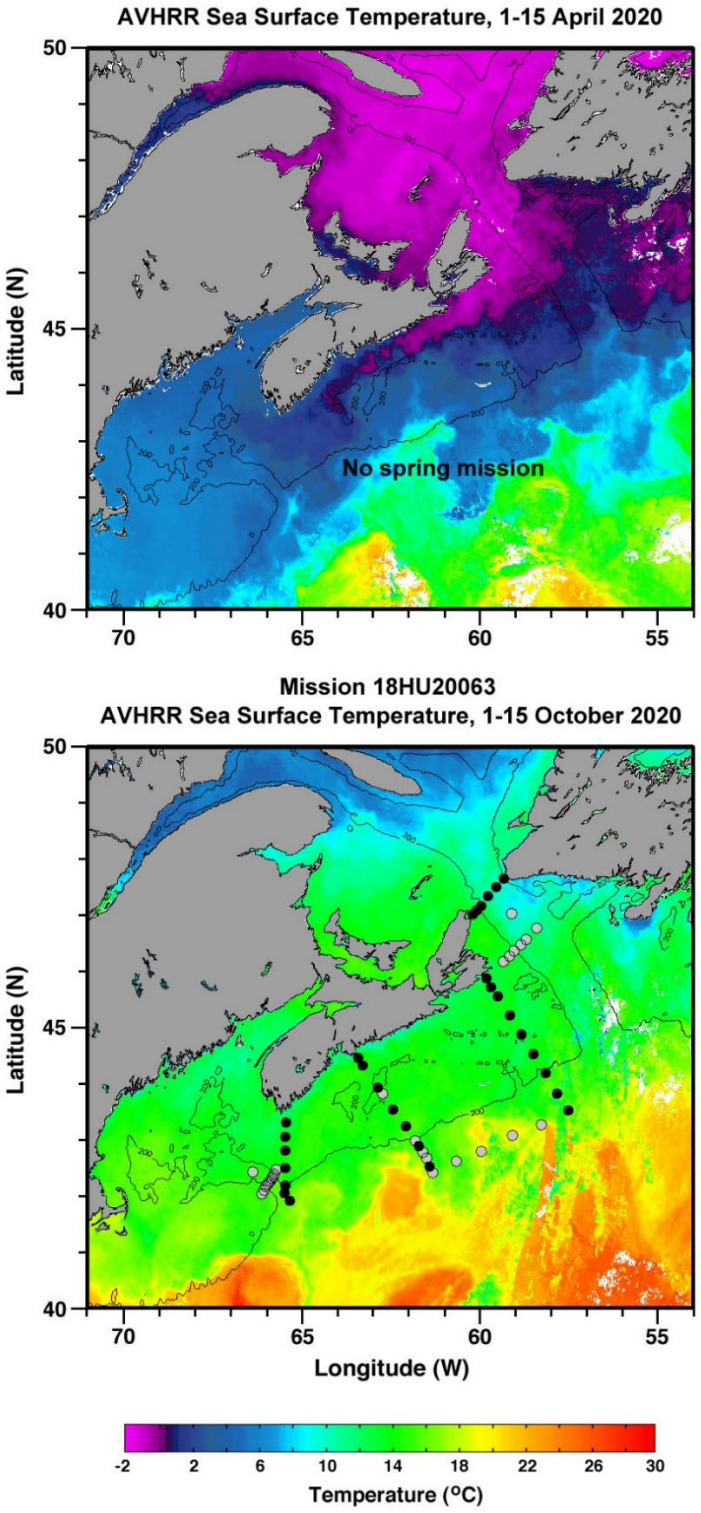

Figure 2. Stations sampled during the 2020 fall survey. Station locations are superimposed on sea-surface-temperature composite images for dates close to the 2020 mission dates (fall mission only). Black markers indicate core stations, and gray markers indicate stations sampled for ancillary programs.

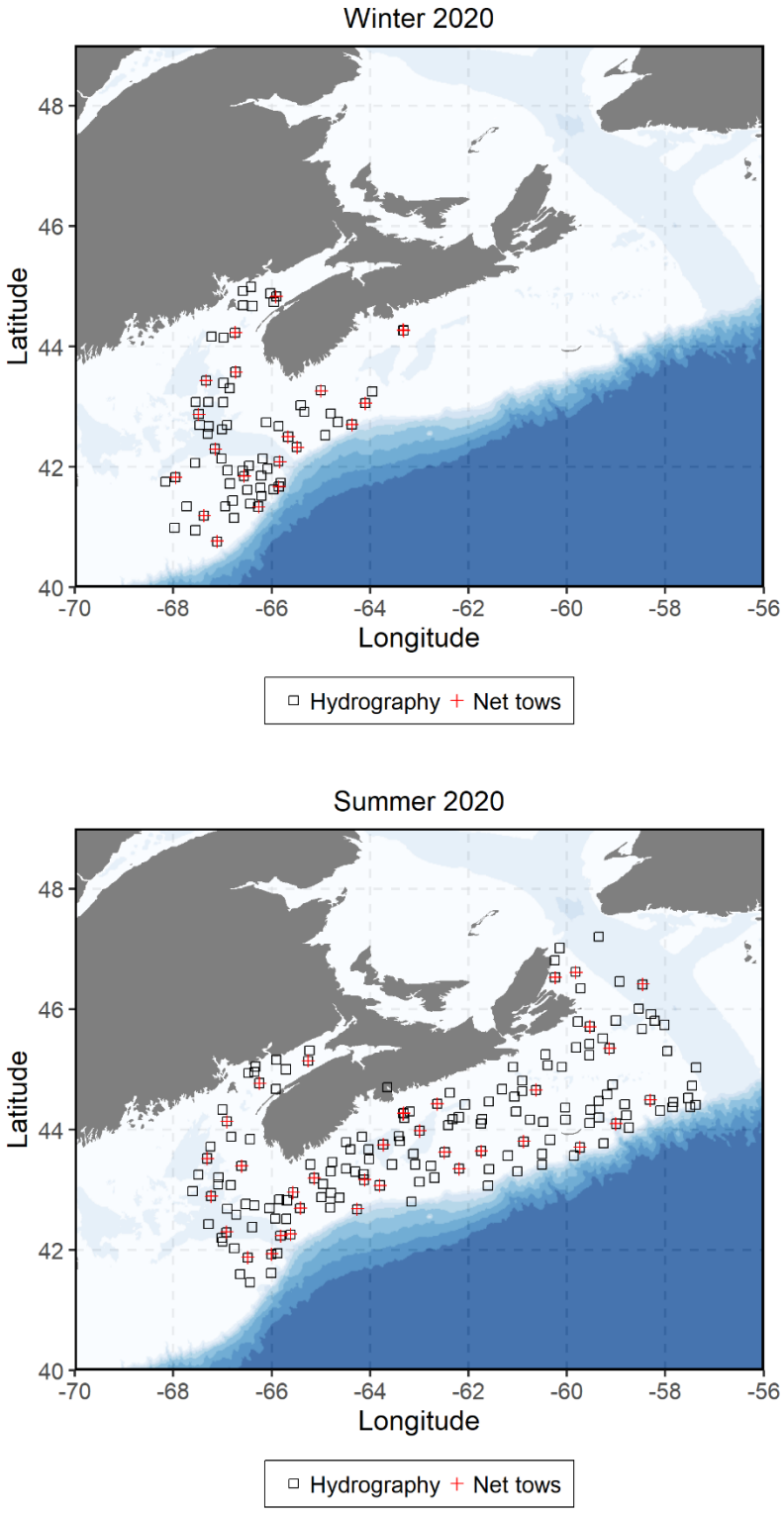

Figure 3. Stations sampled during primary Maritimes Region ecosystem trawl surveys in 2020.

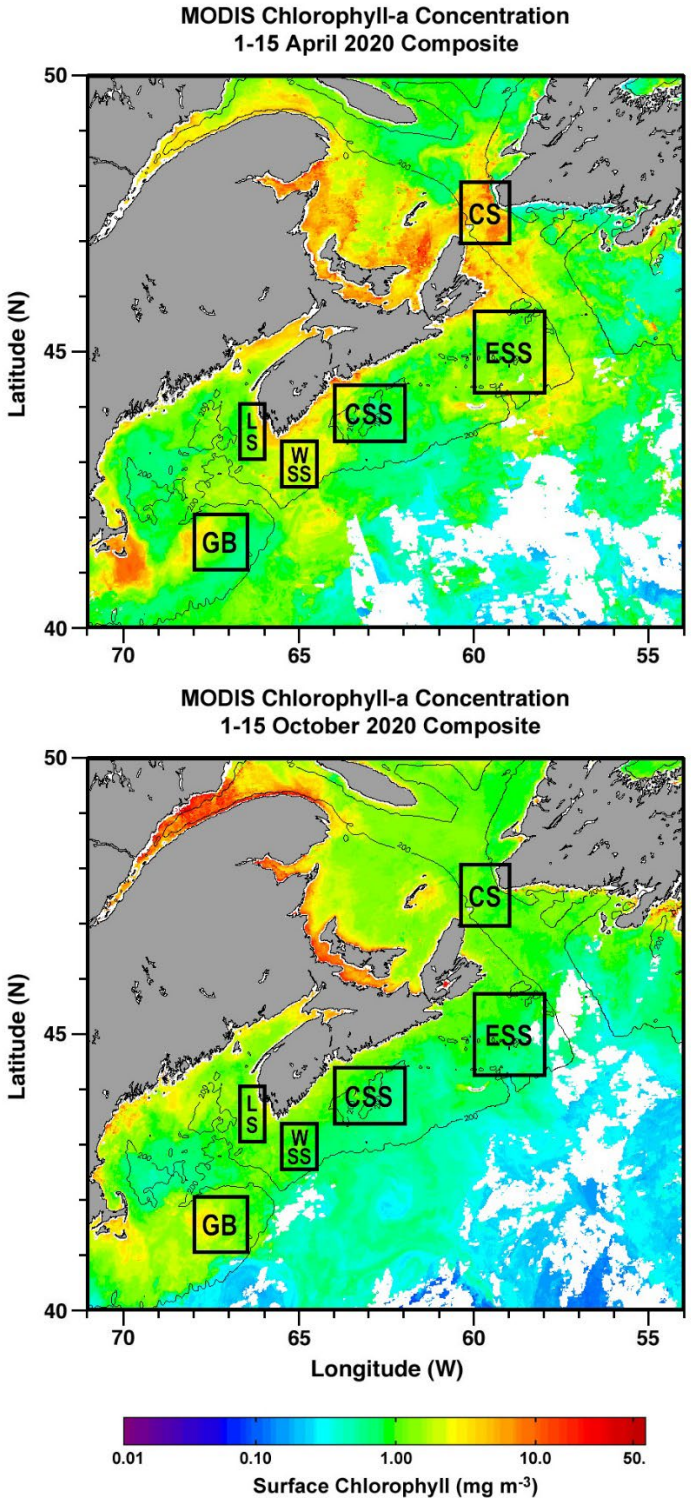

Figure 4. Statistical sub-regions in the Maritimes Region identified for spatial/temporal analysis of satellite ocean colour data. Sub-regions are superimposed on surface chlorophyll a composite images for dates close to the 2020 mission dates (fall mission only). Cabot Strait [CS]; Eastern Scotian Shelf [ESS]; Central Scotian Shelf [CSS]; Western Scotian Shelf [WSS]; Lurcher Shoal [LS]; Georges Bank [GB].

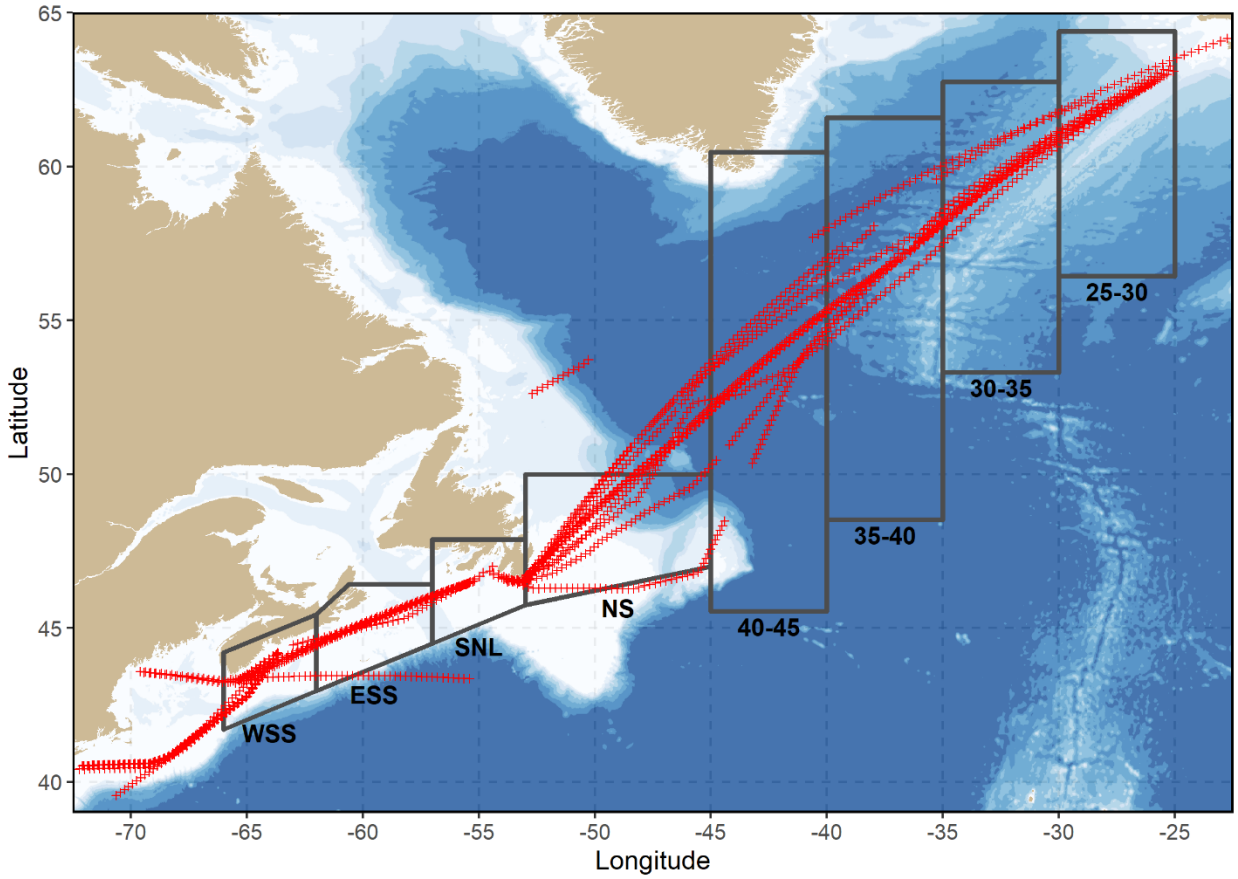

Figure 5. Continuous Plankton Recorder (CPR) lines and stations sampled in 2019 (red markers). Data are analysed by region. Regions are: Western Scotian Shelf (WSS), Eastern Scotian Shelf (ESS), South Newfoundland Shelf (SNL), Newfoundland Shelf (NS), and between longitudes 40–45°W, 35–40°W, 30–35°W, 25–30°W.

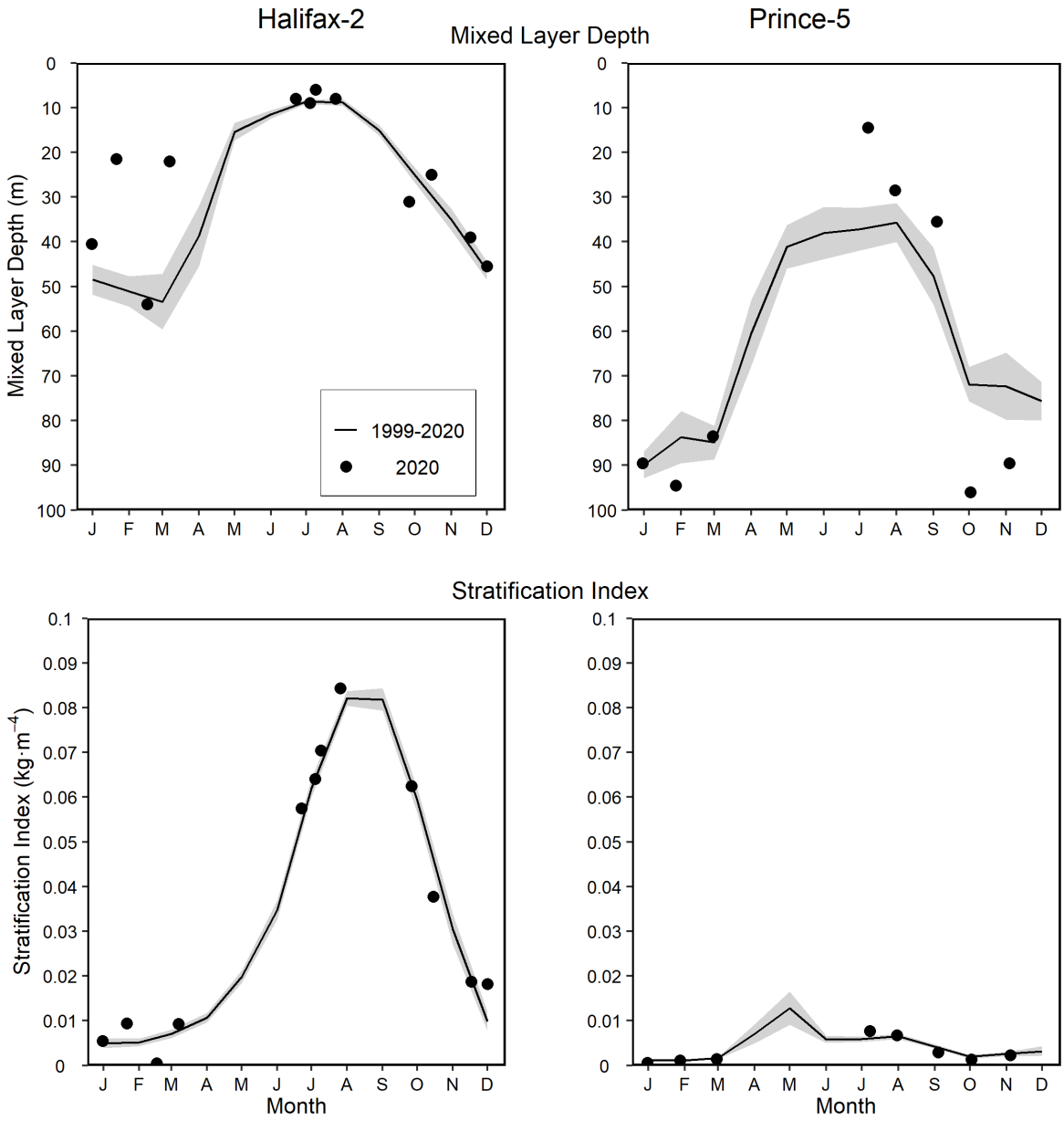

Figure 6. Mixing properties (mixed layer depth, stratification index) at the Maritimes high-frequency sampling stations comparing 2020 data (solid circle) with mean conditions from 1999–2020 (solid line). The gray shaded area represents the standard error of the monthly means. Tick marks on the horizontal axes indicate the 15th day of the month.

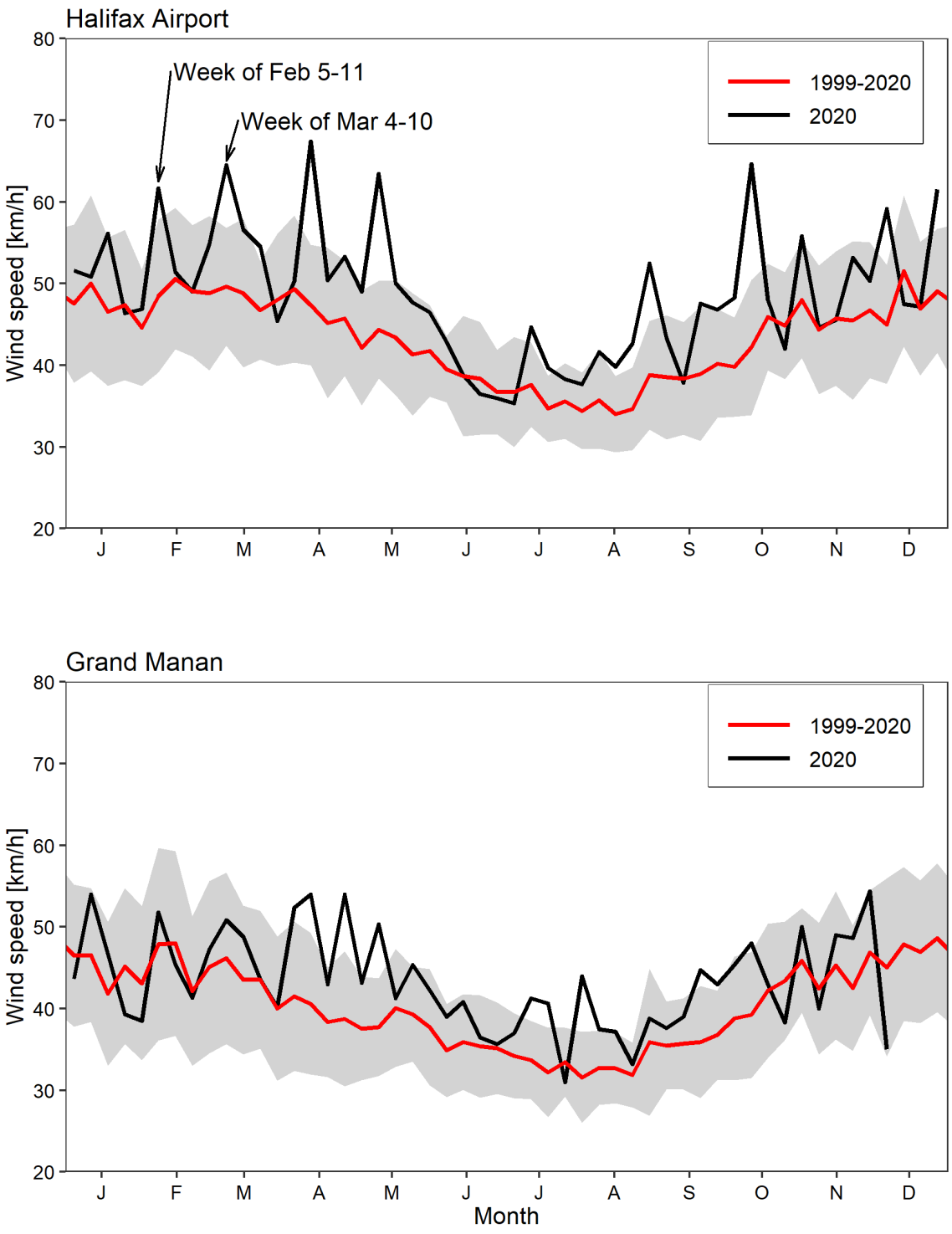

Figure 7. Weekly mean of maximum daily wind gust at Halifax Stanfield International Airport (representative of wind conditions at Halifax-2) and Grand Manan Island (representative of wind conditions at Prince-5) for the year 2020 (black line) and the 1999–2020 climatology (red line). The gray shaded area represents the standard deviation to the climatology computed over 22 years. Tick marks on the horizontal axes indicate the 15th day of the month.

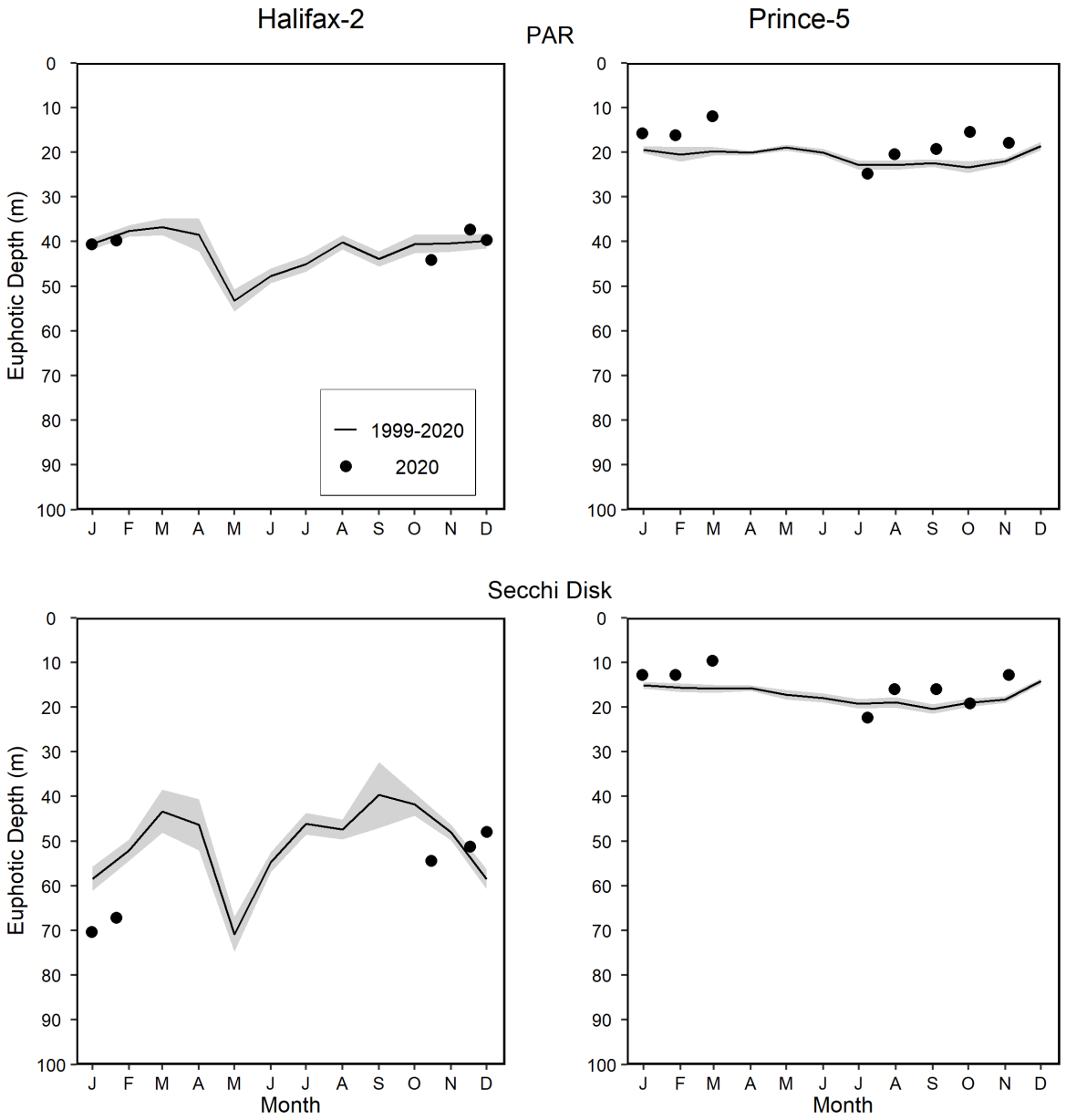

Figure 8. Optical properties (euphotic depth from PAR irradiance meter and Secchi disc) at the Maritimes high-frequency sampling stations. Year 2020 data (solid circle) compared with mean conditions from 1999–2020 (solid line), except 2001–2020 for euphotic depth from PAR at Prince-5. The gray shaded area represents the standard error of the monthly means. Tick marks on the horizontal axes indicate the 15th day of the month.

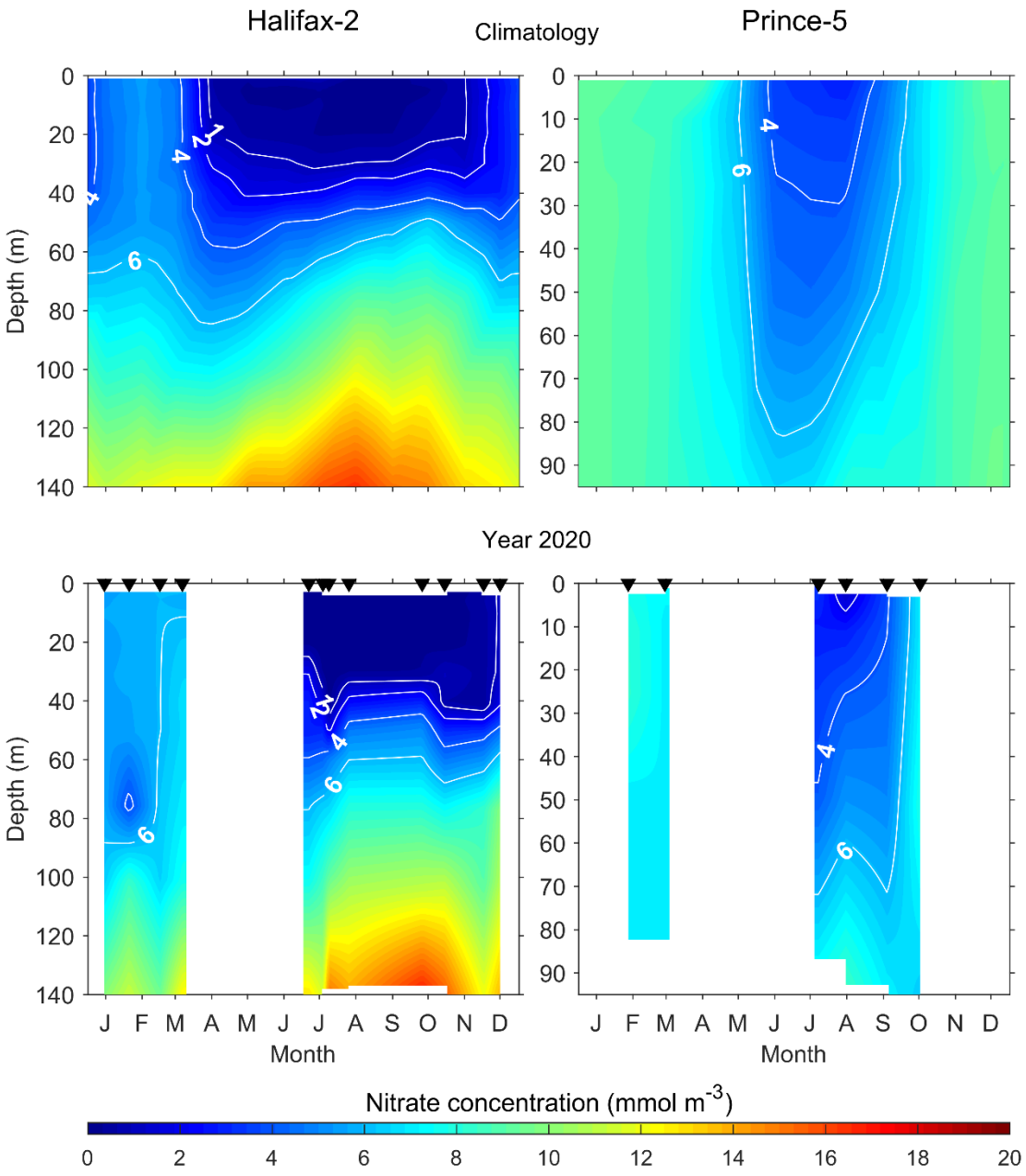

Figure 9. Comparison of annual changes in the vertical structure of nitrate concentrations (mmol·m^{-3}) in 2020 (bottom panels) with climatological conditions from 1999–2020 (upper panels) at the Maritimes high-frequency sampling stations. Black triangles in the bottom panels indicate sampling dates. Tick marks on the horizontal axes indicate the 15th day of the month. White areas indicate no data.

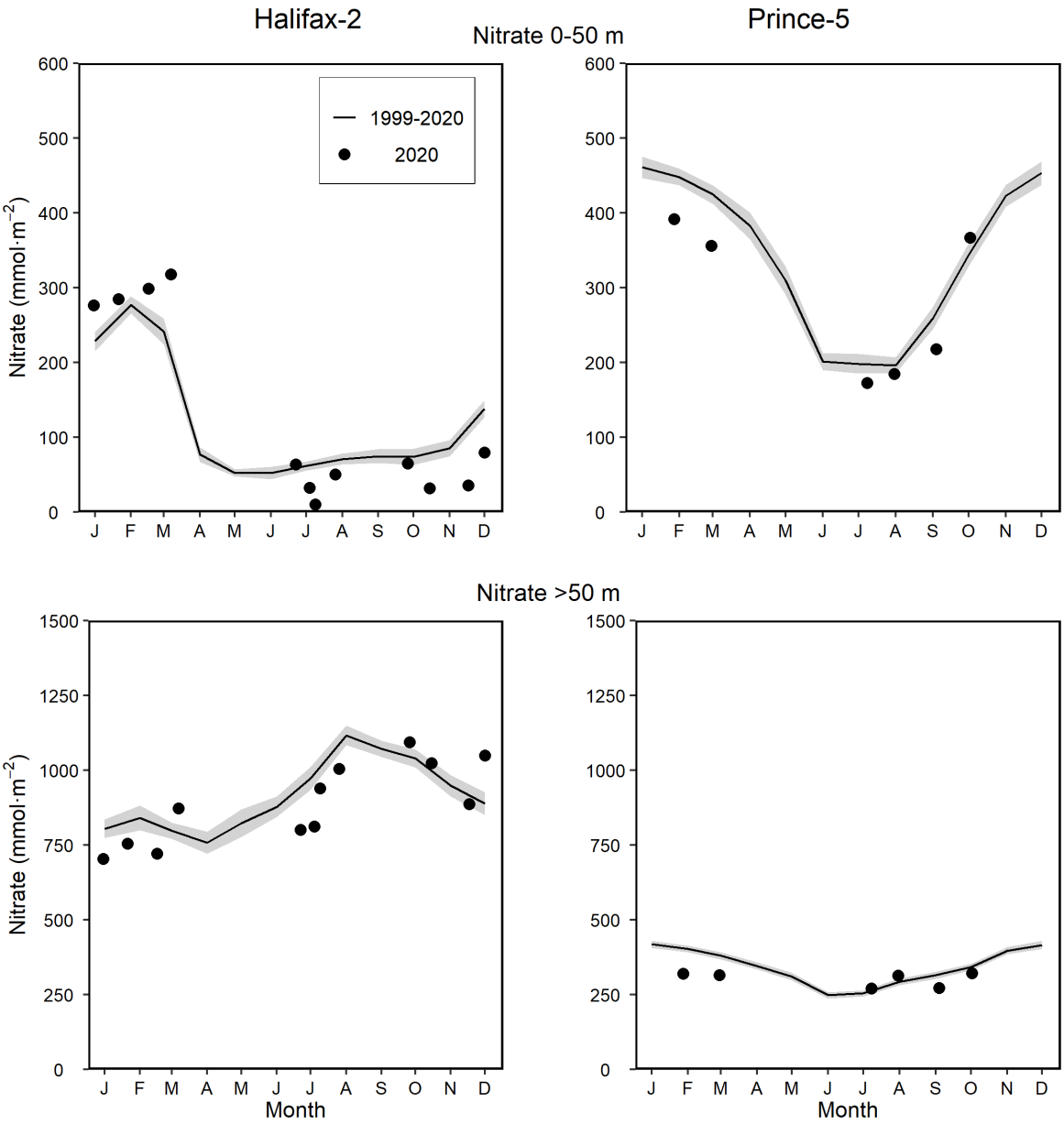

Figure 10. Comparison of 2020 (solid circle) data with mean conditions from 1999–2020 (solid line) at the Maritimes high-frequency sampling stations. Upper panels: surface (0–50 m) nitrate inventory. Lower panels: deep (50–150 m for Halifax-2 and 50–95 m for Prince-5) nitrate inventory. The gray shaded area represents the standard error of the monthly means. Tick marks on the horizontal axes indicate the 15th day of the month.

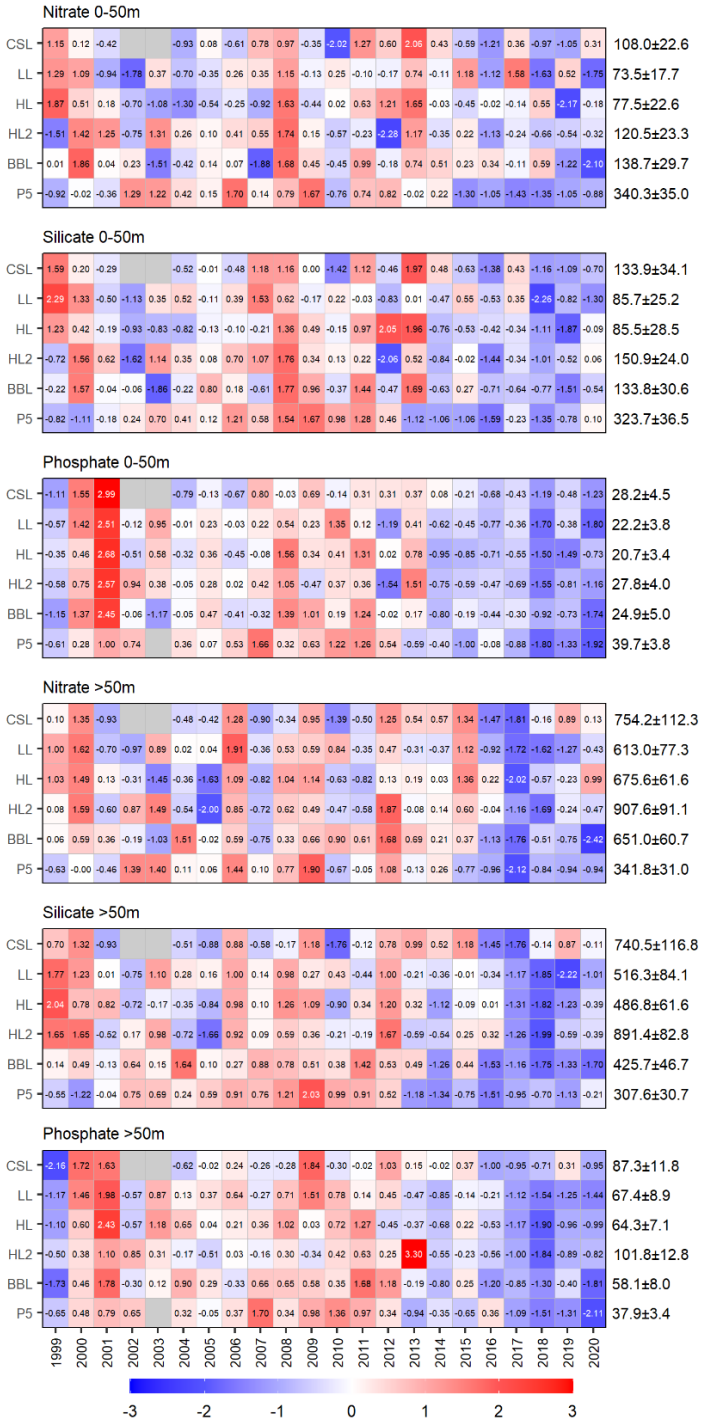

Figure 11. Annual anomaly scorecards for surface (0–50 m) and deep (> 50 m) nitrate, silicate, and phosphate inventories. Values in each cell are anomalies from the mean for the reference period, 1999–2020, in standard deviation (sd) units (mean and sd listed at right, units in mmol/m^3). Red (blue) cells indicate higher- (lower-) than-normal nutrients. Gray cells indicate missing data. CSL: Cabot Strait section; LL: Louisbourg section; HL: Halifax section; HL2: Halifax-2; BBL: Browns Bank section; P5: Prince-5.

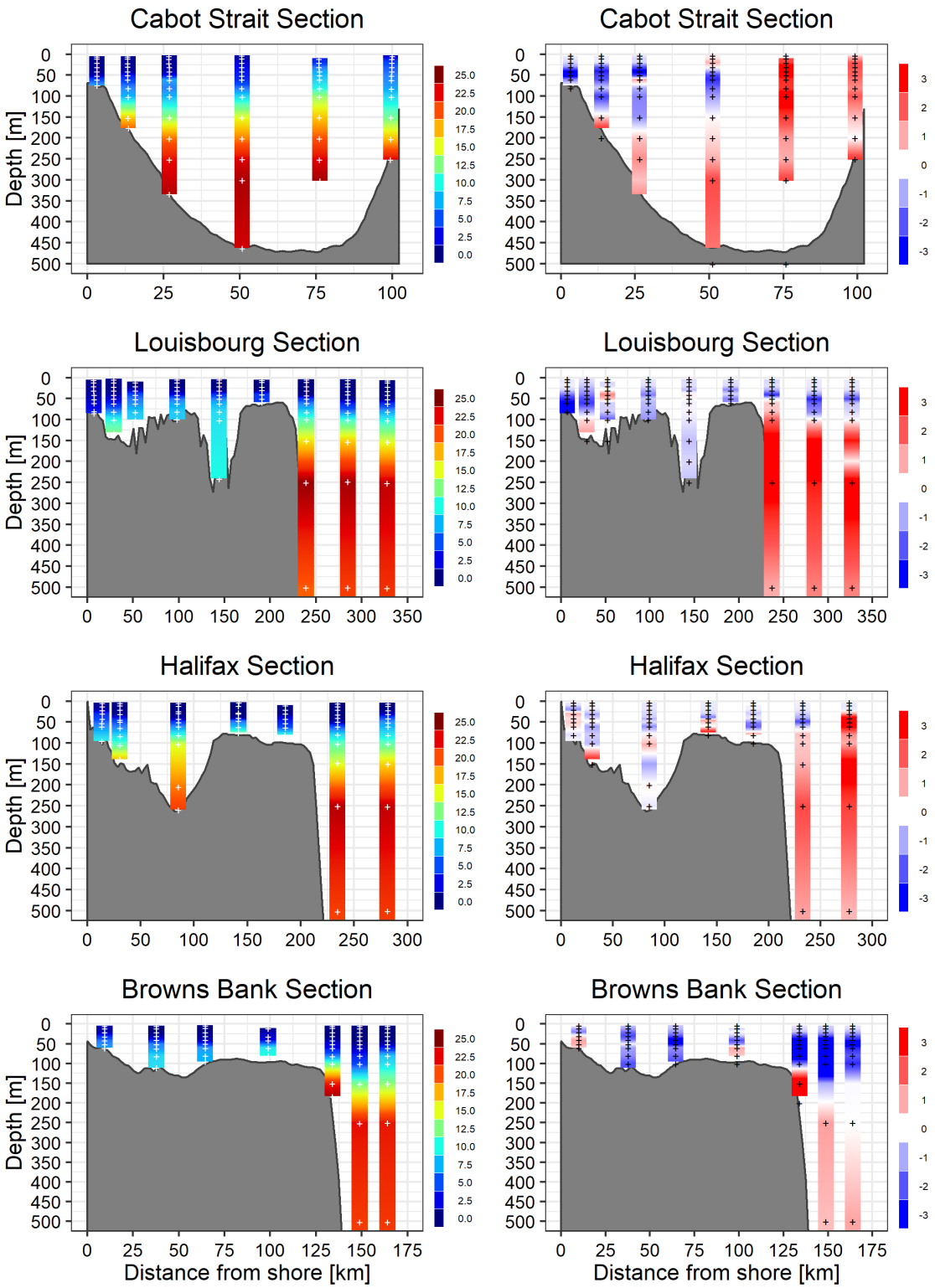

Figure 12. Vertical profiles of nitrate concentration (mmol·m^{-3}) (left panels) and their anomalies (mmol·m^{-3}) from 1999–2020 conditions (right panels) for each occupied stations along the SS sections in fall 2020. White markers on the left panels indicate the actual sampling depths for 2020. Black markers on the right panels indicate the depths at which station-specific climatological values were calculated.

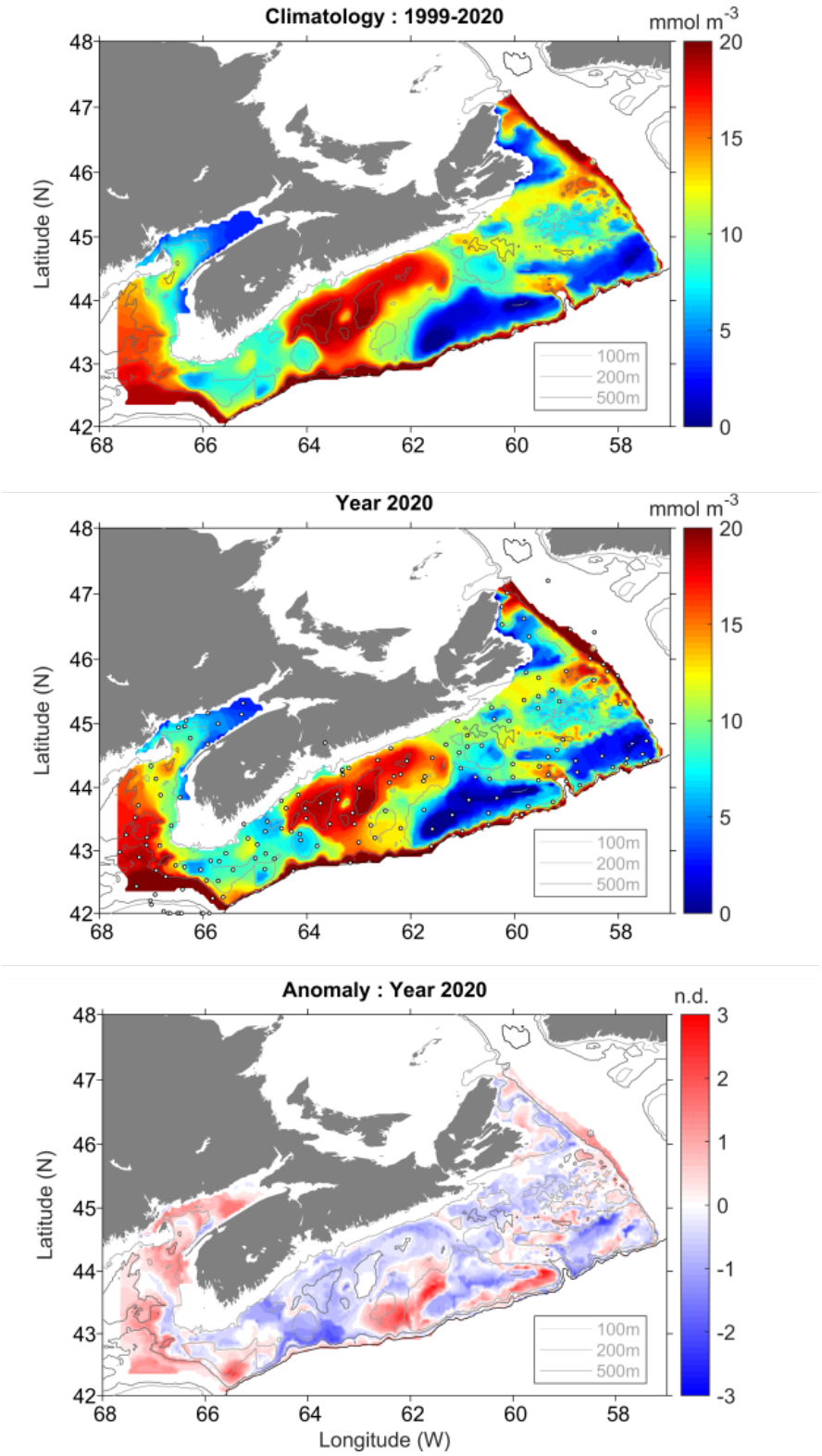

Figure 13. Bottom nitrate concentration during the annual summer ecosystem trawl survey: 1999–2020 climatology (upper panel), 2020 conditions (middle panel), and normalized anomalies (lower panel). Markers in middle panel represent the 2020 sampling locations. nd = no dimensions.

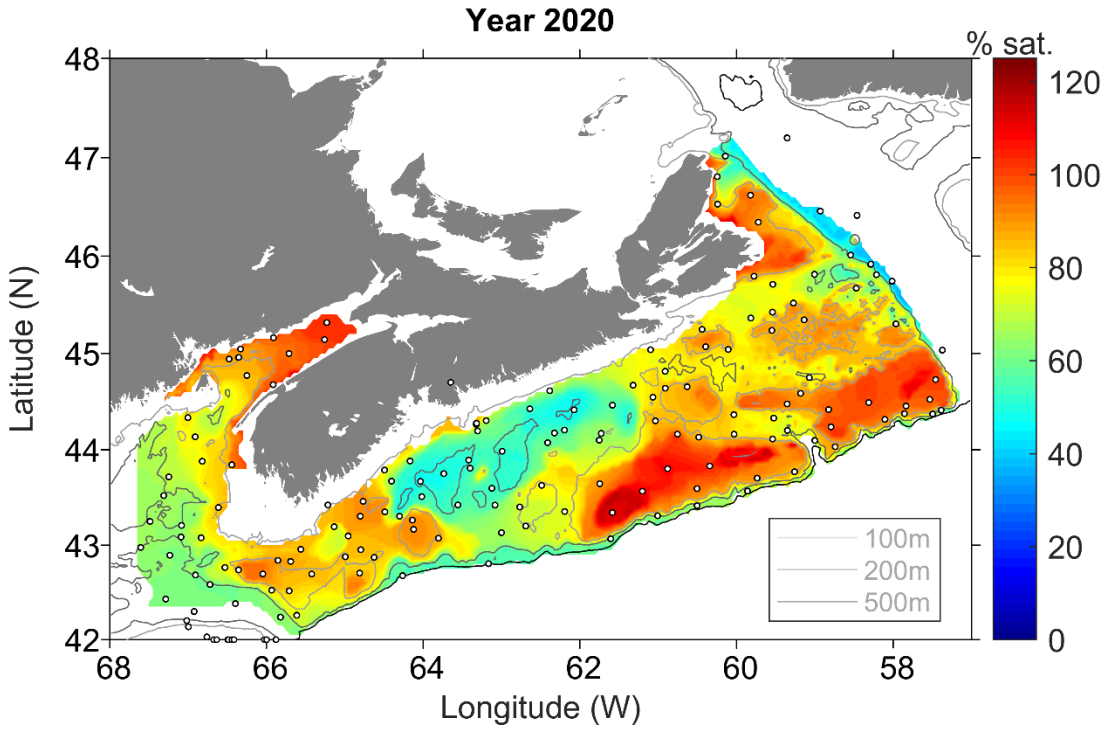

Figure 14. Bottom oxygen saturation level during the annual summer ecosystem trawl survey in 2020. Markers represent the sampling locations.

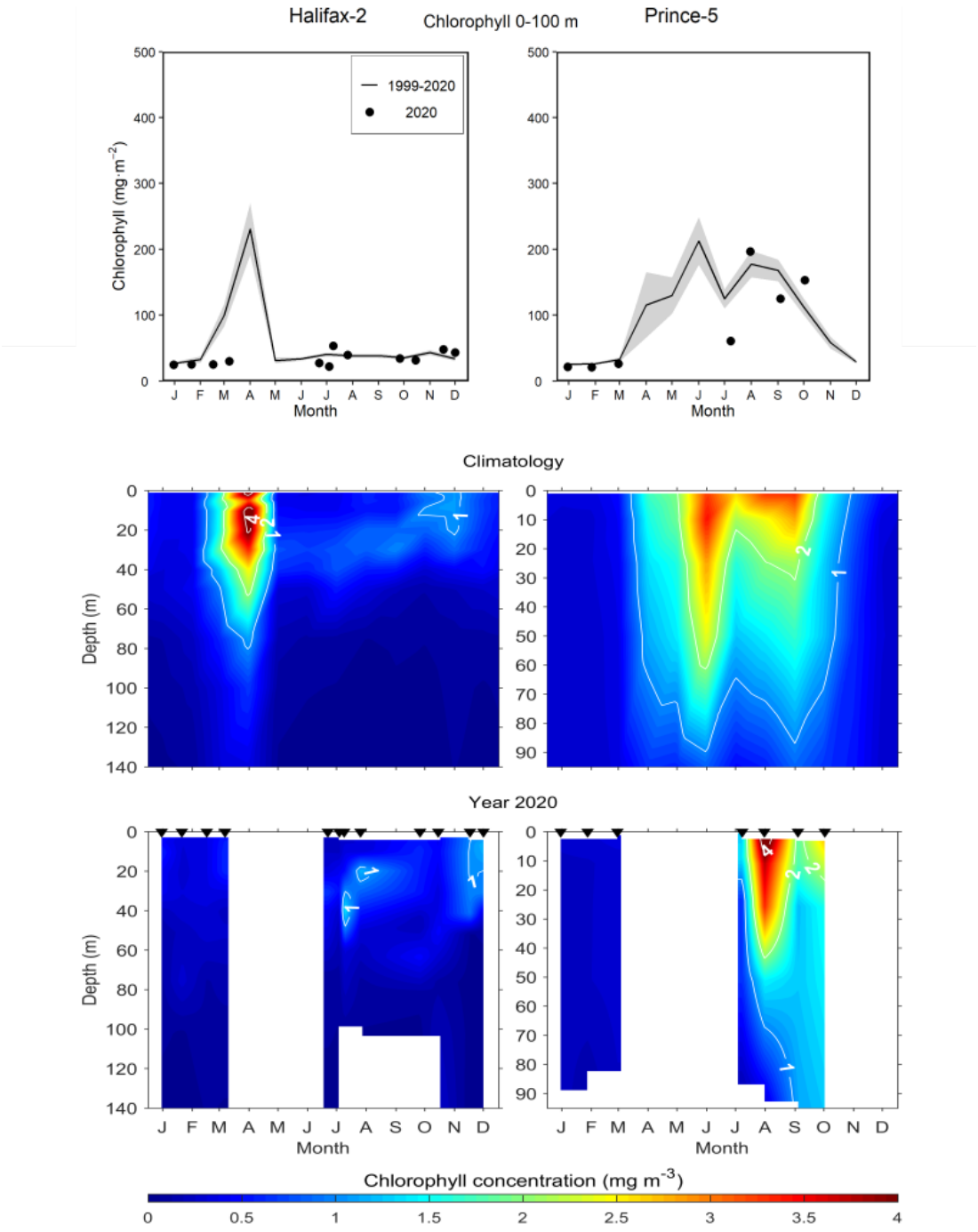

Figure 15. Annual variability in chlorophyll a concentration at the Maritimes time-series stations (left column: Halifax-2, right column: Prince-5). Top row: chlorophyll a inventories (0–100 m at Halifax-2, 0–95 m at Prince-5) in 2020 (open circle) and mean values 1999–2020 (solid line). Vertical lines are 95% confidence intervals of the monthly means. Middle row: Mean (1999–2020) seasonal cycle of the vertical structure of chlorophyll a concentration (mg·m^{-3}). Bottom row: seasonal cycle of the vertical structure of chlorophyll a concentration in 2020. Black triangles in the bottom panels indicate sampling dates. Tick marks on the horizontal axes indicate the 15th day of the month. White areas indicate no data.

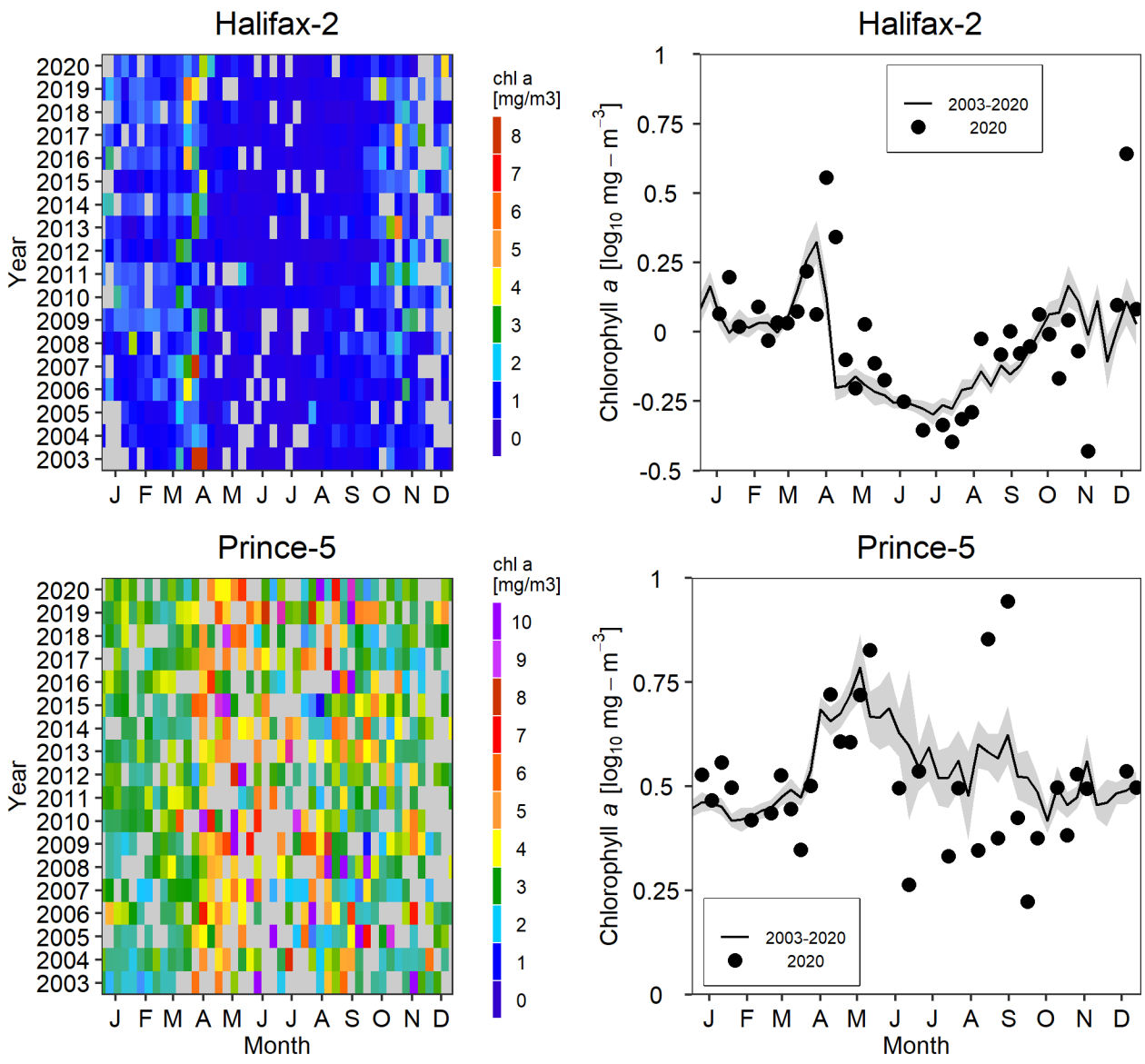

Figure 16. Estimates of surface chlorophyll a concentrations from weekly remotely sensed ocean colour data for Halifax-2 (top panels) and Prince-5 (bottom panels). Data from MODIS 2003–2020. Left panels: Time series of annual variation in chlorophyll a concentrations. Gray pixels indicate missing data. Right panels: Comparison of 2020 (solid circle) surface chlorophyll a estimates with mean conditions from 2003–2020 (solid line). Gray shaded area is the 95% confidence interval of the weekly means. Tick marks on the horizontal axes indicate the 15th day of the month.

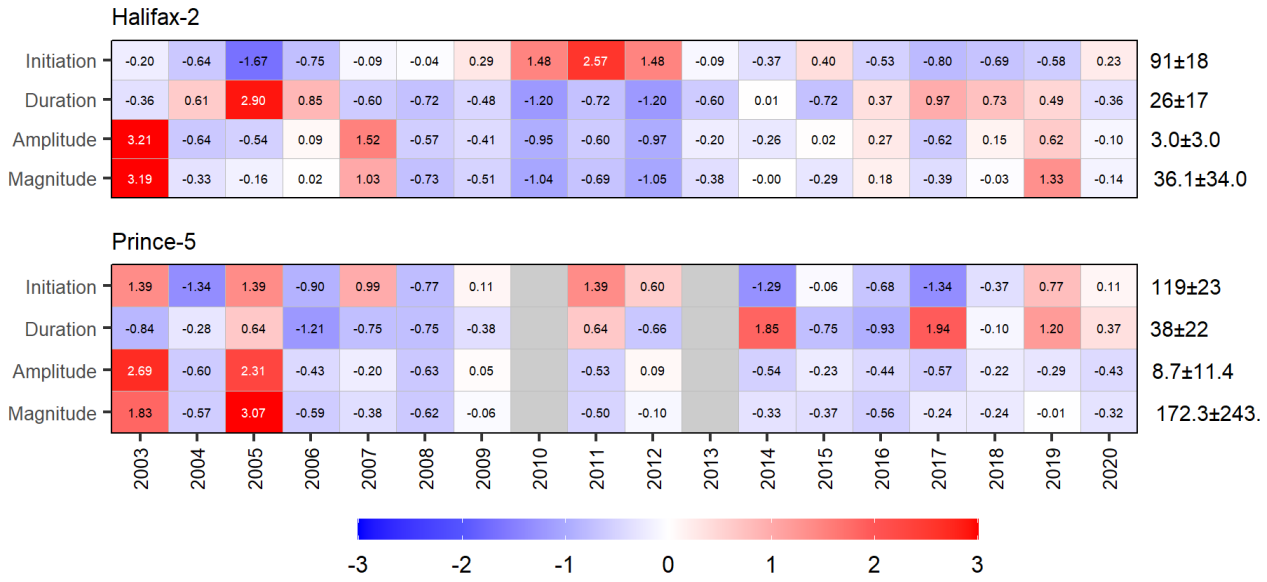

Figure 17. Annual anomaly scorecards for spring bloom parameters for Halifax-2 (top panel) and Prince-5 (bottom panel). Values in each cell are anomalies from the mean for the reference period, 2003–2020, in standard deviation (sd) units (mean and sd listed at right). Red (blue) cells indicate later (earlier) initiation, longer (shorter) duration or higher- (lower-) than-normal amplitude or magnitude. Gray cells indicate missing data.

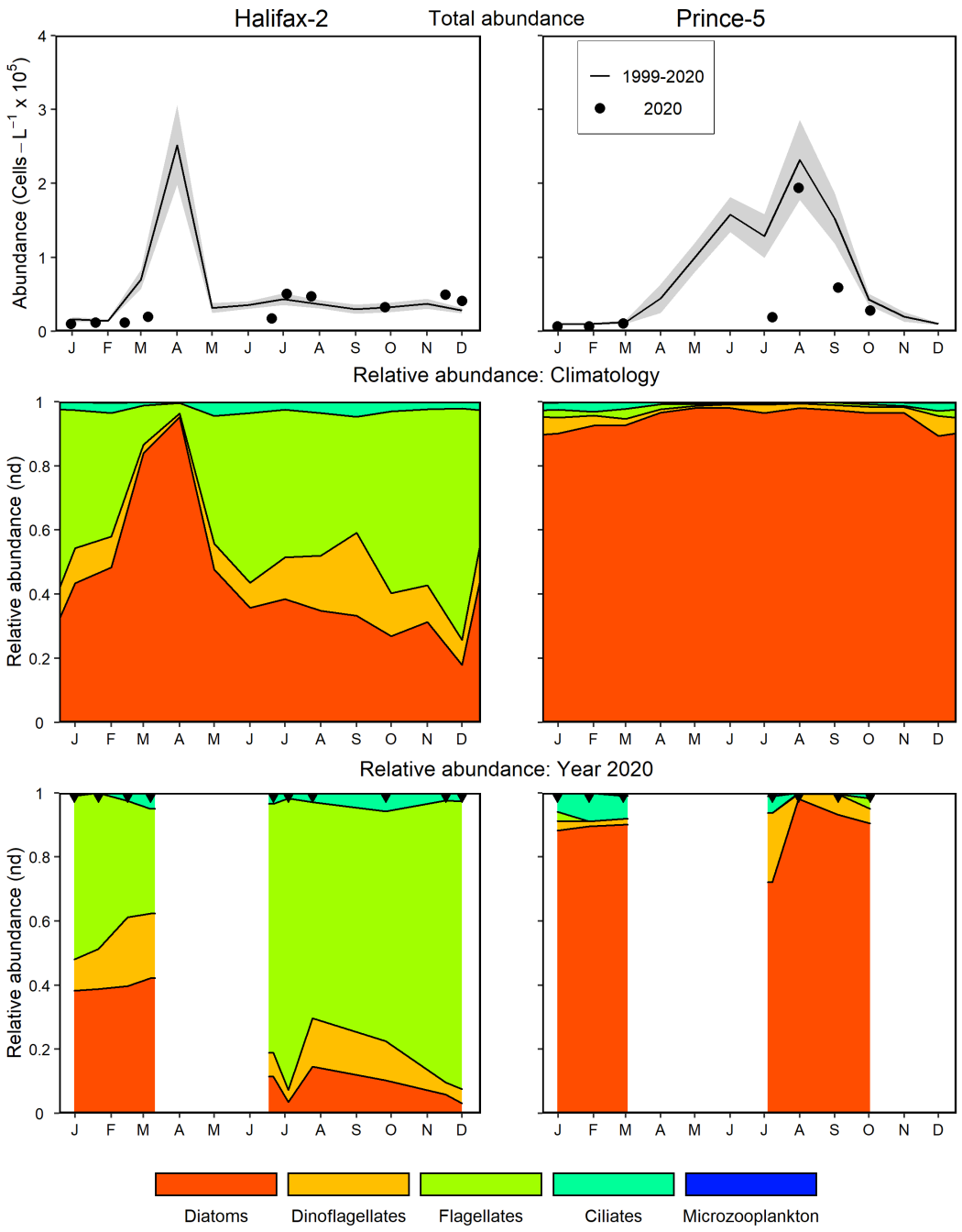

Figure 18. Comparison of 2020 microplankton (phytoplankton and protists) abundance and community composition with mean conditions from 1999–2020 at the Maritimes high-frequency sampling stations (Halifax-2: left panels; Prince-5: right panels). Upper panels: 2020 microplankton abundance (solid circle) and mean conditions from 1999–2020 (solid line). The gray shaded area represents the standard error of the monthly means. Middle panels: Climatological microplankton relative abundance from 1999–2020. Lower panels: 2020 microplankton relative abundance. nd = no dimensions. Black triangles in the bottom panels indicate sampling dates. Tick marks on the horizontal axes indicate the 15th day of the month. White areas indicate no data.

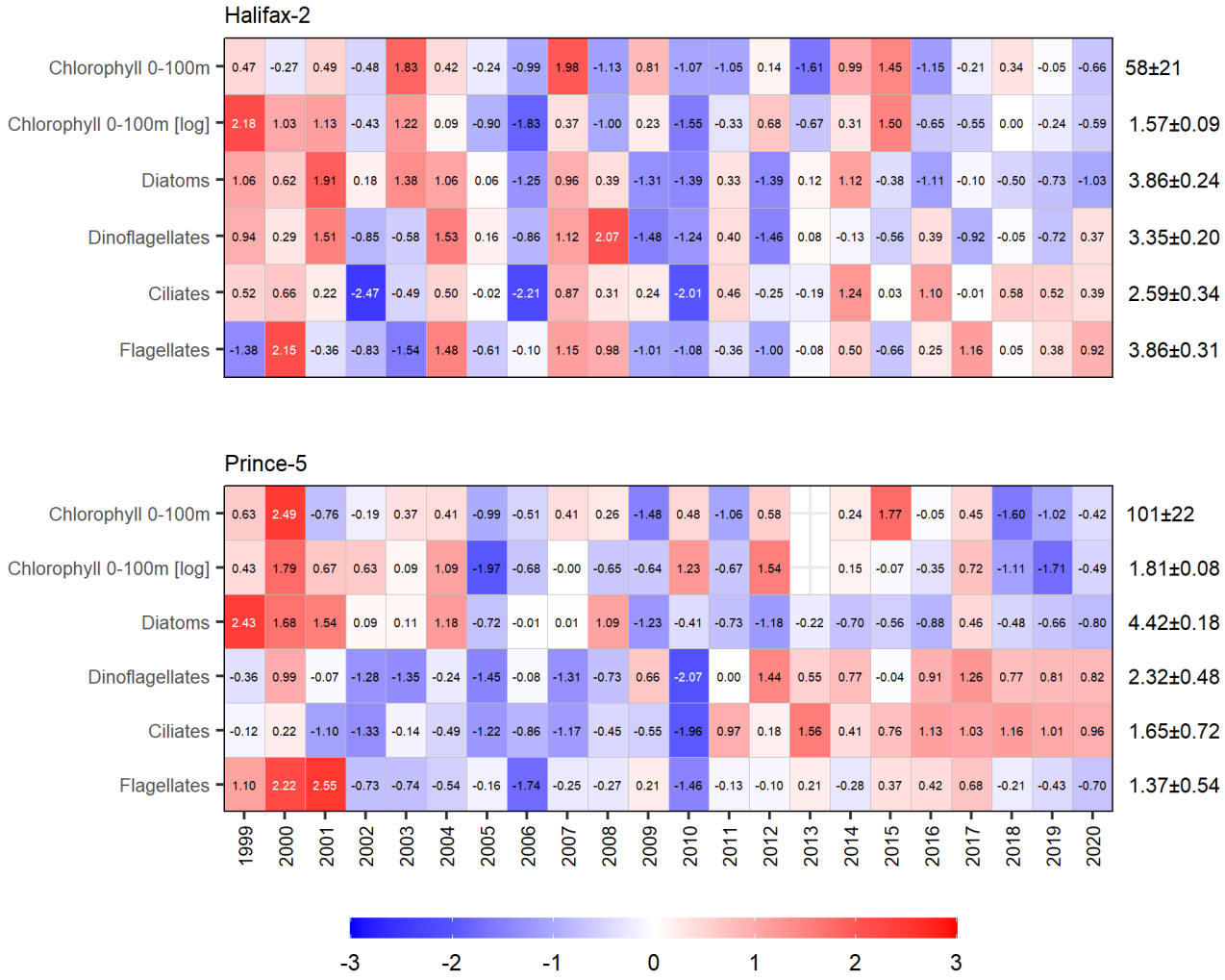

Figure 19. Annual anomaly scorecards for chlorophyll a inventory (0–100 m at Halifax-2, 0–95 m at Prince-5) and microplankton abundance at the Maritimes high-frequency sampling stations. Values in each cell are anomalies from the mean for the reference period, 1999–2020, in standard deviation (sd) units (mean and sd listed at right). Red (blue) cells indicate higher- (lower-) than-normal chlorophyll a inventories or microplankton abundances. Gray cells indicate missing data.

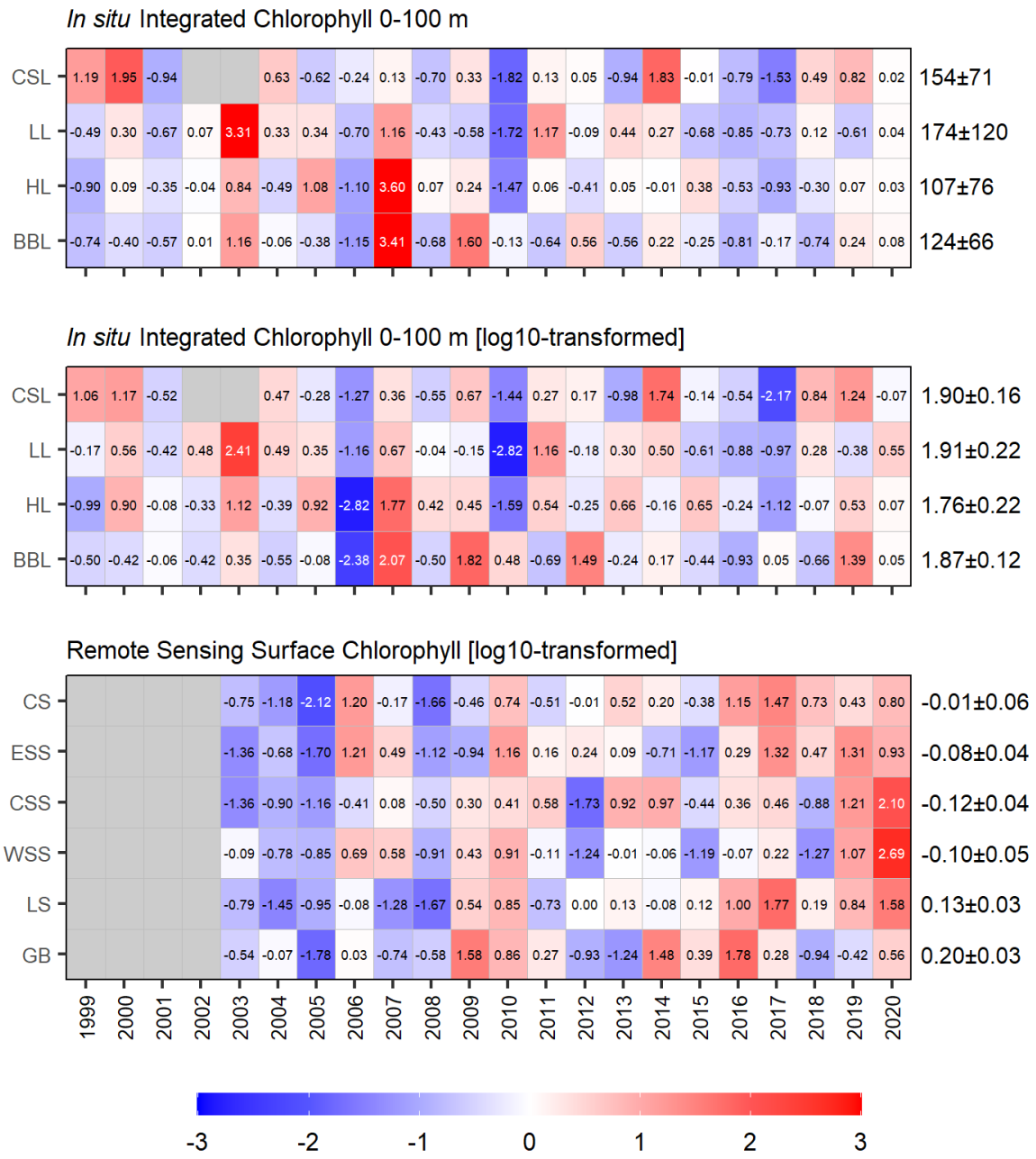

Figure 20. Annual anomaly scorecards for chlorophyll a inventory (0–100 m) from in situ sampling on the Cabot Strait [CSL], Louisbourg [LL], Halifax [HL] and Browns Bank [BBL] sections (top and middle panels) and for surface chlorophyll a concentrations from weekly remotely sensed ocean colour data in the Cabot Strait [CS], Eastern Scotian Shelf [ESS], Central Scotian Shelf [CSS], Western Scotian Shelf [WSS], Lurcher Shoal [LS], and Georges Bank [GB] statistical sub-regions (bottom panel). Data from MODIS 2003–2020. Values in each cell are anomalies from the mean for the reference period, 1999–2020 for in situ chlorophyll a inventory and 2003–2020 for remotely sensed surface chlorophyll a, in standard deviation (sd) units (mean and sd listed at right). Red (blue) cells indicate higher- (lower-) than-normal chlorophyll a inventories or surface chlorophyll a concentrations. Gray cells indicate missing data.

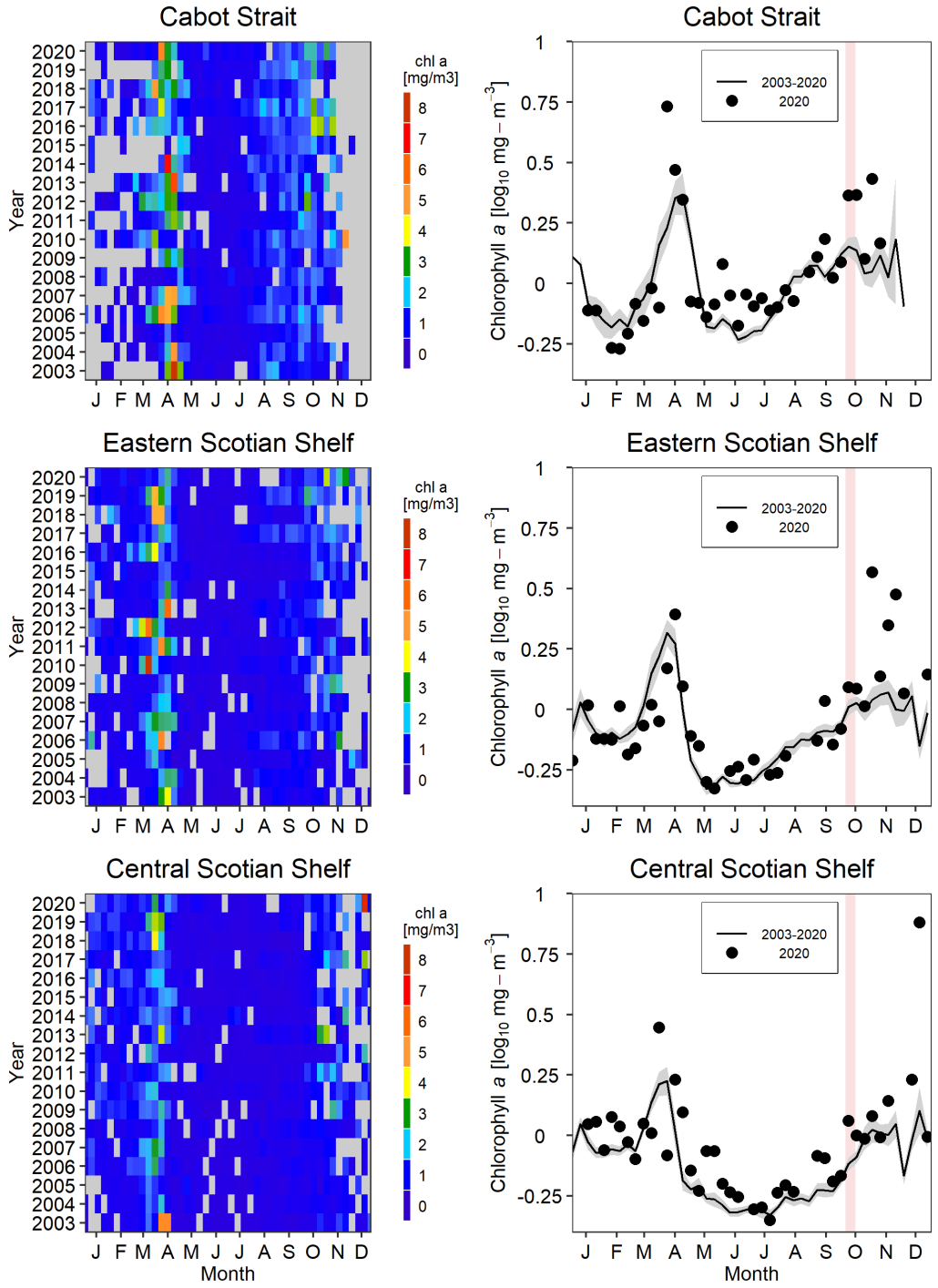

Figure 21a. Estimates of surface chlorophyll a concentrations from weekly remotely sensed ocean colour data in the Cabot Strait (top), Eastern Scotian Shelf (middle), and Central Scotian Shelf (bottom) statistical sub-regions. Data from MODIS 2003–2020. Left panels: Time series of annual variation in chlorophyll a concentrations. Gray pixels indicate missing data. Right panels: Comparison of 2020 (solid circle) surface chlorophyll a estimates with mean conditions from 2003–2020 (solid line) in the same sub-regions. Gray shaded area is the 95% confidence interval of the weekly means. Pink vertical stripes indicate the timing of the seasonal missions. Tick marks on the horizontal axes indicate the 15th day of the month.

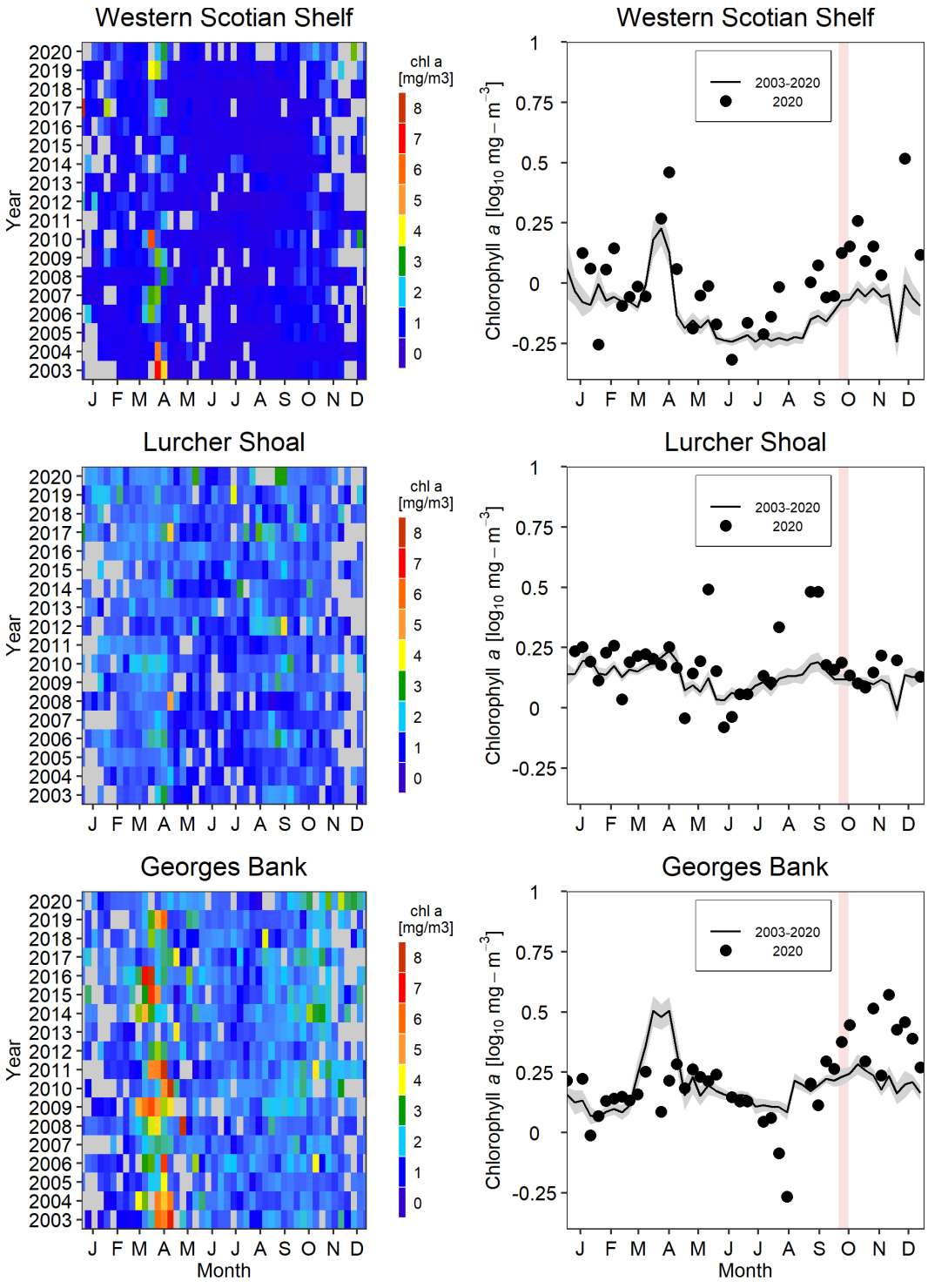

Figure 21b. Estimates of surface chlorophyll a concentrations from weekly remotely sensed ocean colour data in the Western Scotian Shelf (top), Lurcher Shoal (middle), and Georges Bank (bottom) statistical sub-regions. Data from MODIS 2003–2020. Left panels: Time series of annual variation in chlorophyll a concentrations. Gray pixels indicate missing data. Right panels: Comparison of 2020 (solid circle) surface chlorophyll a estimates with mean conditions from 2003–2020 (solid line) in the same sub-regions. Gray shaded area is the 95% confidence interval of the weekly means. Pink vertical stripes indicate the timing of the seasonal missions. Tick marks on the horizontal axes indicate the 15th day of the month.

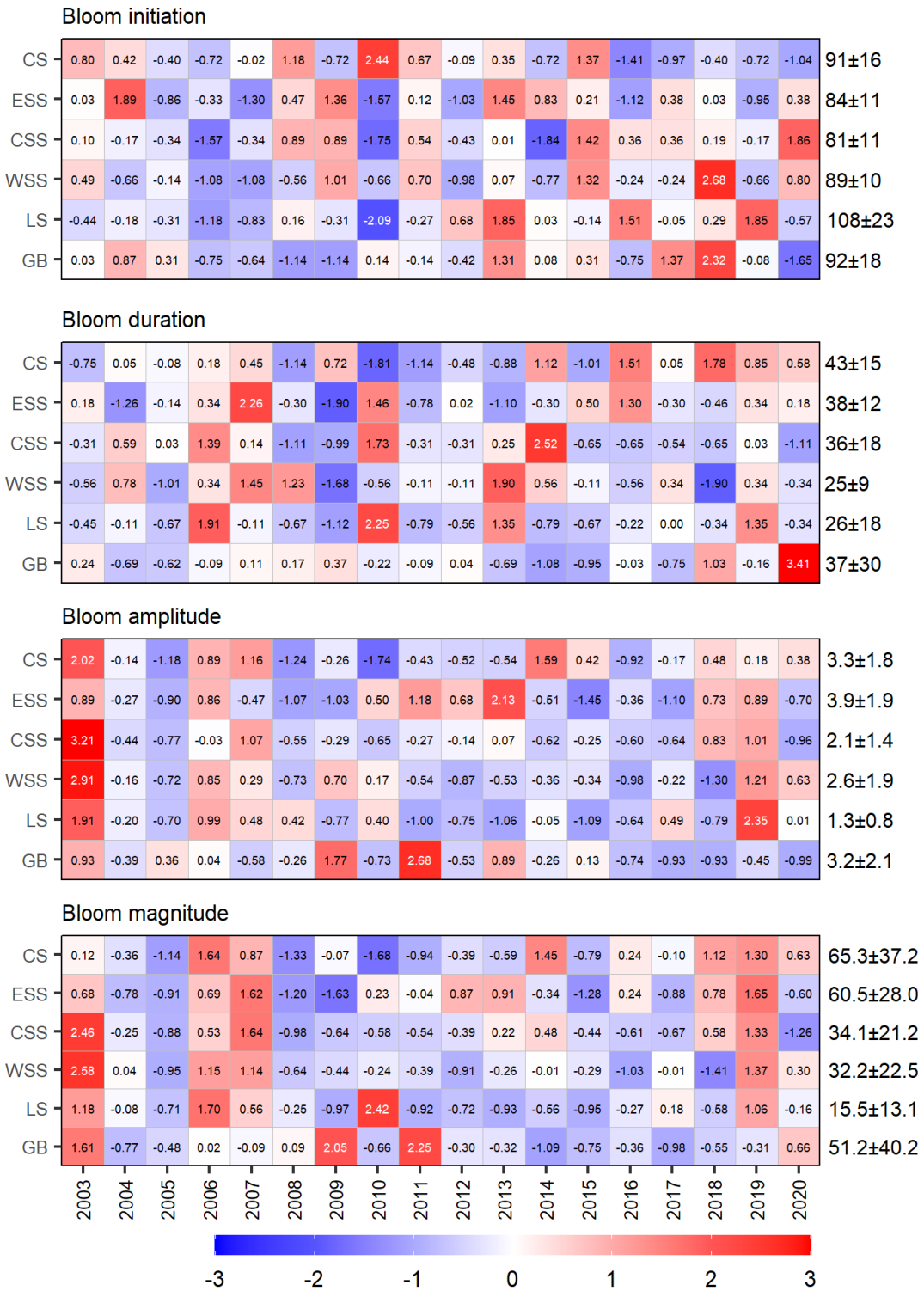

Figure 22. Annual anomaly scorecards for spring bloom parameters. Values in each cell are anomalies from the mean for the reference period, 2003–2020, in standard deviation (sd) units (mean and sd listed at right). Red (blue) cells indicate later (earlier) initiation, longer (shorter) duration or higher- (lower-) than-normal amplitude or magnitude. Gray cells indicate missing data.

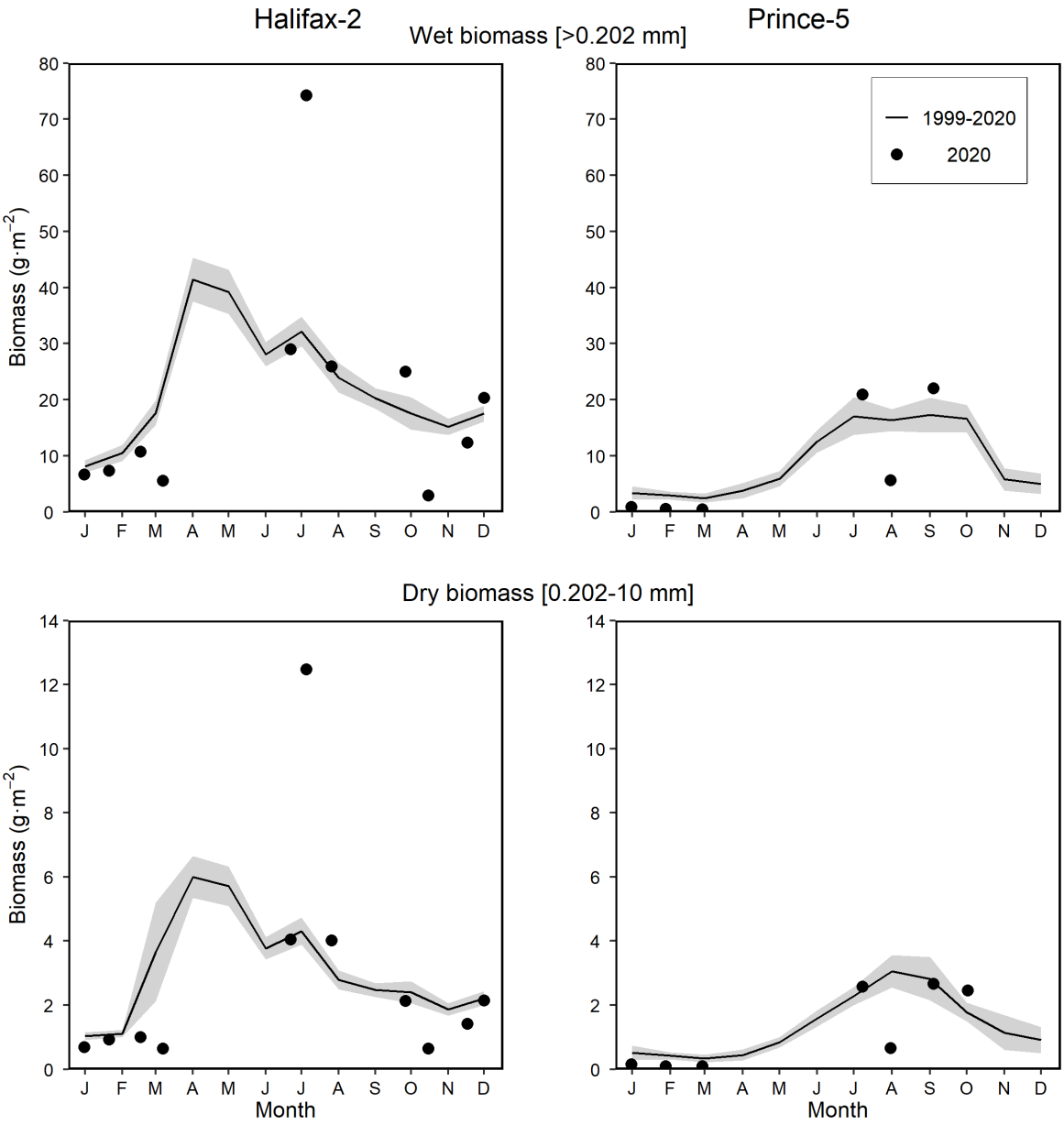

Figure 23. Zooplankton total wet biomass (upper panels) and mesozooplankton dry biomass (bottom panels) (integrated surface to bottom) in 2020 (solid circle) and mean conditions 1999–2020 (solid line) at the Maritimes high-frequency sampling stations. The gray shaded area represents the standard error of the monthly means. Left panels: Halifax-2; right panels: Prince-5. Tick marks on the horizontal axes indicate the 15th day of the month.

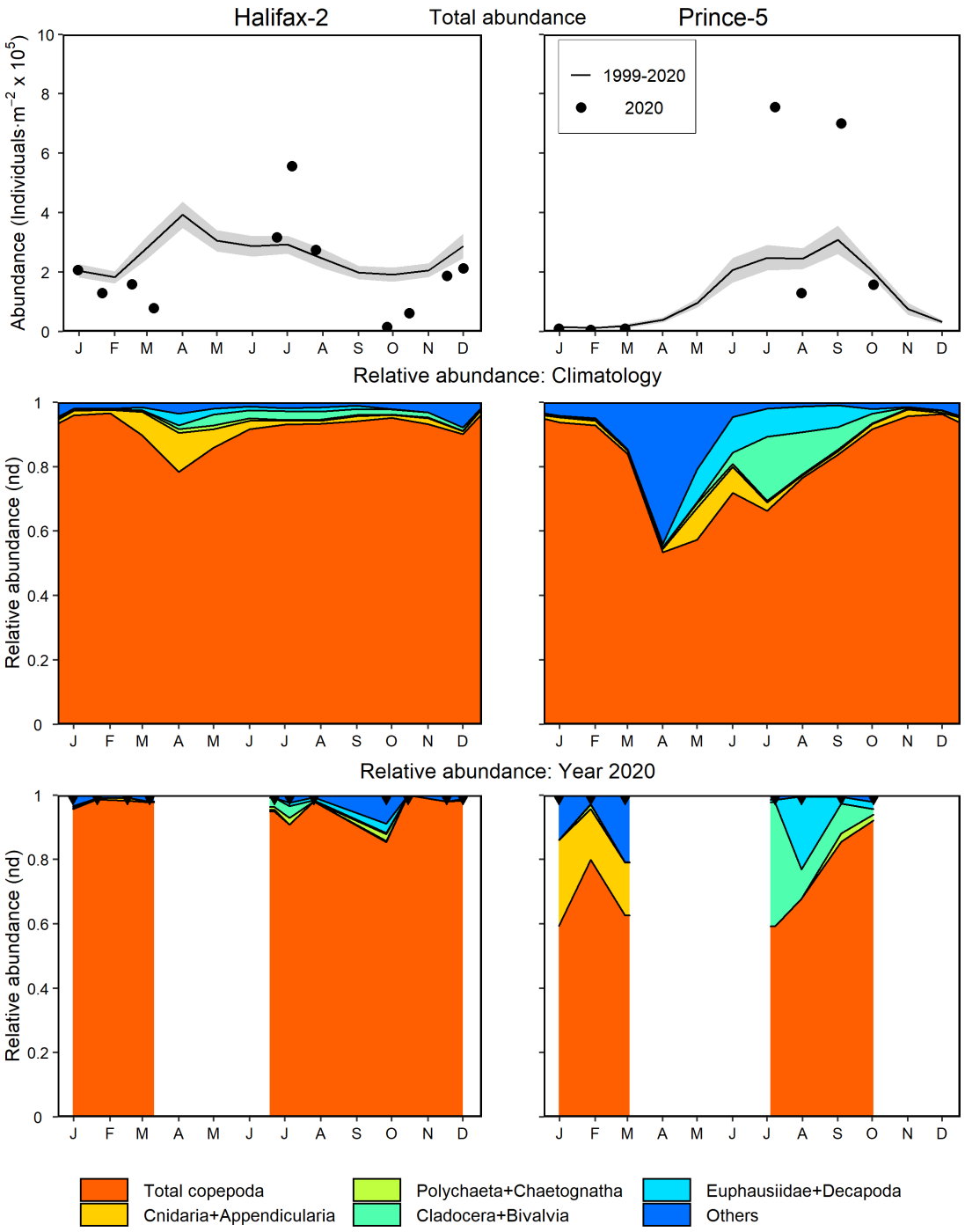

Figure 24. Zooplankton (> 200 µm) abundance and community composition in 2020 and mean conditions 1999–2020 at the Maritimes high-frequency sampling stations (Halifax-2, left panels; Prince-5, right panels). Upper panels: Zooplankton abundance in 2020 (solid circle) and mean conditions 1999–2020 (solid line). The gray shaded area represents the standard error of the monthly means. Middle panels: Climatology of major groups relative abundances 1999–2020. Lower panels: major groups relative abundances in 2020. nd = no dimensions. Black triangles in the bottom panels indicate sampling dates. Tick marks on the horizontal axes indicate the 15th day of the month. White areas indicate no data.

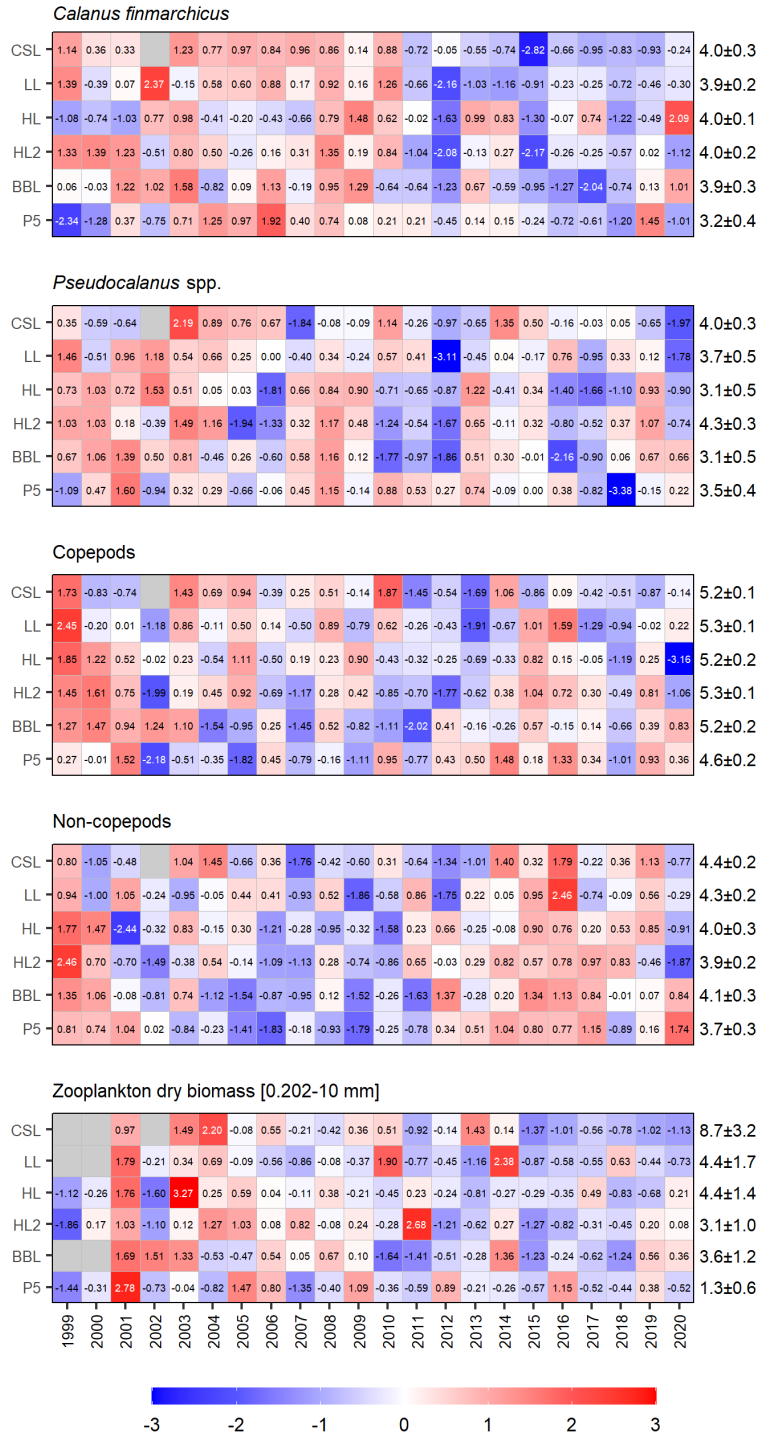

Figure 25. Annual anomaly scorecards for zooplankton abundance and biomass. Values in each cell are anomalies from the mean for the reference period, 1999–2020, in standard deviation (sd) units (mean and sd listed at right). Red (blue) cells indicate higher- (lower-) than-normal abundances or biomass. Gray cells indicate missing data. CSL: Cabot Strait section; LL: Louisbourg section; HL: Halifax section; HL2: Halifax-2; BBL: Browns Bank section; P5: Prince-5.

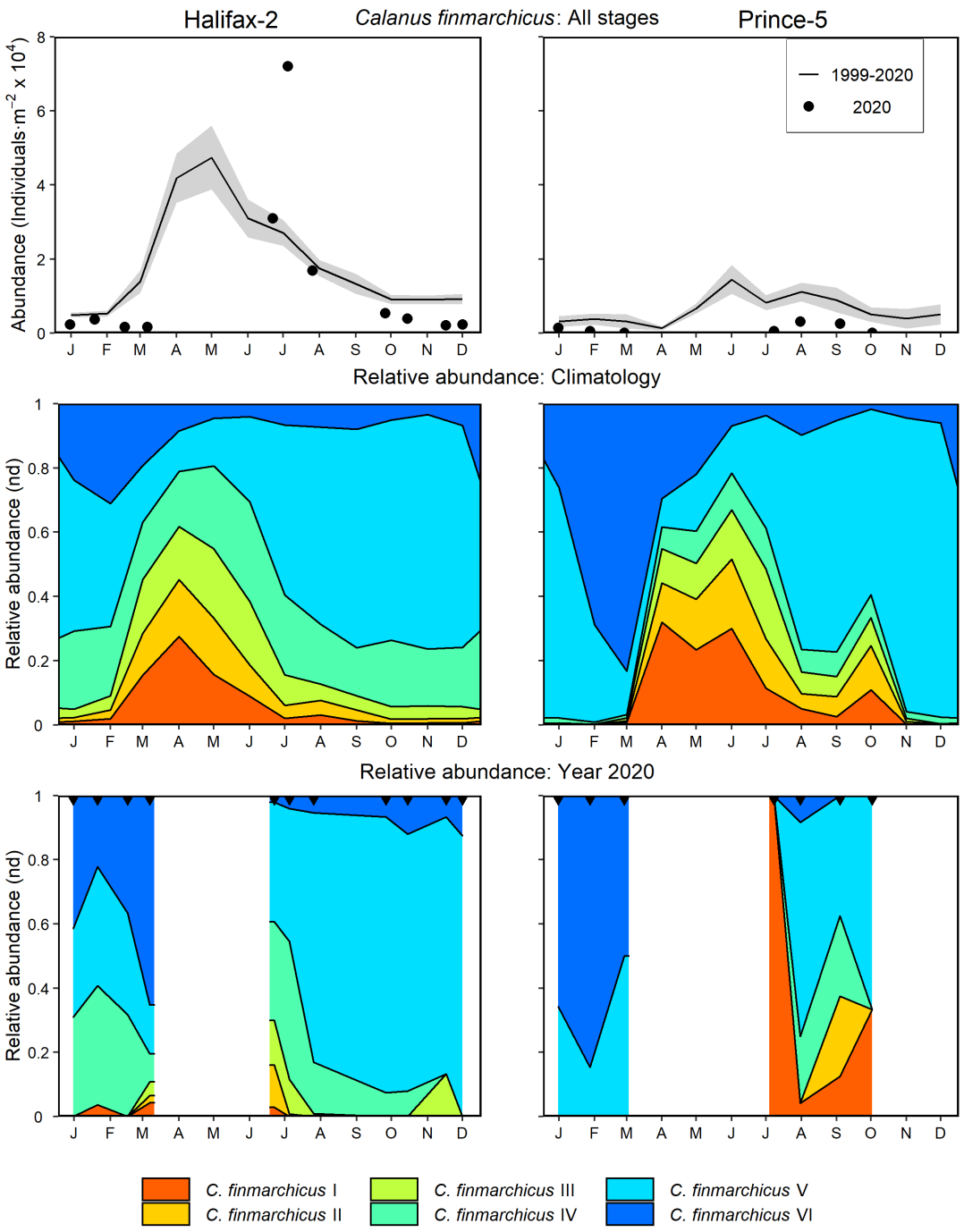

Figure 26. Calanus finmarchicus abundance and developmental stage distributions in 2020 and mean conditions 1999–2020 at the Maritimes high-frequency sampling stations (Halifax-2, left panels; Prince-5, right panels). Upper panels: C. finmarchicus abundance in 2020 (solid circle) and mean conditions 1999–2020 (solid line). The gray shaded area represents the standard error of the monthly means. Middle panels: Climatological C. finmarchicus stage relative abundances, 1999–2020. Lower panels: C. finmarchicus stage relative abundances in 2020. nd = no dimensions. Black triangles in the bottom panels indicate sampling dates. Tick marks on the horizontal axes indicate the 15th day of the month. White areas indicate no data.

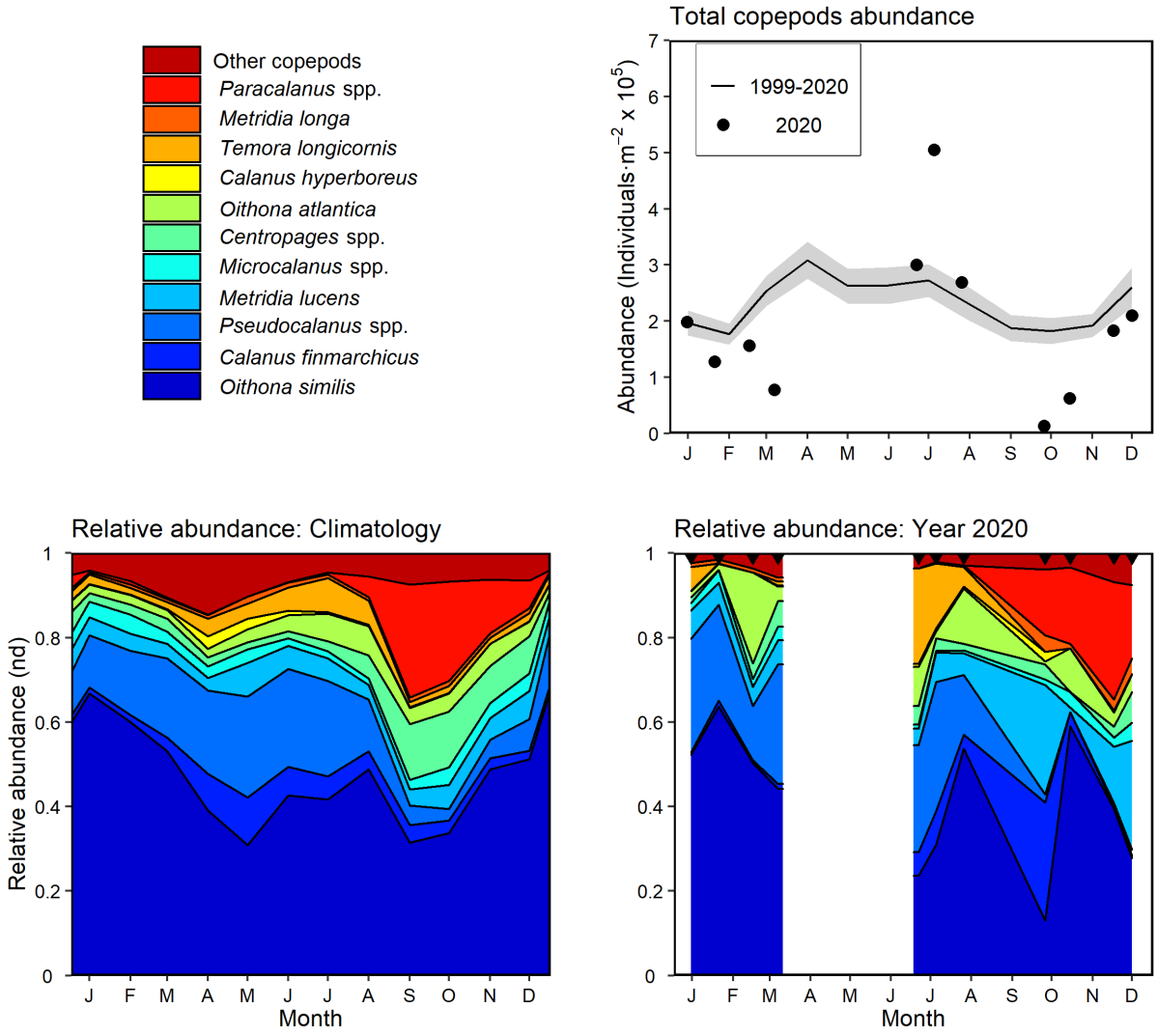

Figure 27a. Variability of dominant copepods at Halifax-2. The top 95% copepod taxa by abundance are shown individually; unidentified copepods (mostly nauplii) are grouped as "others". Upper right panel: copepod abundance in 2020 (solid circle) and mean conditions, 1999–2020 (solid line). The gray shaded area represents the standard error of the monthly means. Bottom left panel: Climatology of copepod relative abundances, 1999–2020. Bottom right panel: copepod relative abundance in 2020. nd = no dimensions. Black triangles in the middle right panel indicate sampling dates. Tick marks on the horizontal axes indicate the 15th day of the month. White areas indicate no data.

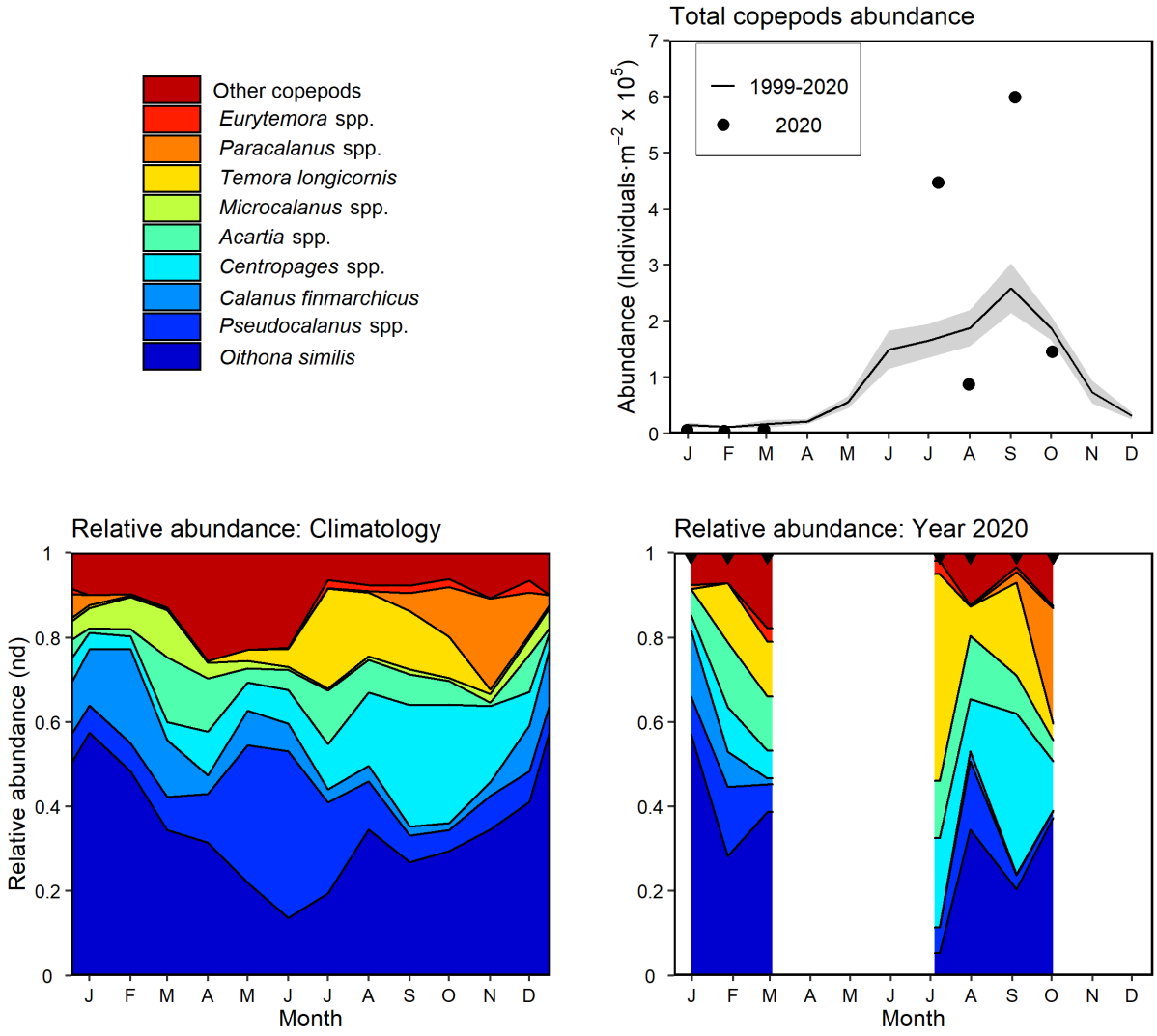

Figure 27b. Variability of dominant copepods at Prince-5. The top 95% copepod taxa by abundance are shown individually; unidentified copepods (mostly nauplii) are grouped as "others". Upper right panel: copepod abundance in 2020 (solid circle) and mean conditions, 1999–2020 (solid line). The gray shaded area represents the standard error of the monthly means. Bottom left panel: Climatology of copepod relative abundances, 1999–2020. Bottom right panel: copepod relative abundance in 2020. nd = no dimensions. Black triangles in the middle right panel indicate sampling dates. Tick marks on the horizontal axes indicate the 15th day of the month. White areas indicate no data.

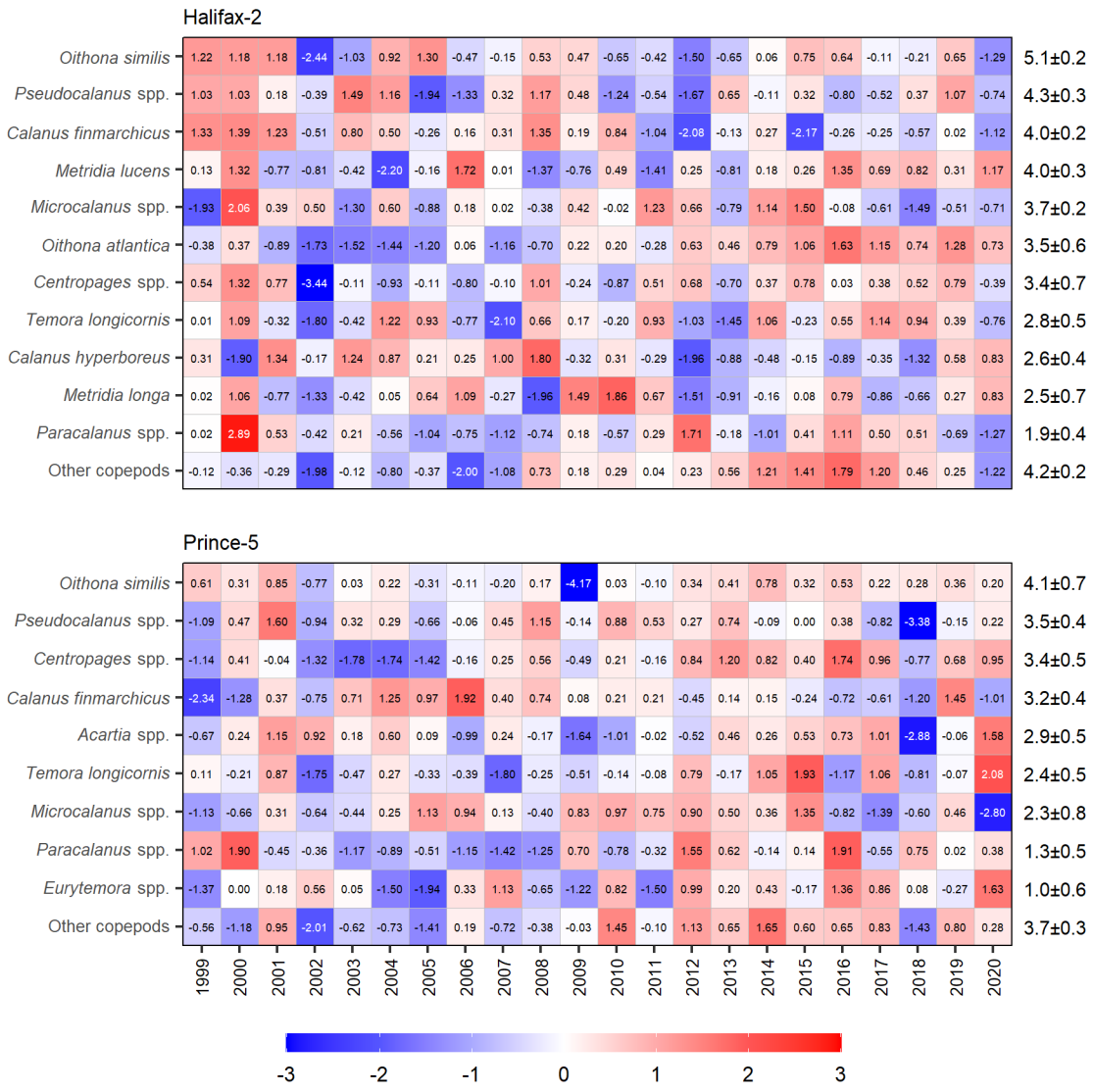

Figure 28. Annual anomaly scorecards for dominant copepods abundances at the Maritimes high-frequency sampling stations (top panel: Halifax-2; bottom panel: Prince-5). Values in each cell are anomalies from the mean for the reference period, 1999–2020, in standard deviation (sd) units (mean and sd listed at right). Red (blue) cells indicate higher- (lower-) than-normal abundances. Gray cells indicate missing data.

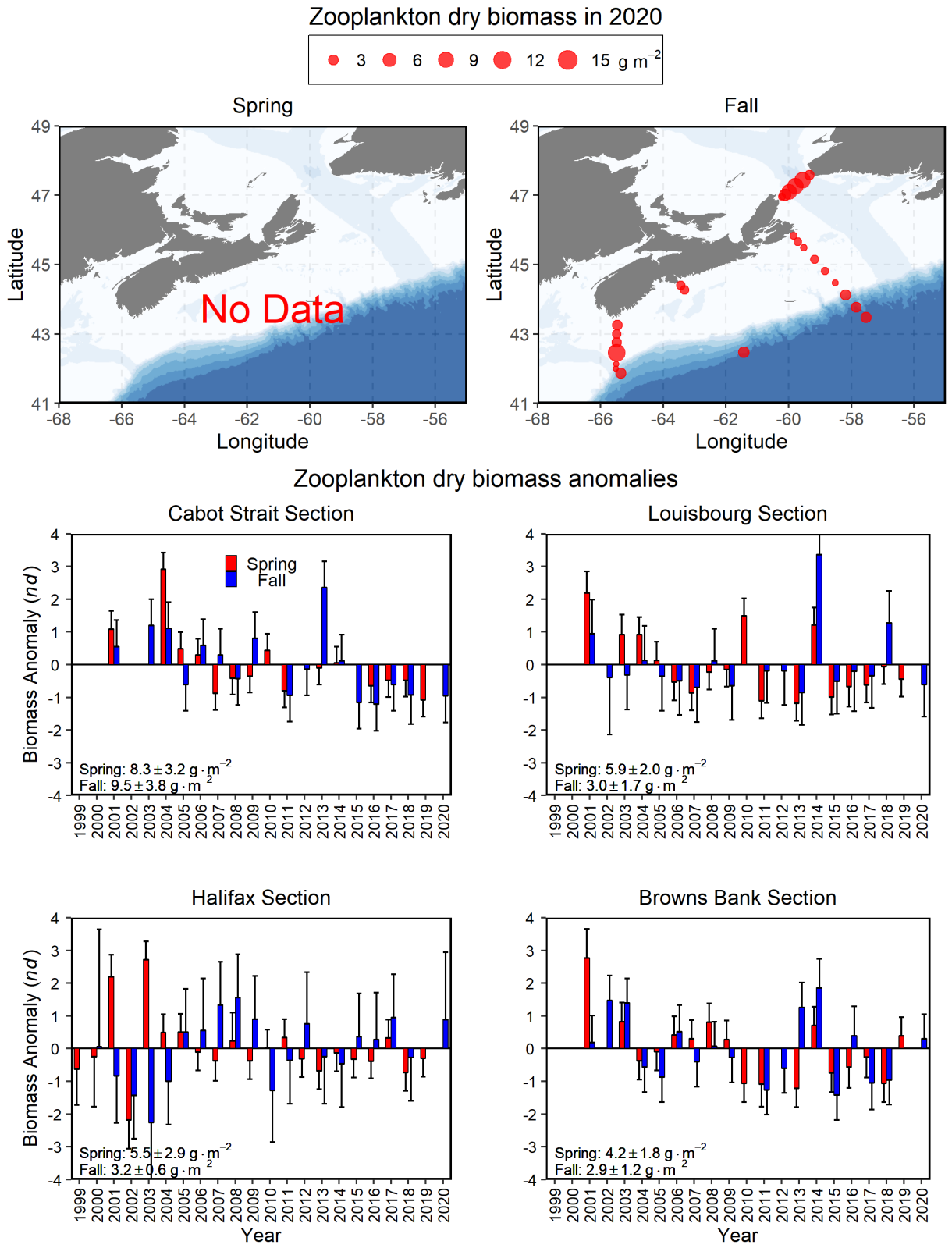

Figure 29. Spatial distribution of zooplankton dry biomass in 2020 (upper panels) and time series of zooplankton dry biomass anomalies on Scotian Shelf sections (middle and lower panels) in spring and fall, 1999–2020. Vertical lines in lower panels represent standard errors.

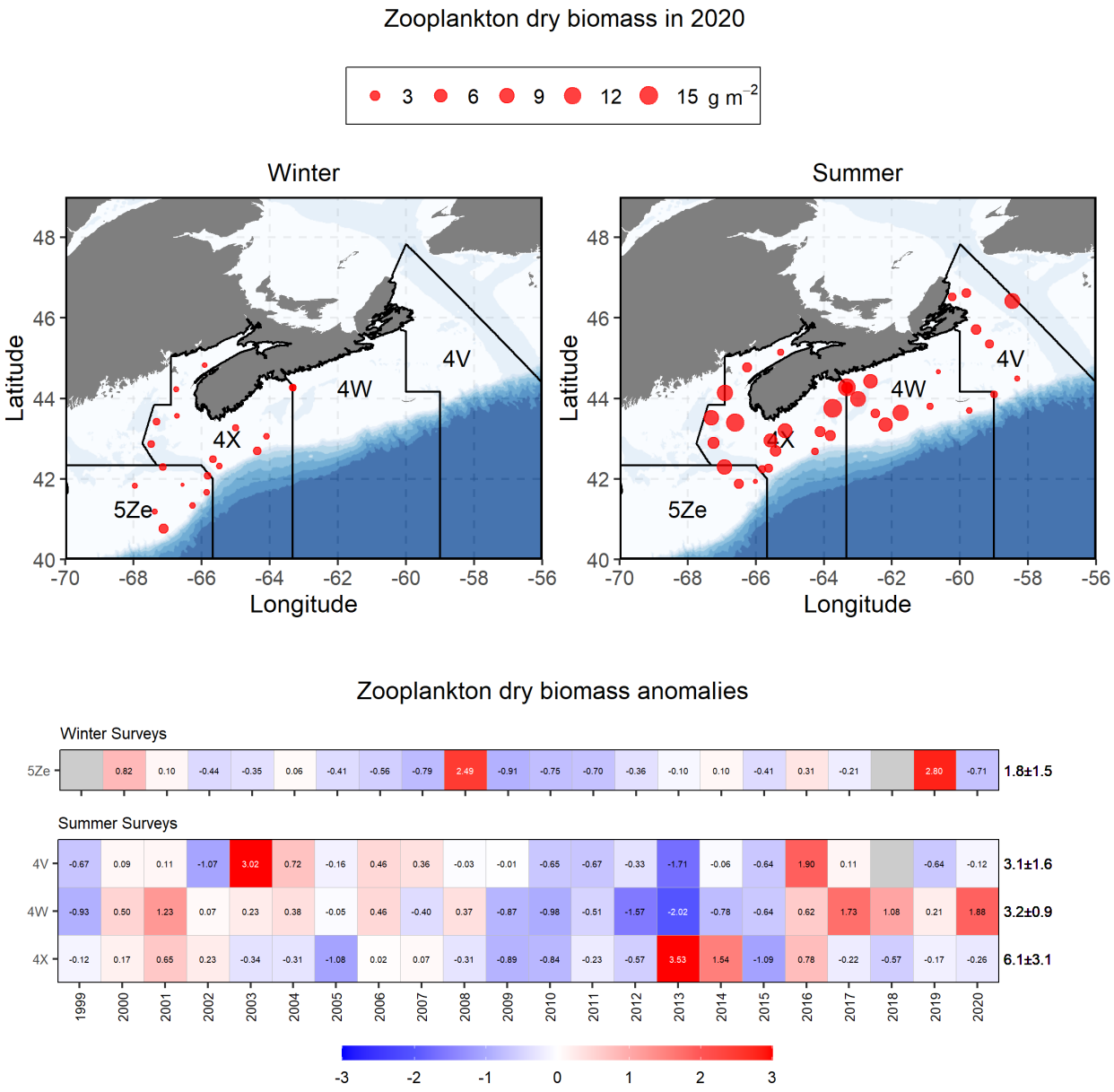

Figure 30. Spatial distribution of zooplankton dry biomass in 2020 (upper panels) and seasonal anomaly scorecards of zooplankton dry biomass (lower panels) from ecosystem trawl surveys on Georges Bank (5Ze in winter) and the Scotian Shelf and eastern Gulf of Maine (4X, 4W, and 4V in summer), 1999–2020. Values in each cell are anomalies from the mean for the reference period, 1999–2020, in standard deviation (sd) units (mean and sd listed at right). Red (blue) cells indicate higher- (lower-) than-normal biomass. Gray cells indicate missing data.

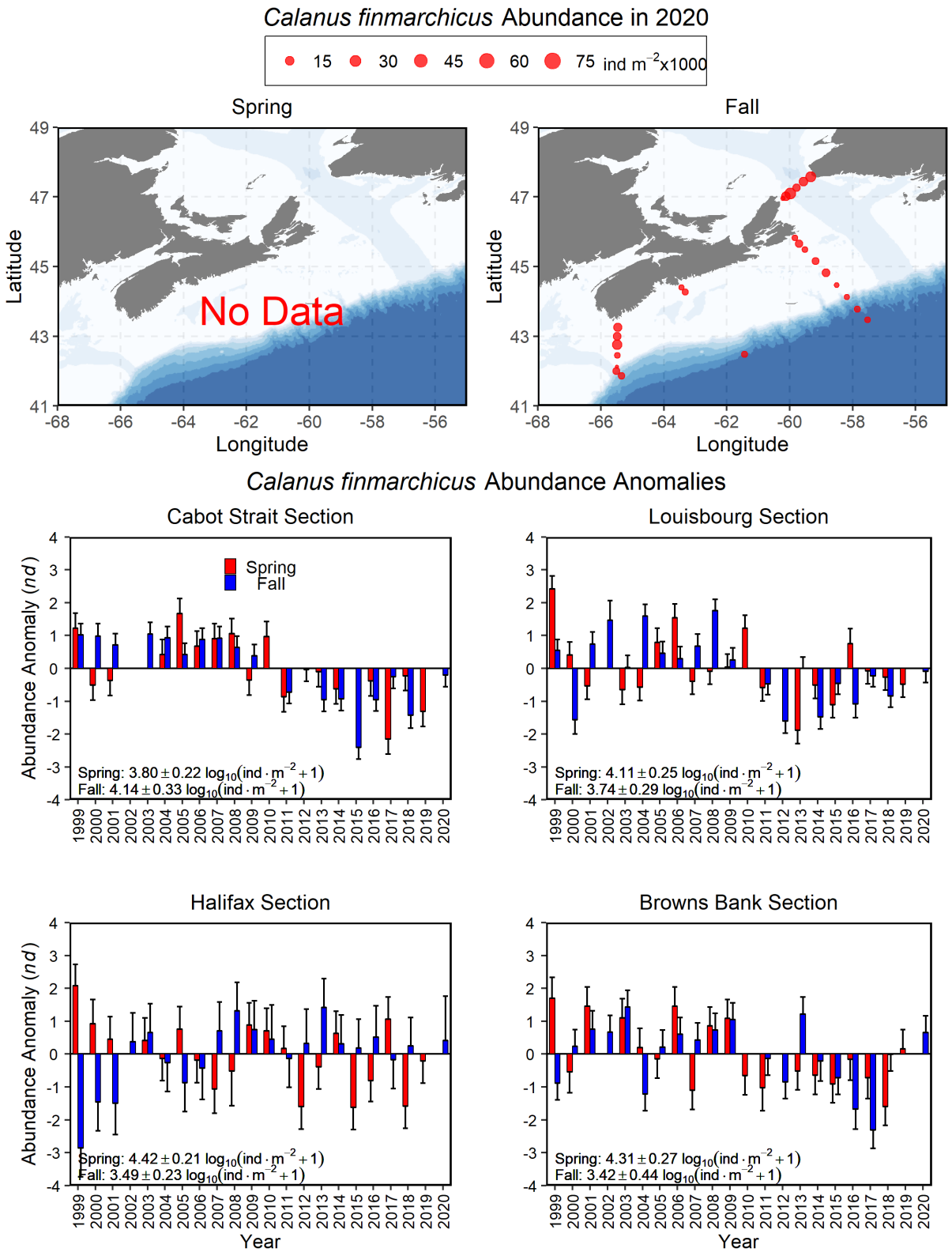

Figure 31. Spatial distribution of Calanus finmarchicus abundance in 2020 (upper panels) and time series of C. finmarchicus abundance anomalies on Scotian Shelf sections (middle and lower panels) in spring and fall, 1999–2020. Vertical lines in lower panels represent standard errors.

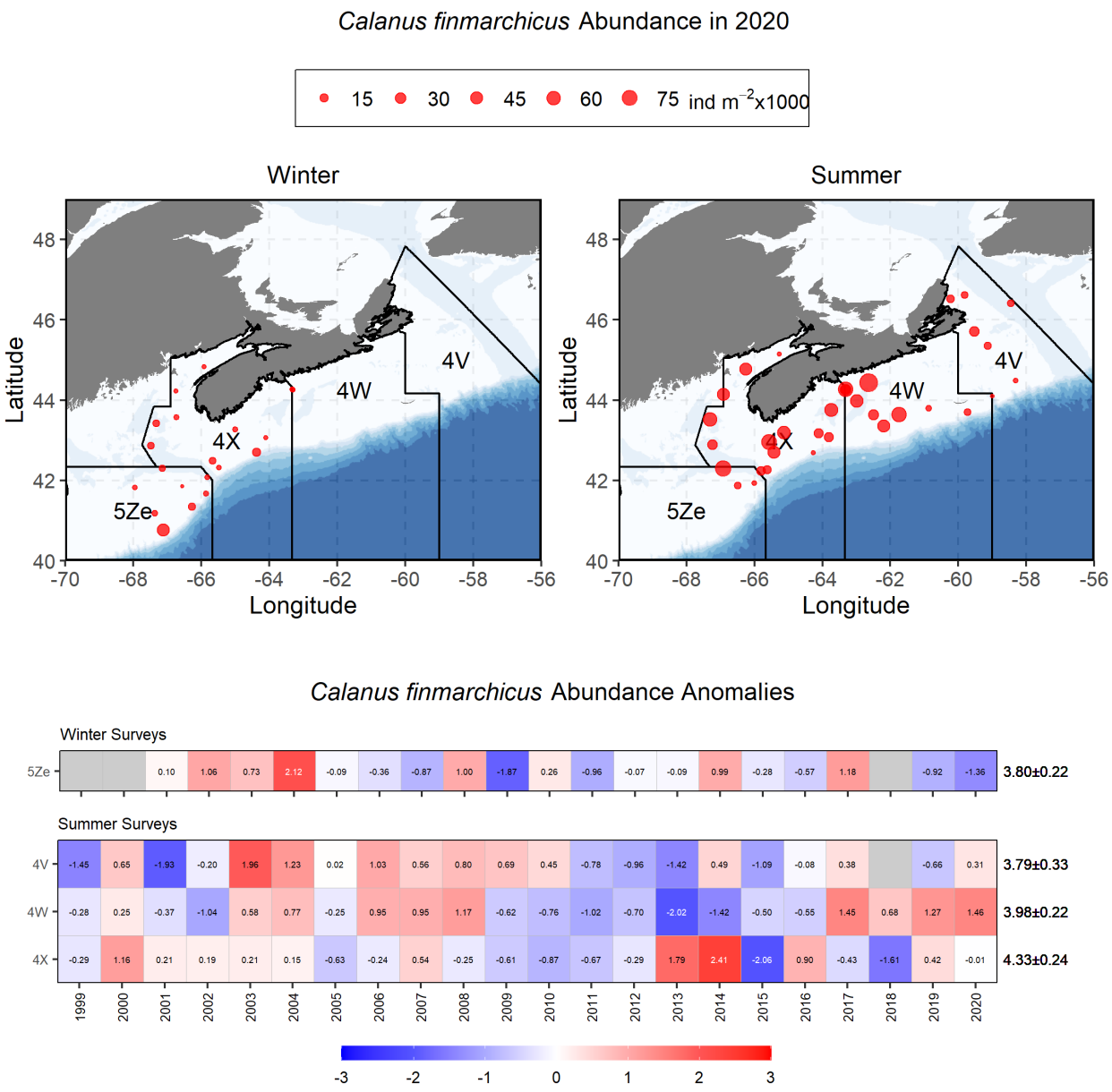

Figure 32. Spatial distribution of Calanus finmarchicus abundance in 2020 (upper panels) and seasonal anomaly scorecards of C. finmarchicus abundance (lower panels) from ecosystem trawl surveys on Georges Bank (5Ze in winter) and the Scotian Shelf and eastern Gulf of Maine (4X, 4W, and 4V in summer), 1999–2020. Values in each cell are anomalies from the mean for the reference period, 1999–2020, in standard deviation (sd) units (mean and sd listed at right). Red (blue) cells indicate higher-(lower-) than-normal abundances. Gray cells indicate missing data.

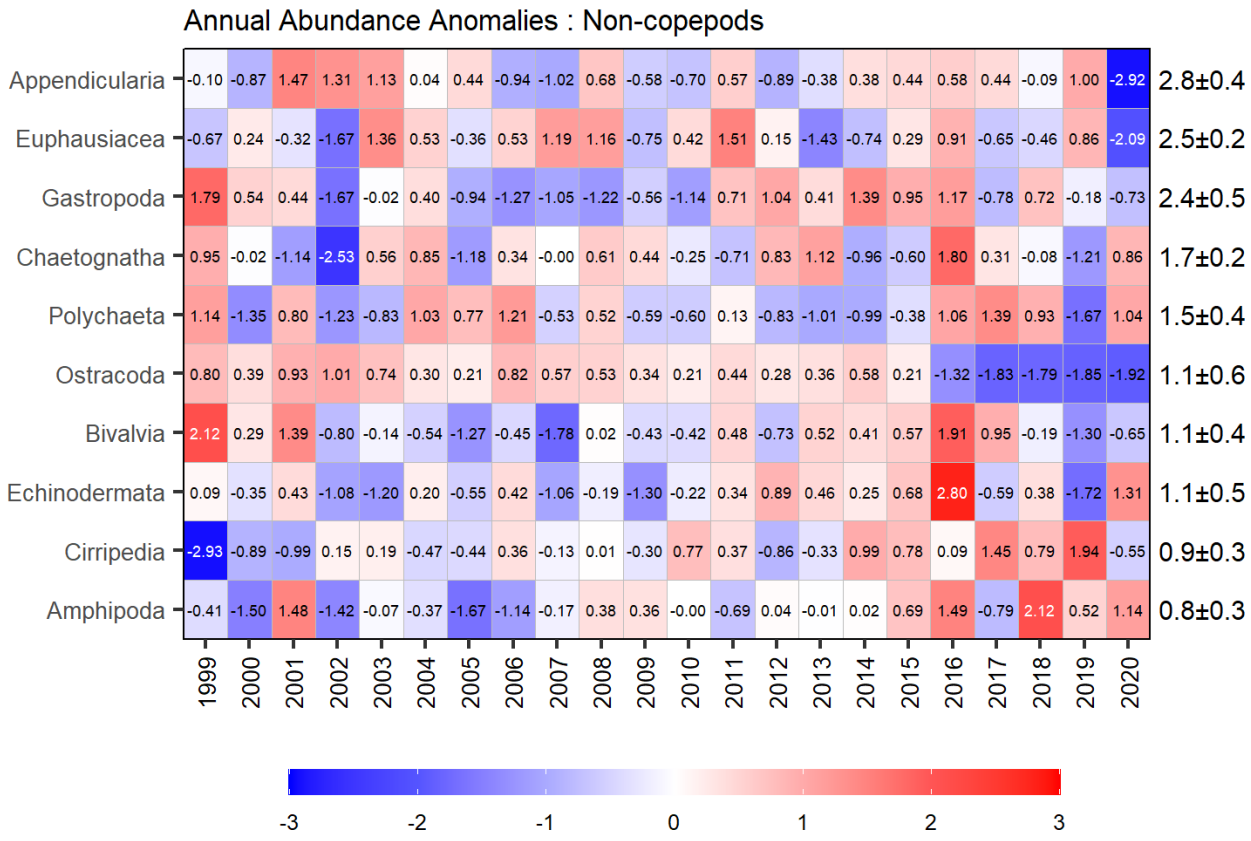

Figure 33. Annual anomaly scorecard for non-copepod groups abundances on the Scotian Shelf sections, ordered from higher- to lower-abundance. Values in each cell are anomalies from the mean for the reference period, 1999–2020, in standard deviation (sd) units (mean and sd listed at right). Red (blue) cells indicate higher- (lower-) than-normal abundances.

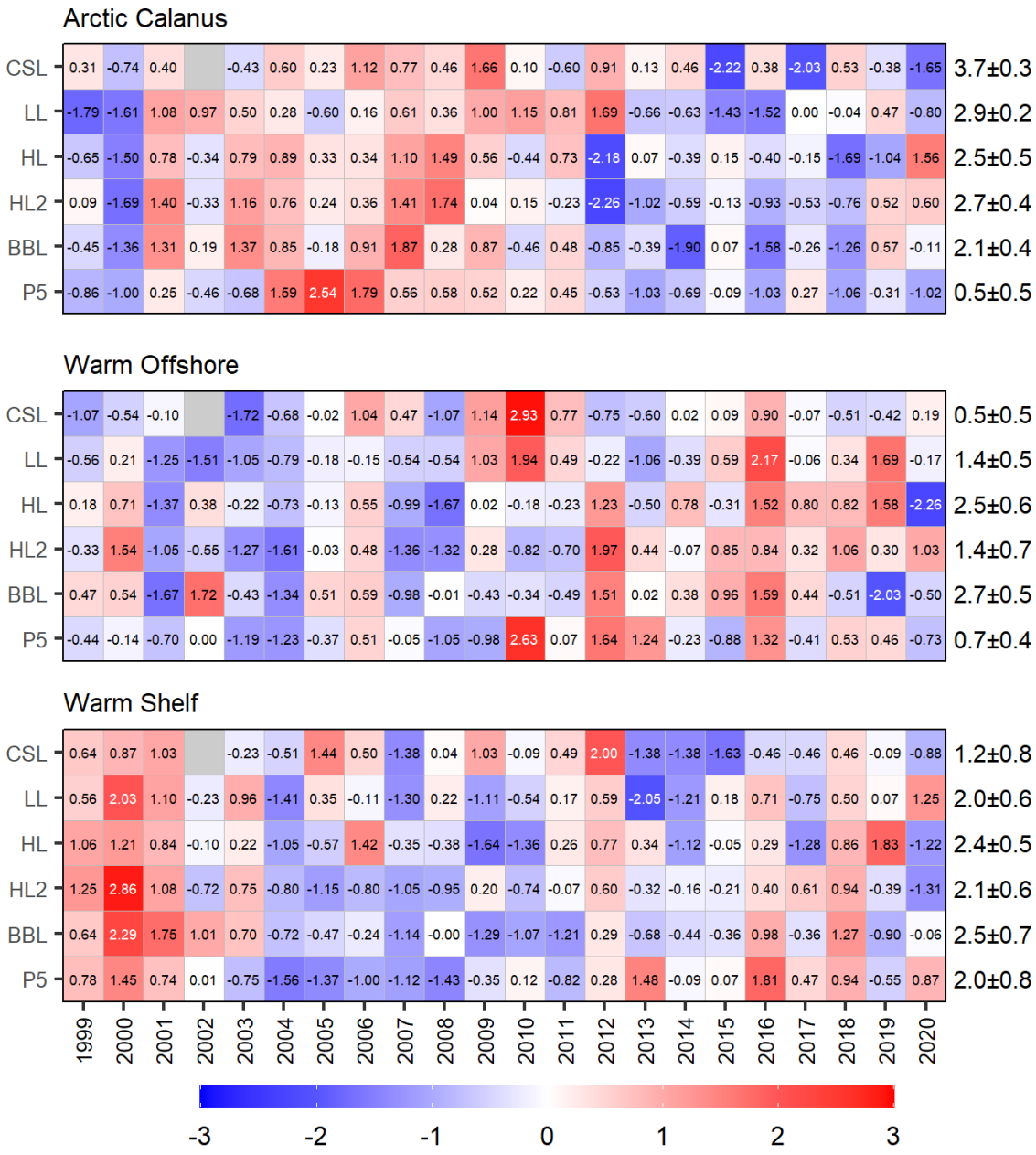

Figure 34. Annual anomaly scorecards for copepod indicator species grouped abundances. Values in each cell are anomalies from the mean for the reference period, 1999–2020, in standard deviation (sd) units (mean and sd listed at right). Red (blue) cells indicate higher- (lower-) than-normal abundances. Gray cells indicate missing data. CSL: Cabot Strait section; LL: Louisbourg section; HL: Halifax section; HL2: Halifax-2; BBL: Browns Bank section; P5: Prince-5. Gray cells indicate missing data.

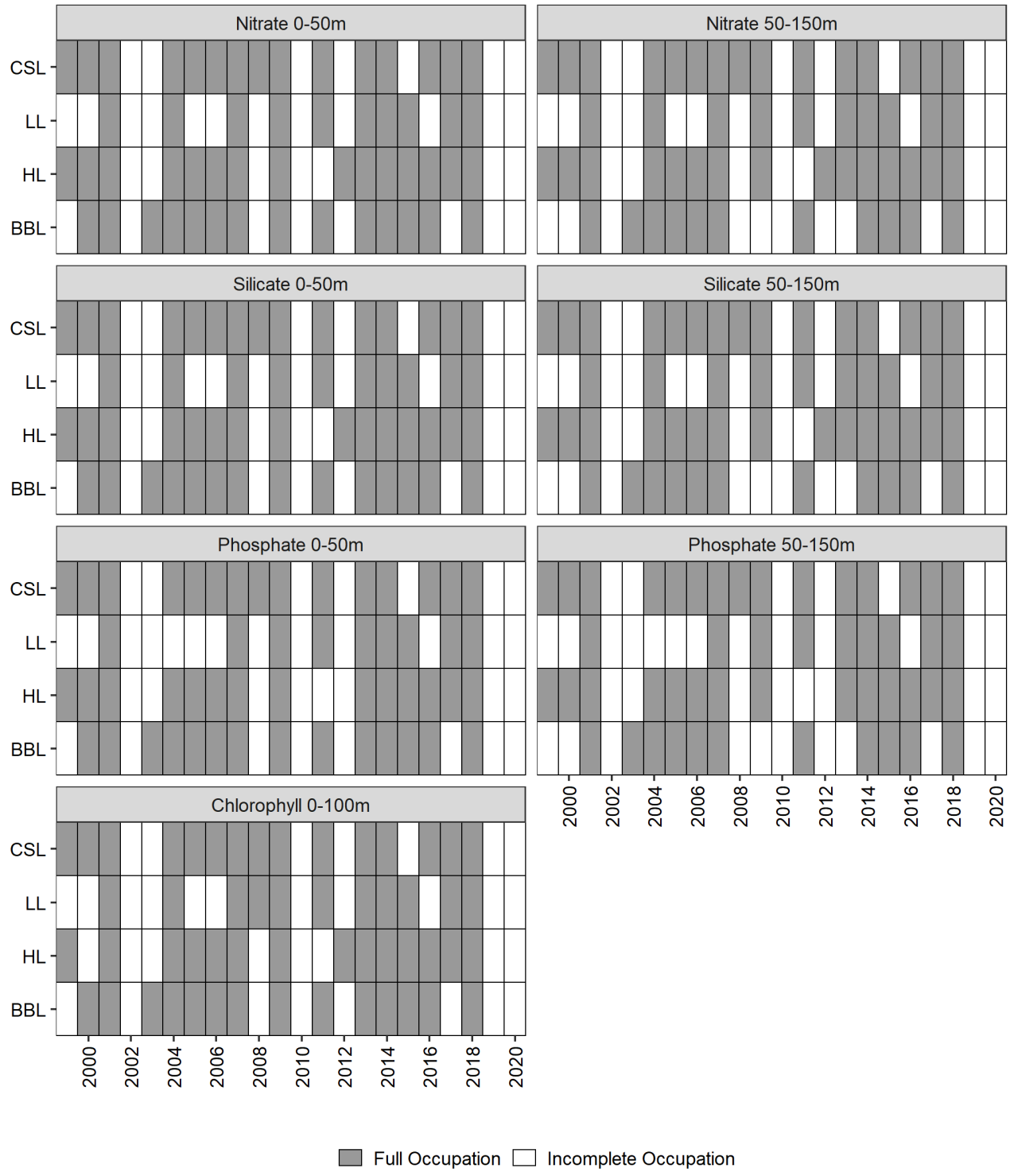

Figure 35a. Summary of sections occupation for the nutrients and chlorophyll a indices. Gray cells indicate years with full annual occupation (i.e., spring and fall) for a given index and section. White cells indicate years with incomplete annual occupation resulting from missing sampling at either one or multiple stations on a section. CSL: Cabot Strait section; LL: Louisbourg section; HL: Halifax section; BBL: Browns Bank section.

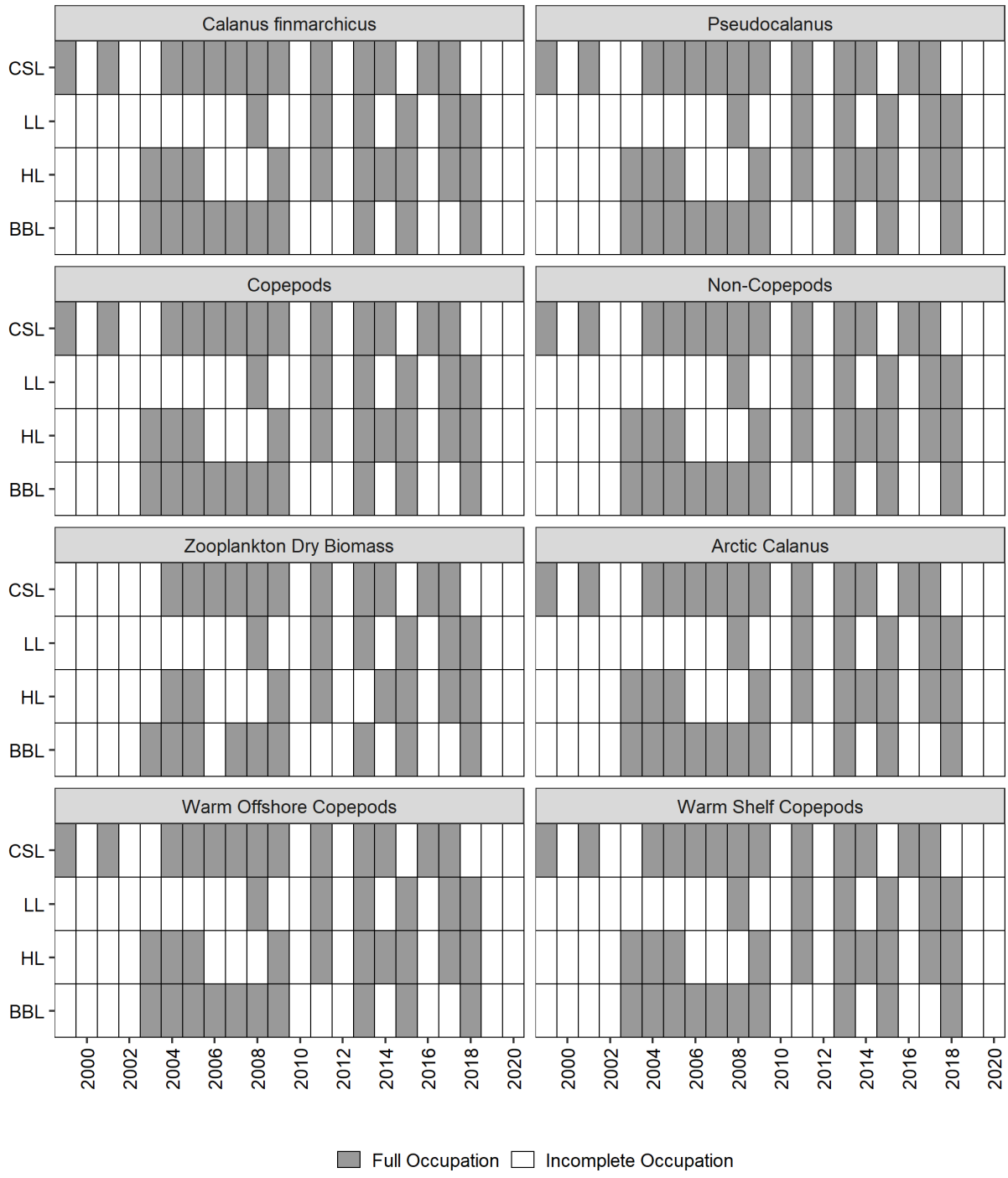

Figure 35b. Summary of sections occupation for the zooplankton indices. Gray cells indicate years with full annual occupation (i.e., spring and fall) for a given index and section. White cells indicate years with incomplete annual occupation resulting from missing sampling at either one or multiple stations on a section. CSL: Cabot Strait section; LL: Louisbourg section; HL: Halifax section; BBL: Browns Bank section.

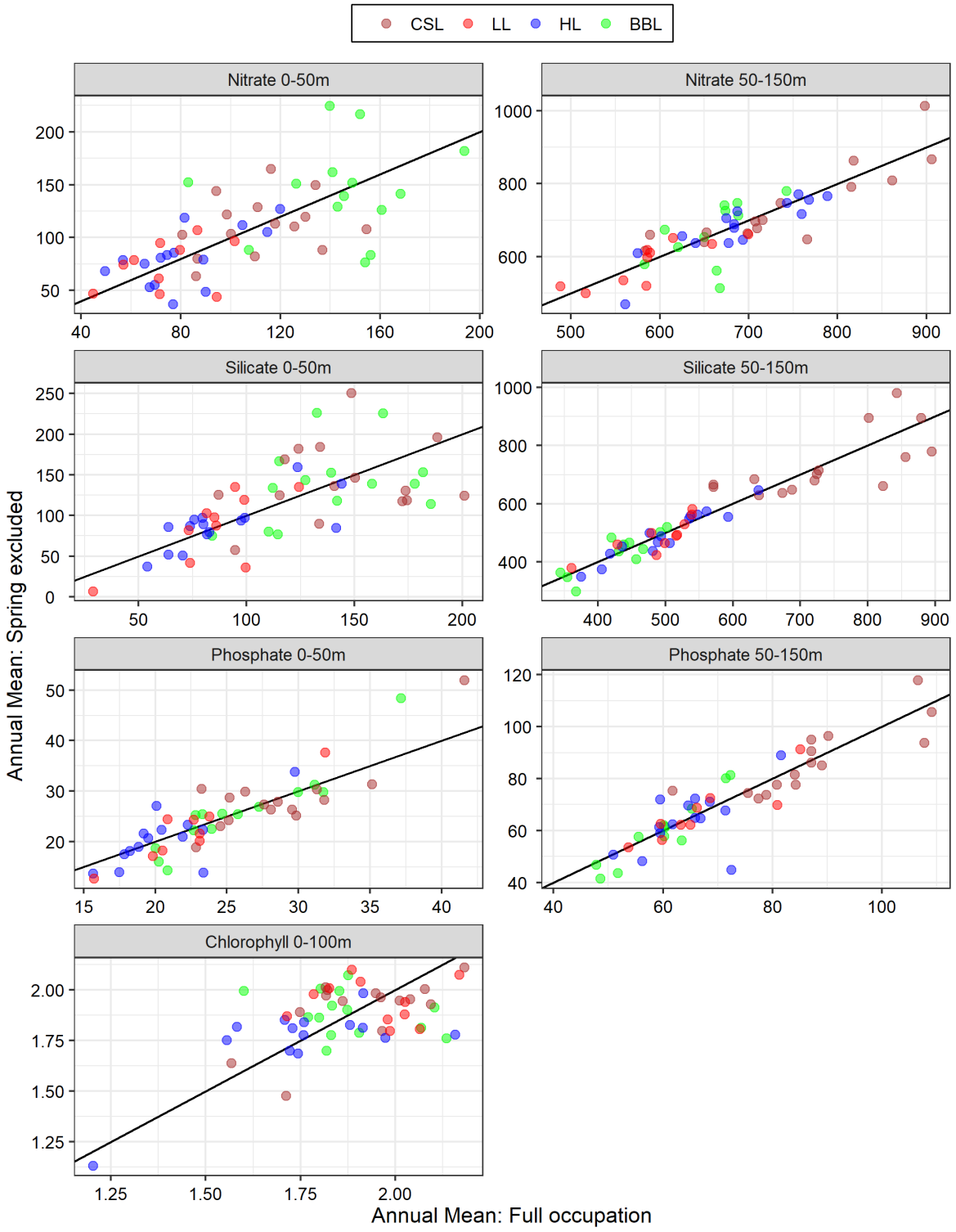

Figure 36a. Relationship between the annual unbiased mean (x-axis) and the estimated annual mean resulting from the exclusion of spring data (y-axis) for the nutrients and chlorophyll a indices. Data points represent the individual years with full occupation for each index and section. CSL: Cabot Strait section; LL: Louisbourg section; HL: Halifax section; BBL: Browns Bank section. The black line is the identity line.

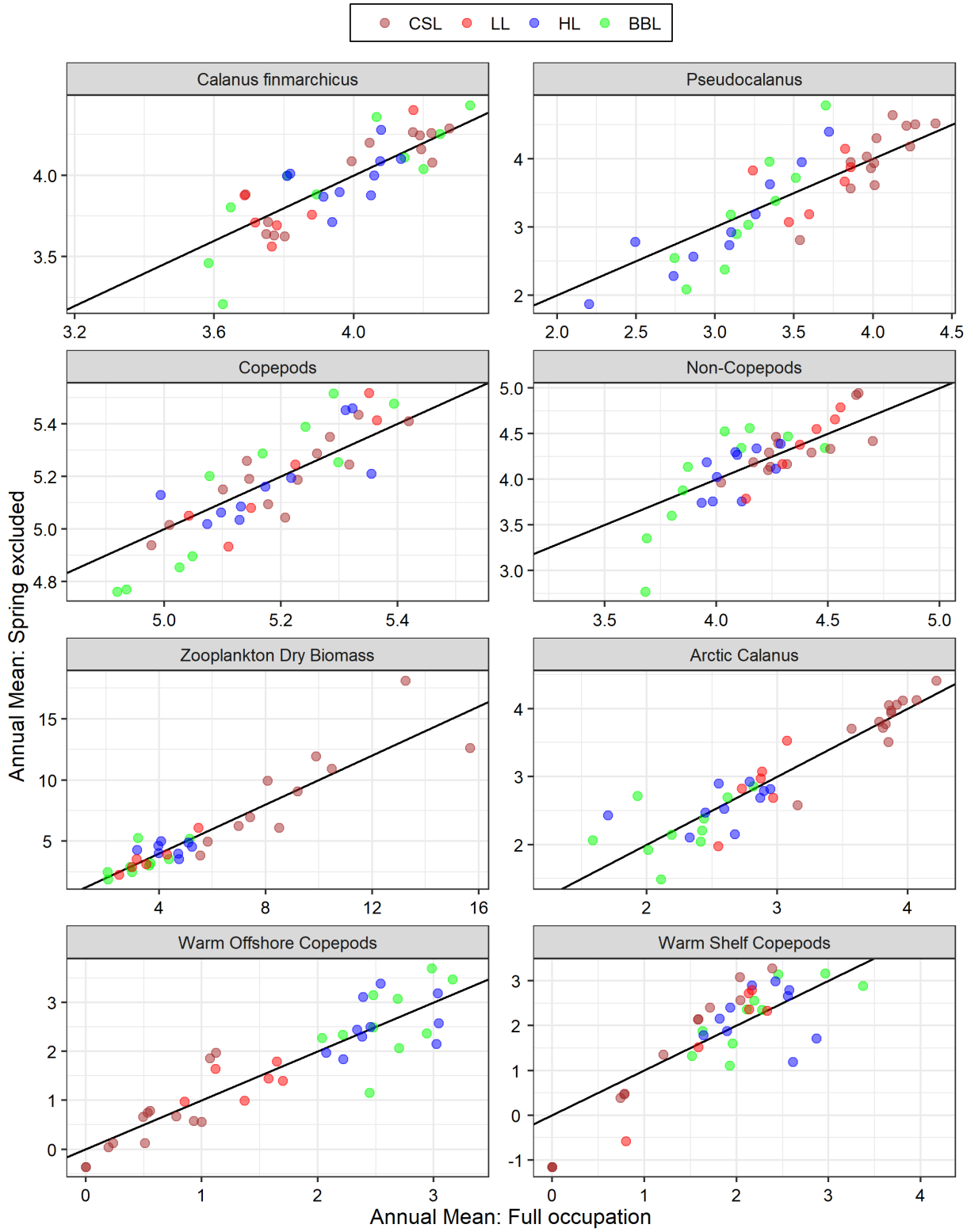

Figure 36b. Relationship between the unbiased annual mean (x-axis) and the estimated annual mean resulting from the exclusion of spring data (y-axis) for the zooplankton indices. Data points represent the individual years with full occupation for each index and section. CSL: Cabot Strait section; LL: Louisbourg section; HL: Halifax section; BBL: Browns Bank section. The black line is the identity line.

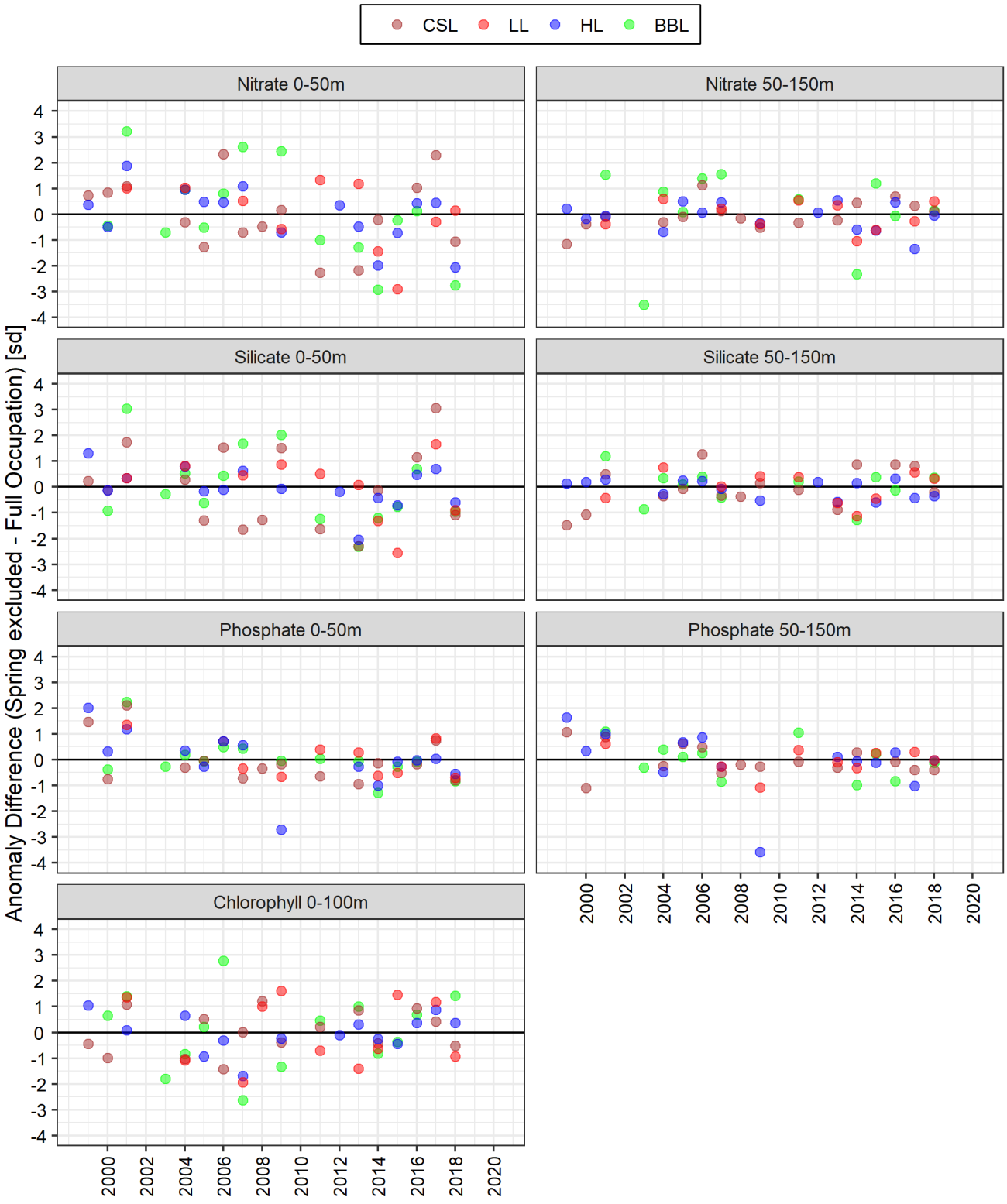

Figure 37a. Difference between the annual normalized anomaly resulting from the exclusion of spring data and the unbiased anomaly calculated from full occupation for the nutrients and chlorophyll a indices. Data points represent the years with full occupation for each index and section. CSL: Cabot Strait section; LL: Louisbourg section; HL: Halifax section; BBL: Browns Bank section.

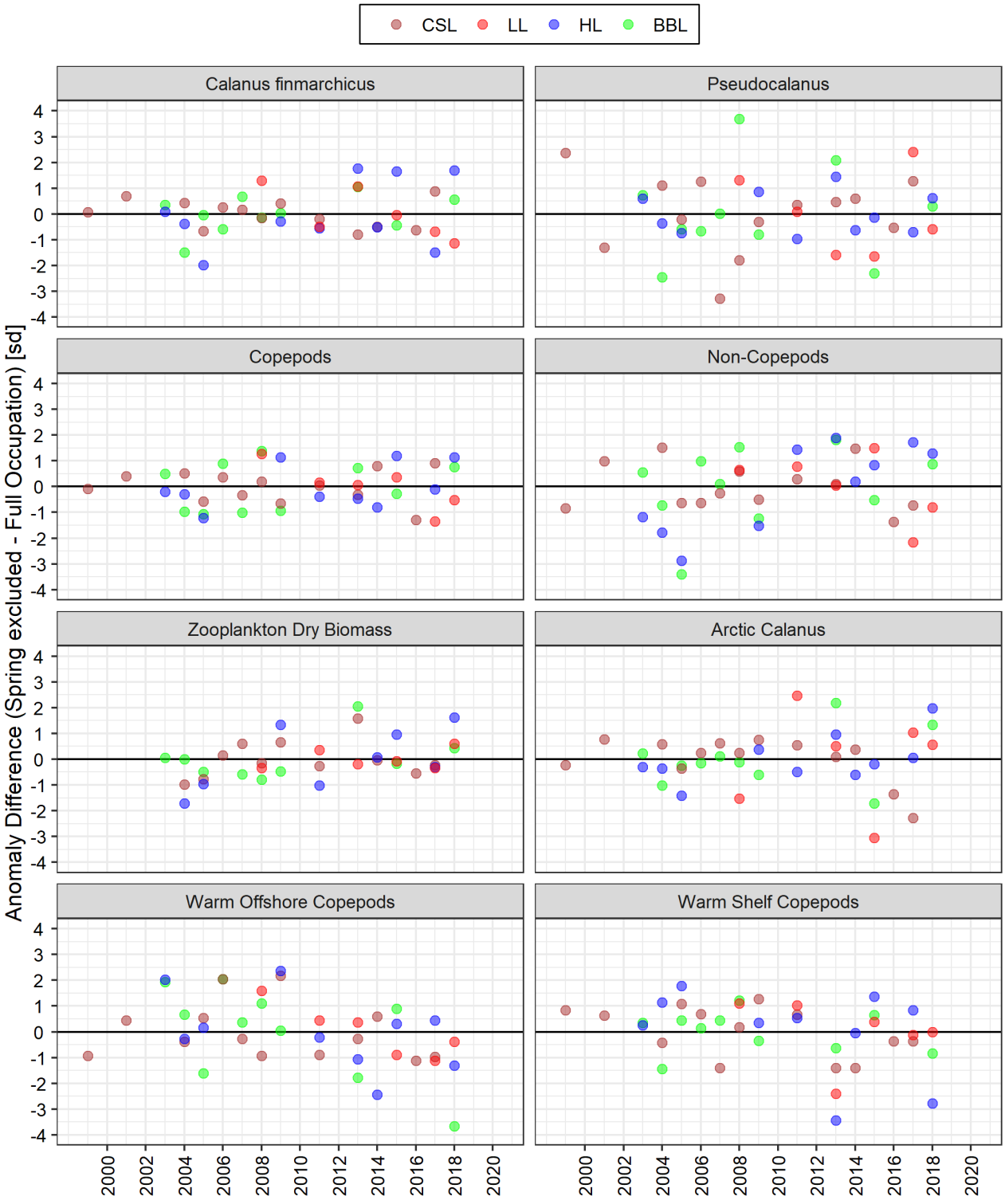

Figure 37b. Difference between the annual normalized anomaly resulting from the exclusion of spring data and the unbiased anomaly calculated from full occupation for the zooplankton indices. Data points represent the years with full occupation for each index and section. CSL: Cabot Strait section; LL: Louisbourg section; HL: Halifax section; BBL: Browns Bank section.

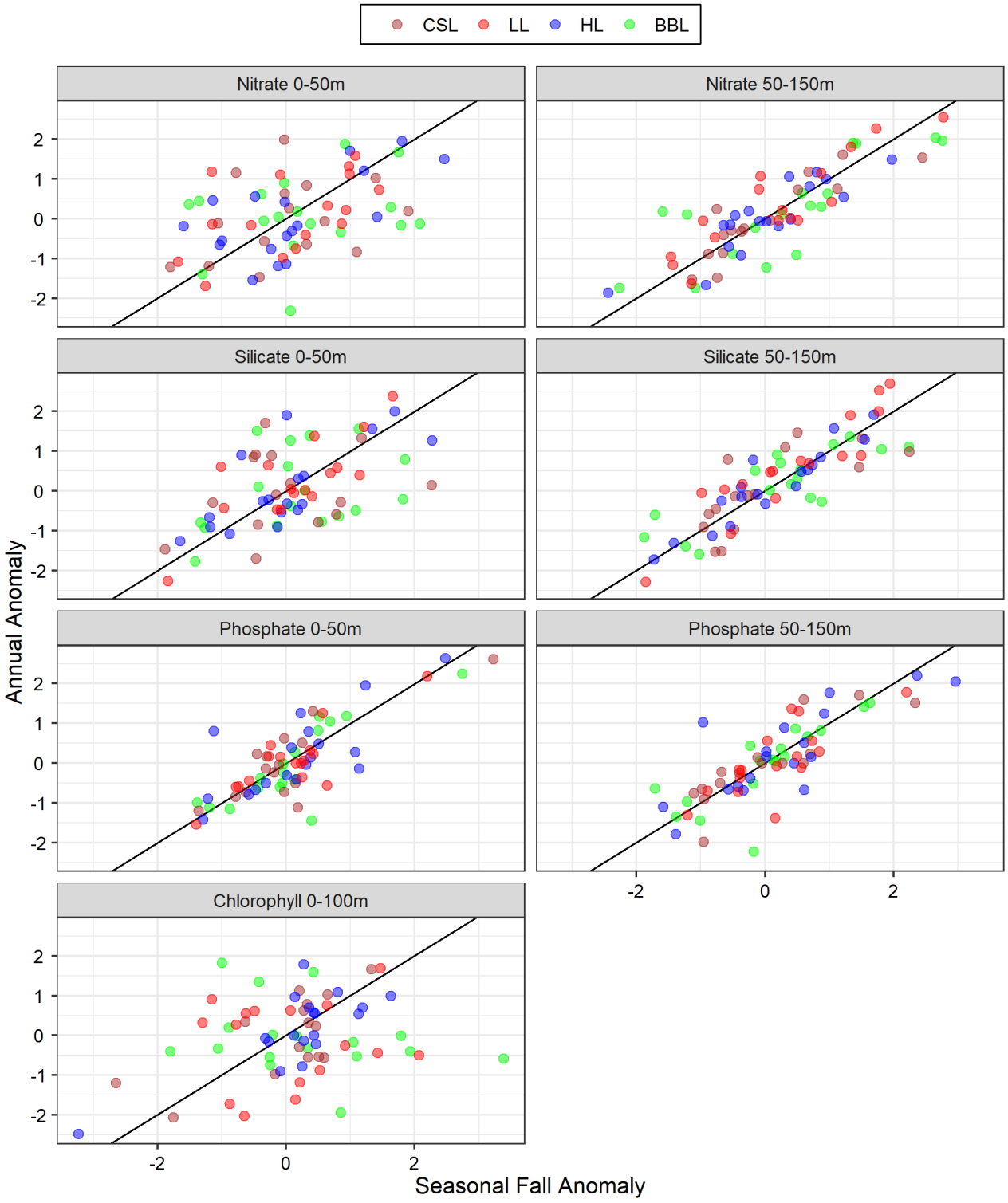

Figure 38a. Relationship between the unbiased annual and fall normalized anomalies for the nutrients and chlorophyll a indices. Data points represent the individual years with full occupation for each index and section. CSL: Cabot Strait section; LL: Louisbourg section; HL: Halifax section; BBL: Browns Bank section. The black line is the identity line.

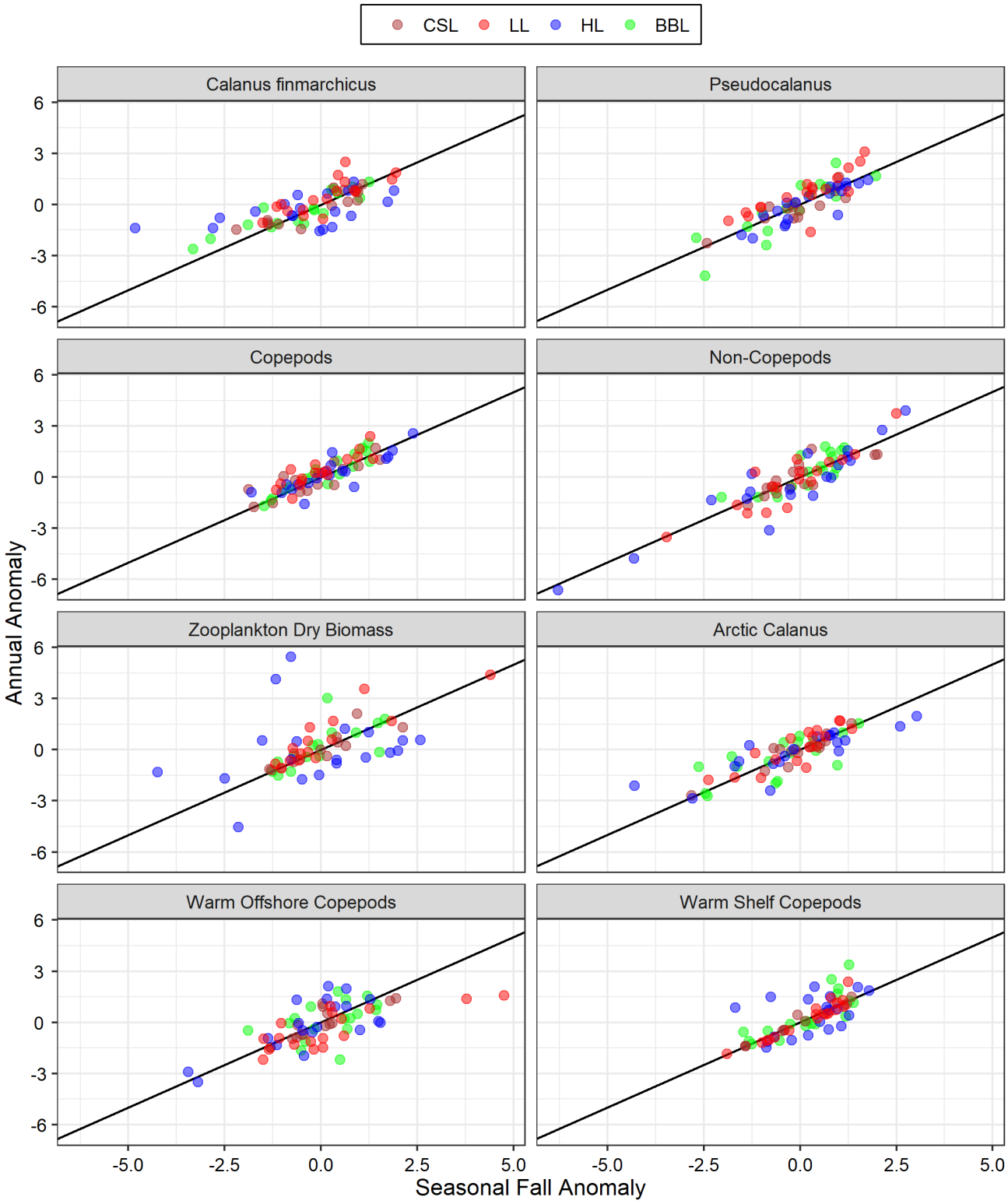

Figure 38b. Relationship between the unbiased annual and fall normalized anomalies for the zooplankton indices. Data points represent the individual years with full section occupation for each index and section. CSL: Cabot Strait section; LL: Louisbourg section; HL: Halifax section; BBL: Browns Bank section. The black line is the identity line.

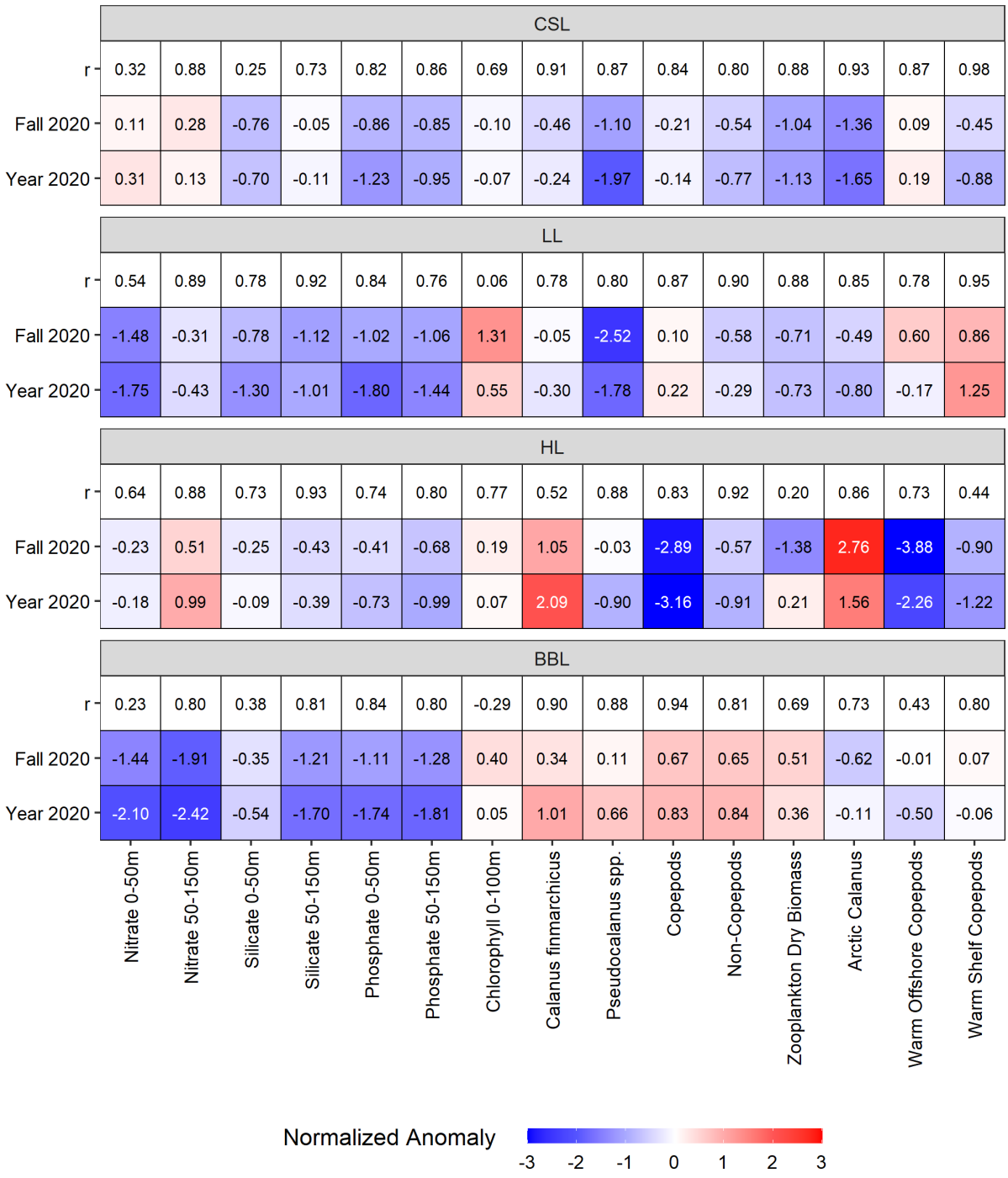

Figure 39. Comparison of 2020 annual and fall normalized anomalies. For each section, the first row indicates the correlation coefficient (r) between the annual and the fall anomalies calculated from data for the years with full occupation for each index and section. The second row indicates 2020 normalized fall anomalies for each index. The third row indicates 2020 annual normalized anomalies for each index, estimated from the general linear model. CSL: Cabot Strait section; LL: Louisbourg section; HL: Halifax section; BBL: Browns Bank section.

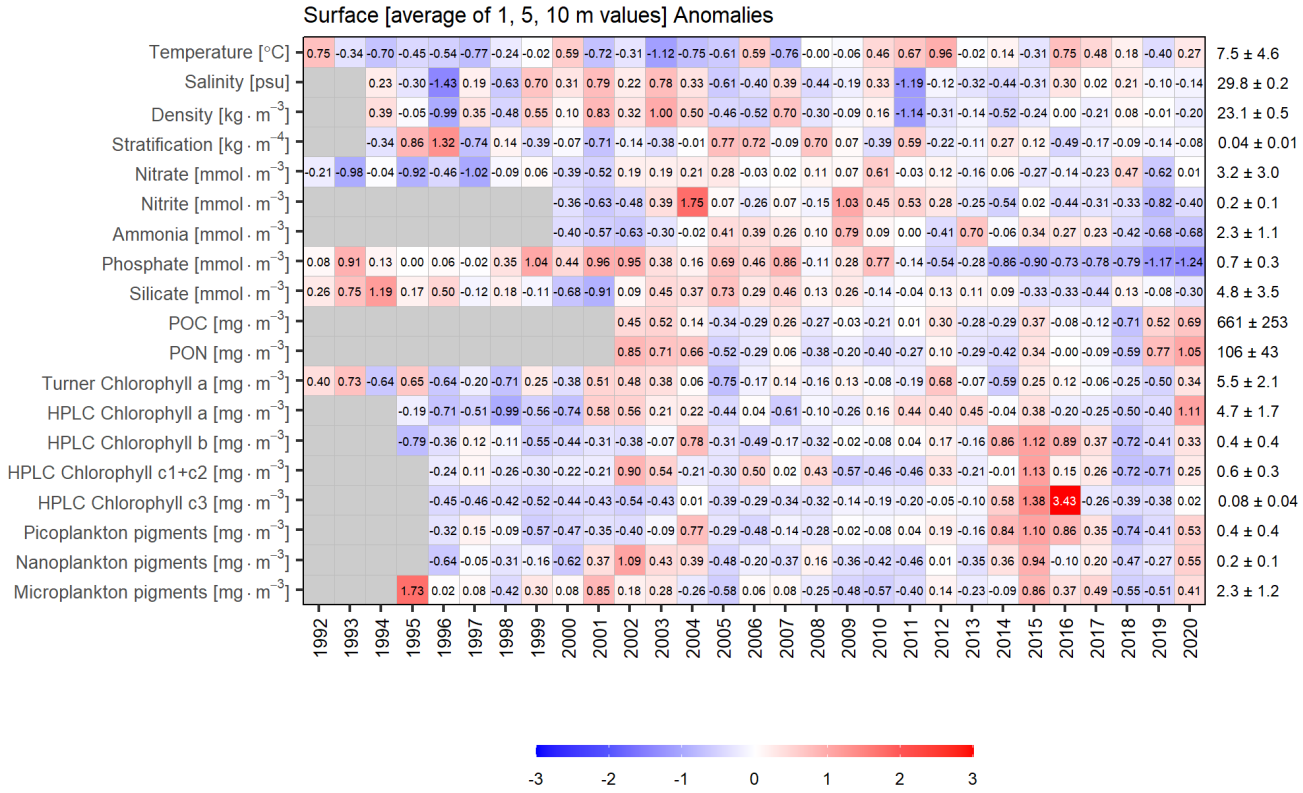

Figure 40. Annual anomaly scorecard for environmental and phytoplankton conditions in the upper water column (2 m, 5 m, and 10 m) in Bedford Basin. Values in each cell are anomalies from the mean for the reference period, 1999–2020, in standard deviation (sd) units (mean and sd listed at right). Red (blue) cells indicate higher- (lower-) than-normal levels for a given variable. Gray cells indicate missing data. POC and PON represent particulate organic carbon and nitrogen, respectively.

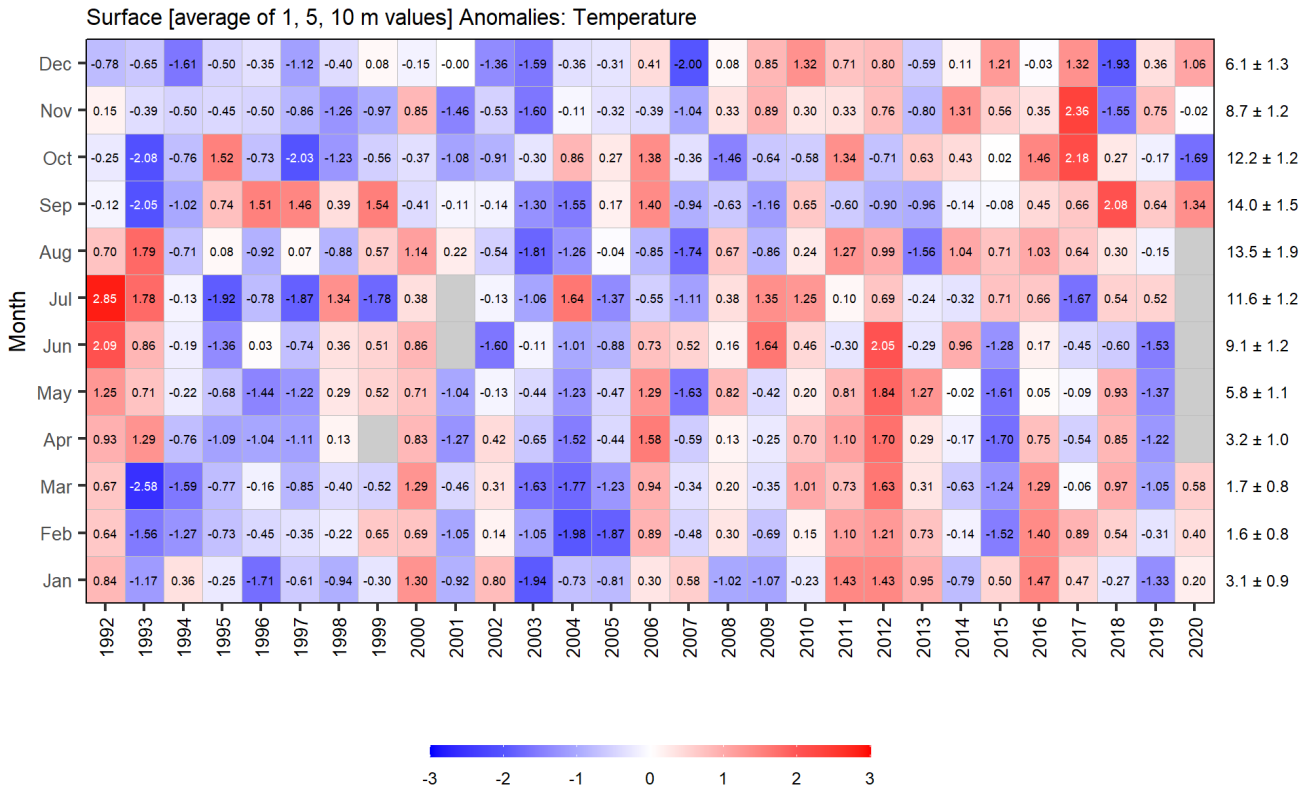

Figure 41. Monthly anomaly scorecard for temperature in the upper water column (2 m, 5 m, and 10 m) in Bedford Basin. Values in each cell are anomalies from the monthly means for the reference period, 1999–2020, in standard deviation (sd) units (mean and sd listed at right). Red (blue) cells indicate higher-(lower-) than-normal temperature. Gray cells indicate missing data.

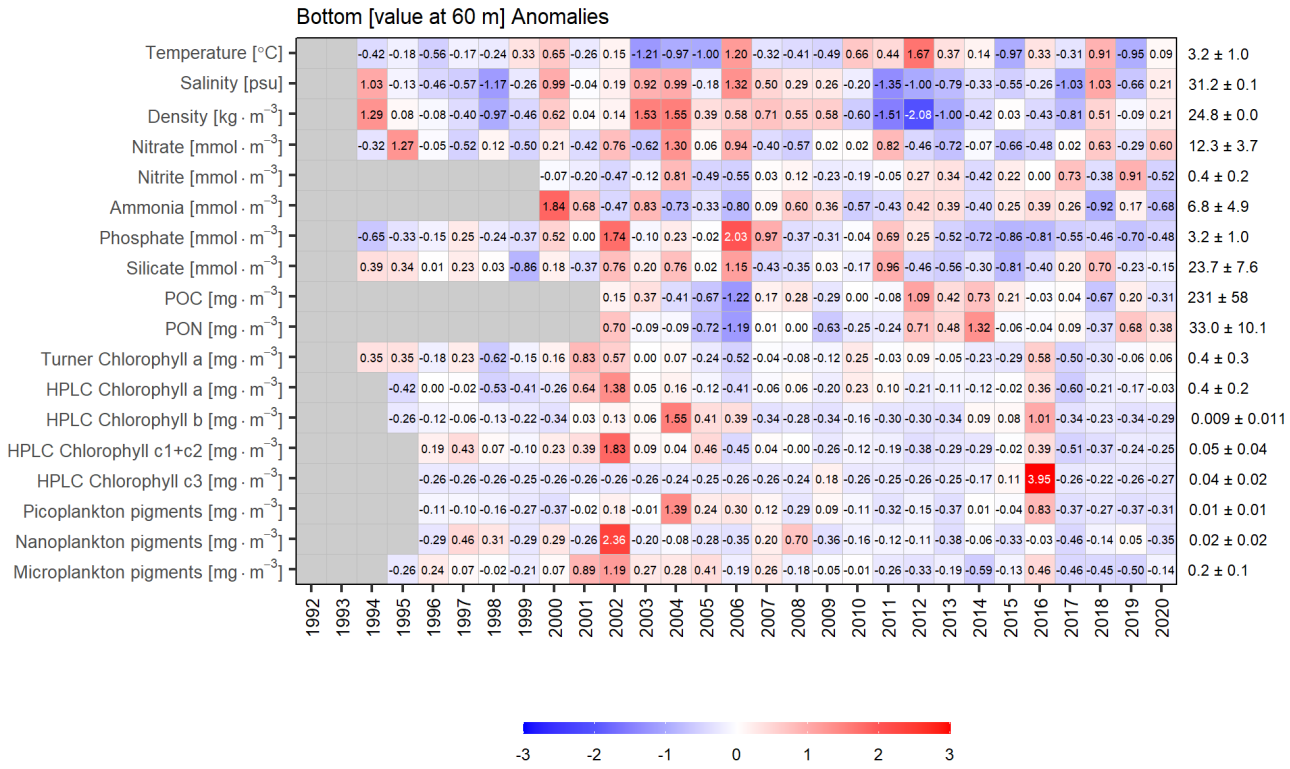

Figure 42. Annual anomaly scorecard for environmental and phytoplankton conditions at 60 m in Bedford Basin. Values in each cell are anomalies from the mean for the reference period, 1999–2020, in standard deviation (sd) units (mean and sd listed at right). Red (blue) cells indicate higher- (lower-) than-normal levels for a given variable. Gray cells indicate missing data. POC and PON represent particulate organic carbon and nitrogen, respectively.

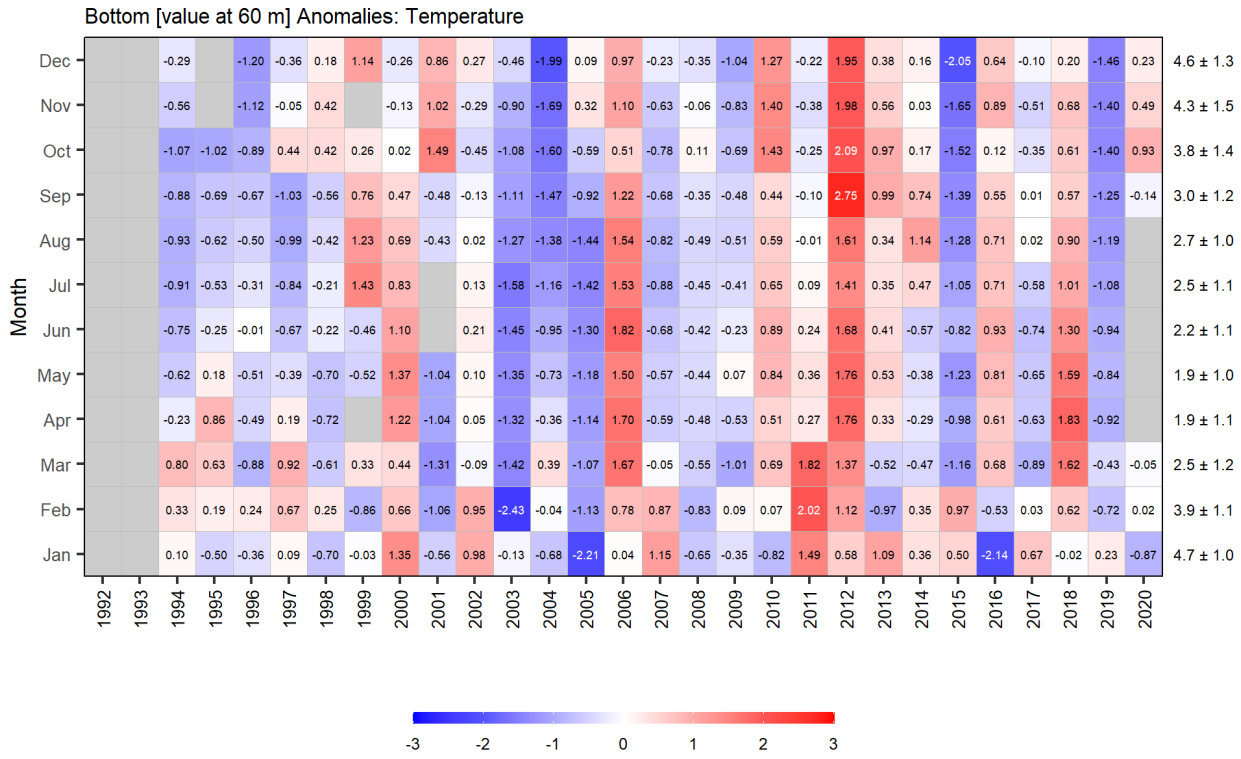

Figure 43. Monthly anomaly scorecard for temperature at 60 m in Bedford Basin. Values in each cell are anomalies from the monthly means for the reference period, 1999–2020, in standard deviation (sd) units (mean and sd listed at right). Red (blue) cells indicate higher- (lower-) than-normal temperatures. Gray cells indicate missing data.

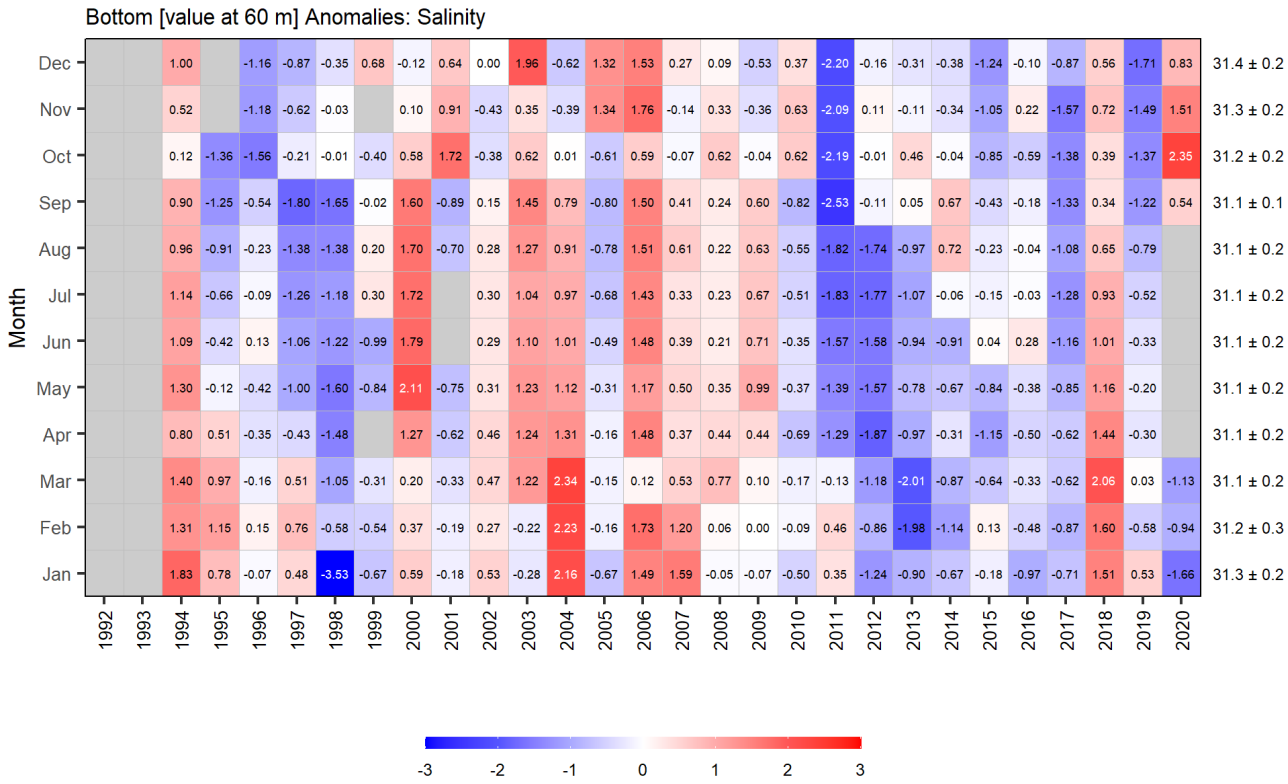

Figure 44. Monthly anomaly scorecard for salinity at 60 m in Bedford Basin. Values in each cell are anomalies from the monthly means for the reference period, 1999–2020, in standard deviation (sd) units (mean and sd listed at right). Red (blue) cells indicate higher- (lower-) than-normal salinities. Gray cells indicate missing data.

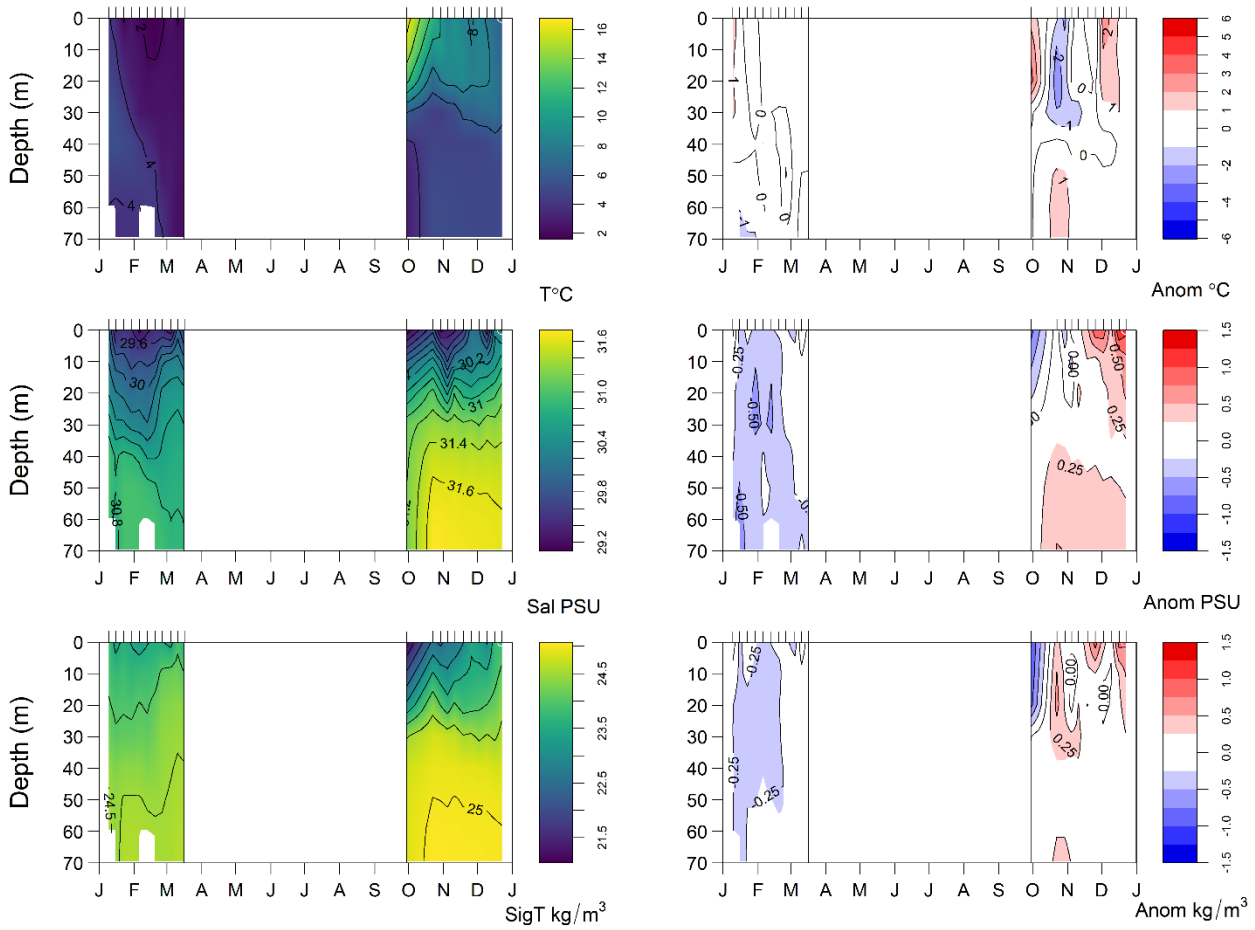

Figure 45. Annual cycle of temperature (top left panel), salinity (middle left panel), and density (lower left panel) in Bedford Basin in 2020 and their anomalies with respect to 1999–2020 monthly means (right panels). Tick marks on the top horizontal axes indicate sampling dates. Tick marks on the bottom horizontal axes indicate the 1st day of the month. No information is shown for the period without sampling from mid-March to late September.

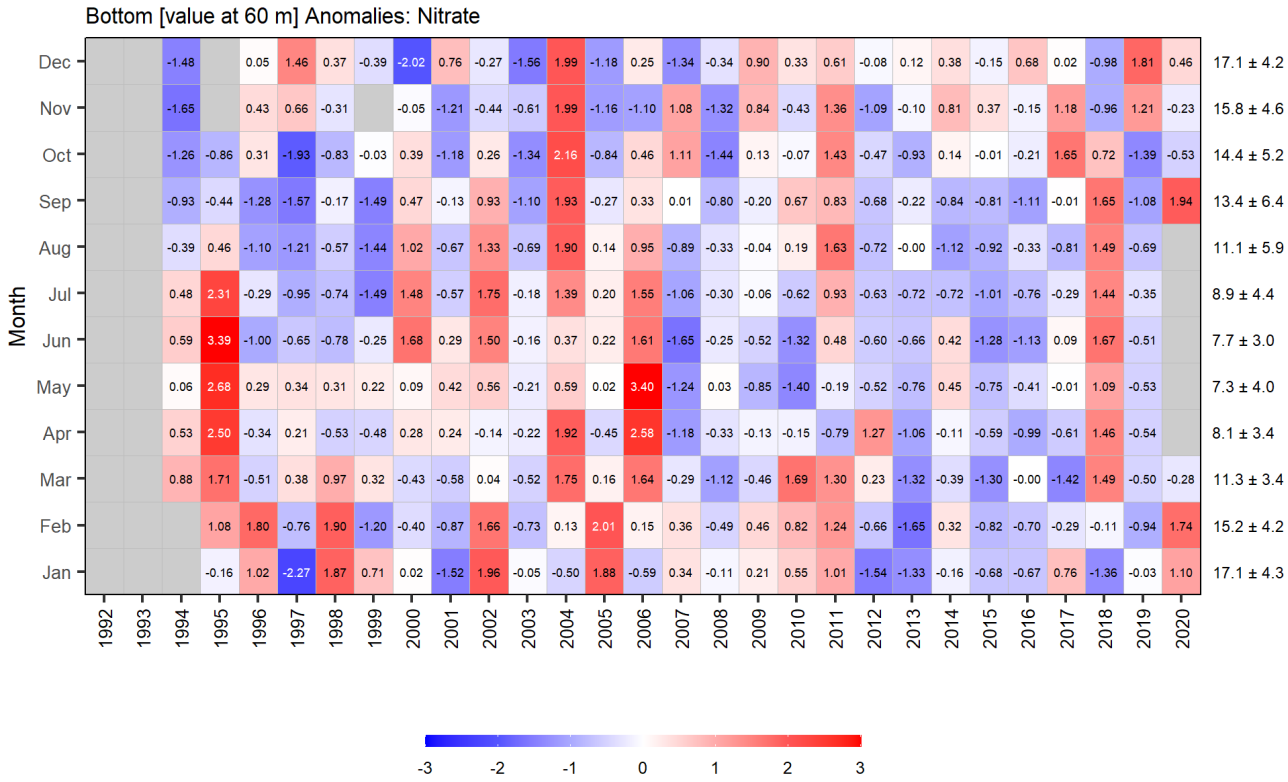

Figure 46. Monthly anomaly scorecard for nitrate at 60 m in Bedford Basin. Values in each cell are anomalies from the monthly means for the reference period, 1999–2020, in standard deviation (sd) units (mean and sd listed at right). Red (blue) cells indicate higher- (lower-) than-normal nitrate concentrations. Gray cells indicate missing data.

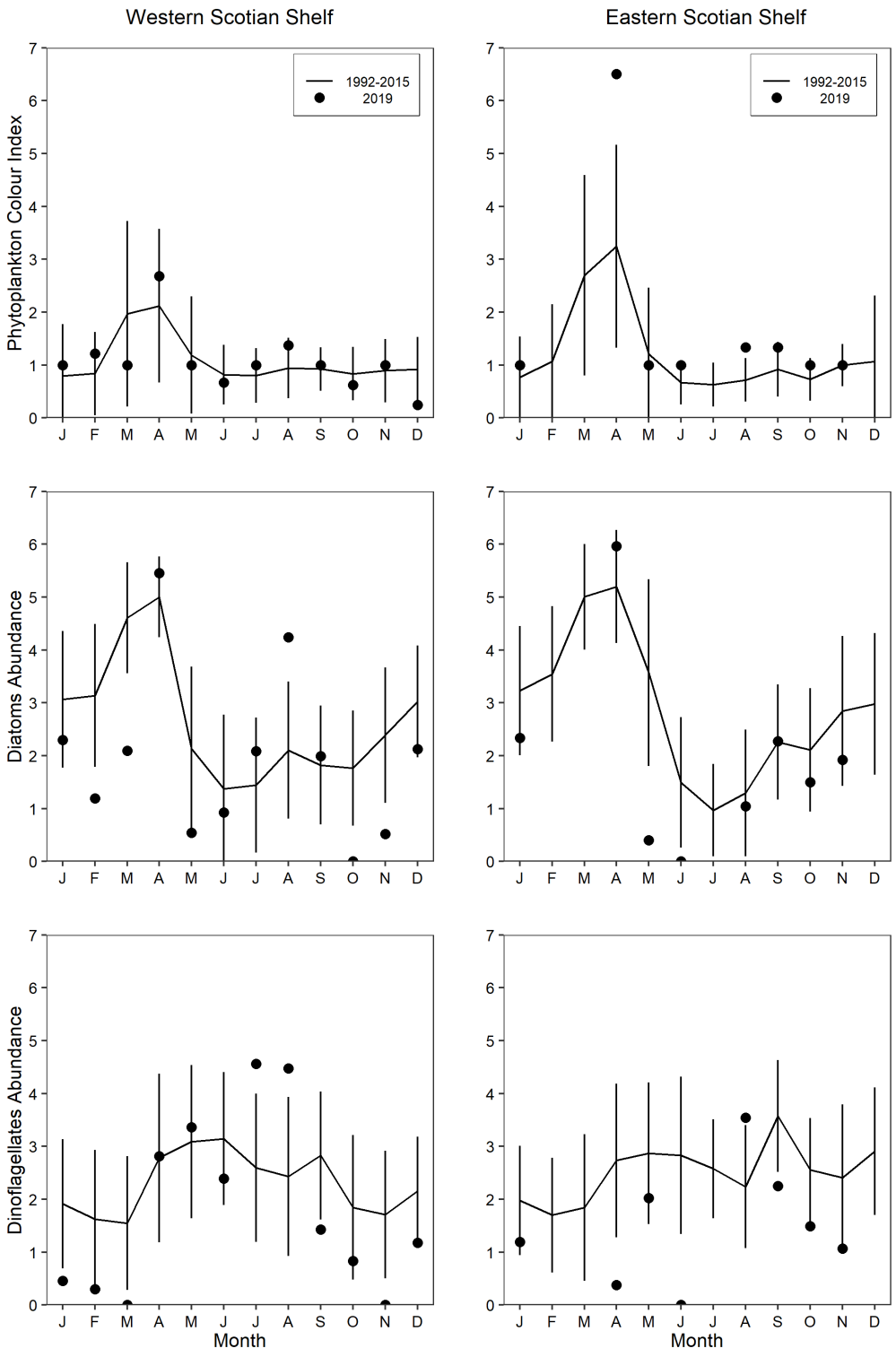

Figure 47. CPR phytoplankton abundance indices in 2019 and mean conditions, 1992–2015 (solid line) on the Western Scotian Shelf (left column) and Eastern Scotian Shelf (right column). Vertical lines show the standard deviations of the monthly averages.

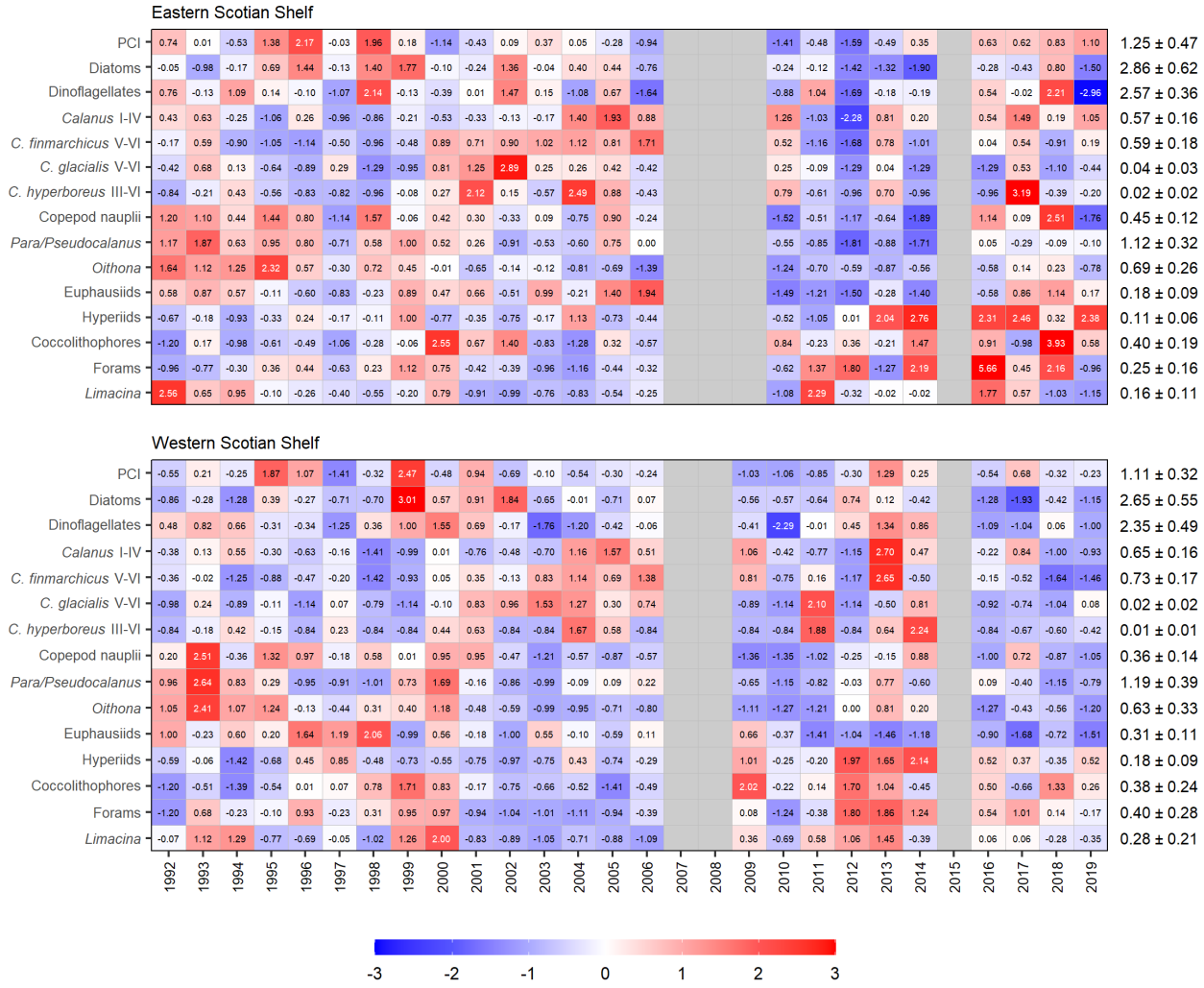

Figure 48. Annual anomaly scorecard for the abundances of phytoplankton and zooplankton taxa observed with the CPR on the Eastern Scotian Shelf (upper panel) and Western Scotian Shelf (lower panel). Values in each cell are anomalies from the annual means for the reference period, 1992–2015, in standard deviation (sd) units (mean and sd listed at right). Red (blue) cells indicate higher- (lower-) than-normal abundances. Gray cells correspond to years where either there was sampling in 8 or fewer months, or years where there was a gap in sampling of 3 or more consecutive months. PCI represents the phytoplankton color index.

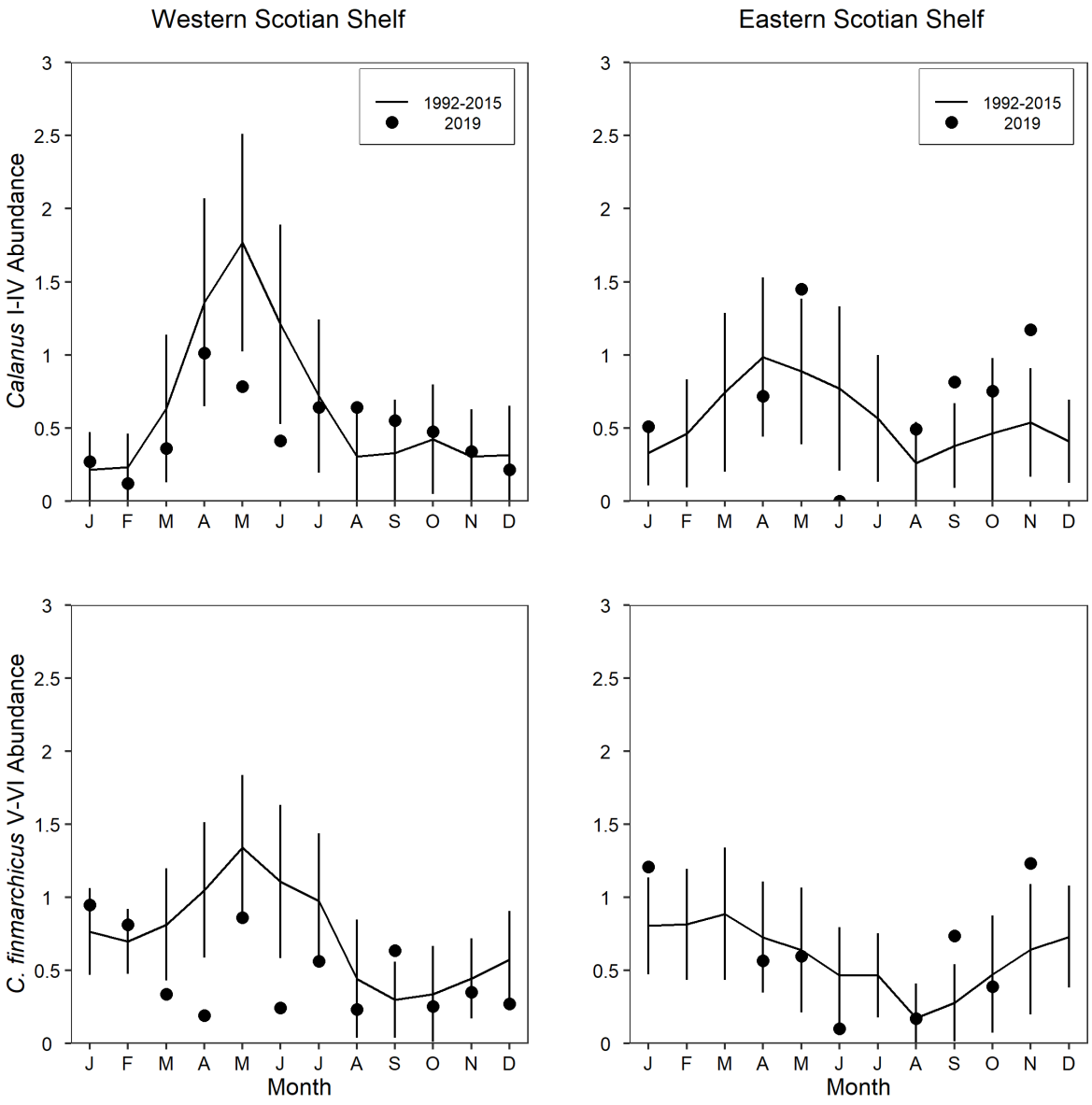

Figure 49. CPR abundance indices for Calanus I–IV (mostly Calanus finmarchicus, upper row) and C. finmarchicus V–VI (lower row) in 2019 and mean conditions, 1992–2015 (solid line) on the Western Scotian Shelf (left column) and Eastern Scotian Shelf (right column). Vertical lines represent standard deviations of the monthly averages.